Purdue University Purdue e-Pubs

ECE Masters Theses

Electrical and Computer Engineering

7-25-2008

Diesel Particulate Filter Diagnostics Using Correlation and Spectral Analysis

Pranati R. Surve

Purdue University - Main Campus, psurve@purdue.edu

Follow this and additional works at: http://docs.lib.purdue.edu/ecetheses

Surve, Pranati R., "Diesel Particulate Filter Diagnostics Using Correlation and Spectral Analysis" (2008). *ECE Masters Theses.* Paper 18. http://docs.lib.purdue.edu/ecetheses/18

This document has been made available through Purdue e-Pubs, a service of the Purdue University Libraries. Please contact epubs@purdue.edu for additional information.

PURDUE UNIVERSITY GRADUATE SCHOOL Thesis/Dissertation Acceptance

This is to certify that the thesis/dissertation prepared

This is to certify that the thesis/dissertation prepared	
By Pranati Surve	
Entitled Diesel Particulate Filter Diagnostics Using Correlation and Spectral Ar	nalysis
For the degree of Master of Science in Electrical and Computer Engineering	
Is approved by the final examining committee:	
P. H. Meckl	
Chair V. Balakrishnan	
S. D. Pekarek	
J. P. Gore	
To the best of my knowledge and as understood by the student in the <i>Research Copyright Disclaimer (Graduate School Form 20)</i> , this thesis/dissertation adhe Purdue University's "Policy on Integrity in Research" and the use of copyrighted	res to the provisions of
Approved by Major Professor(s): P. H. Meckl	
Approved by: M. J. T. Smith Head of the Graduate Program	July 22, 2008

PURDUE UNIVERSITY GRADUATE SCHOOL

Research Integrity and Copyright Disclaimer

Title of Thesis/Dissertation:
Diesel Particulate Filter Diagnostics Using Correlation and Spectral Analysis
For the degree of _Master of Science in Engineering
I certify that in the preparation of this thesis, I have observed the provisions of <i>Purdue University Executive Memorandum No. C-22</i> , September 6, 1991, <i>Policy on Integrity in Research.</i> *
Further, I certify that this work is free of plagiarism and all materials appearing in this thesis/dissertation have been properly quoted and attributed.
I certify that all copyrighted material incorporated into this thesis/dissertation is in compliance with the United States' copyright law and that I have received written permission from the copyright owners for my use of their work, which is beyond the scope of the law. I agree to indemnify and save harmless Purdue University from any and all claims that may be asserted or that may arise from any copyright violation.
Pranati Surve
Signature of Candidate
July 21, 2008
Date

^{*}Located at http://www.purdue.edu/policies/pages/teach_res_outreach/c_22.html

DIESEL PARTICULATE FILTER DIAGNOSTICS USING CORRELATION AND SPECTRAL ANALYSIS

A Thesis

Submitted to the Faculty

of

Purdue University

by

Pranati Ramdas Surve

In Partial Fulfillment of the

Requirements for the Degree

of

Master of Science in Electrical and Computer Engineering

August 2008

Purdue University

West Lafayette, Indiana

ACKNOWLEDGMENTS

This work would not have been possible without the help and support of many individuals. First and foremost, I would like to thank my advisor, Dr. Peter Meckl for guiding me throughout the course of my work. I would also like to thank my other committee members, Dr. Venkataramanan Balakrishnan, Dr. Jay Gore and Dr. Steve Pekarek for their critical suggestions. I would also like to extend my gratitude to Dr. Patricia Davies and Dr. Michael Zoltowski for helping me with signal processing. This work was supported by Cummins Inc. and would not have been possible without the contribution of Mr. Benjamin Zwissler from Cummins Inc. who provided test data. Furthermore, I would like to thank David Jamerson and Daniel Smith for answering all my questions. I got the opportunity to come to Purdue and study here through a Purdue-Cummins scholarship program and I am thankful to everyone involved in this program. Most of all, I would like to thank my colleagues, Patrick Cunningham, Alok Joshi, Gayatri Adi, Scott James and Chintan Shah for their help. Finally, I would like to thank all my friends, well wishers and family members for their encouragement and support.

TABLE OF CONTENTS

	Page
LIST OF TABLES	vii
LIST OF FIGURES	viii
ABBREVIATIONS	xii
SYMBOLS	xiiii
ABSTRACT	xv
1. INTRODUCTION	1
1.1. Motivation for Diesel Particulate Filter Implementation	1
1.1.1. Particulate Matter Composition and Health Hazards	2
1.1.2. EPA Regulations	4
1.2. DPF Background	5
1.3. Causes of DPF Failure	8
1.4. Document Organization	9
2. LITERATURE REVIEW	11
2.1. Offline Diagnostic Methods	11
2.2. Insertion Techniques	12
2.3. Engine and DPF Sensor Signal Based Methods	13
2.3.1. Drawback of Mean Value Pressure Drop Approach - Particu	ulate Micro-
structural Variability	15
2.3.2. Drawback of Mean Value Pressure Drop Approach - Non-u	niform Soot
Distribution	20
2.4. Transfer Function Methods	20
3. TEST PROCEDURES	22
3.1 Type of Filter Failure	22

	Page
3.2. Test cycle	23
3.3. Data Recording	26
4. TEMPERATURE SIGNALS – TIME DOMAIN ANALYSIS	27
4.1. Introduction	27
4.2. Magnitude Difference	28
4.3. Cross-correlation Method	30
4.3.1. Method of Magnitude	31
4.3.2. Time Delay Detection	35
5. PRESSURE SIGNALS – FREQUENCY DOMAIN ANALYSIS	41
5.1. Introduction	41
5.2. Approach	41
5.3. Method of Analysis	43
5.3.1. Transient engine operation and raw pressure signals	44
5.3.2. Fourier Transform and Energy Spectrum	47
5.3.3. Integrating energy per hertz bin	49
5.3.4. Ratio of Energy Signals	51
5.4. Frequency Range Selection.	52
5.5. Detecting Filter Condition	54
6. DPF FAILURE DETECTION ALGORITHM	57
6.1. Approach	59
6.2. Algorithm	63
6.3. Computational Burden	69
6.4. Sensitivity to Sensor Error	69
7. CONCLUSION AND FUTURE WORK	75
7.1. Conclusions	75
7.2. Research Contribution	77
7.3. Scope for Future Work	78
LIST OF REFERENCES	79

	Page
APPENDIX	
A. DPF TRANSFER FUNCTION CHARACTERISTICS	83

LIST OF TABLES

Table		Page
Table 1.1	Heavy duty US EPA diesel particulate matter regulation	4
Table 1.2	Heavy duty EU diesel particulate matter regulation	5
Table 3.1	Types of damaged and undamaged filter cases tested	23
Table 4.1	Summary of delay count between pre and post-DPF temperature sig	gnals for
	various filter cases tested	39
Table 6.1	Logarithmic function fitted to the 5-point average peak trend data o	f energy
	ratio plot for various filter cases tested	61
Table 6.2	Logarithmic function fitted to the area under the curve trend data of	energy
	ratio plot for various filter cases tested	62

LIST OF FIGURES

Figure	Page
Figure 1.1	Diesel exhaust particulate size distribution - mass and number weightings $\boldsymbol{3}$
Figure 1.2	Wall flow diesel particulate filter structure
Figure 3.1	Speed-load map for FTP75 transient test cycle
Figure 3.2	Speed-load map for LA92 transient test cycle
Figure 3.3	Speed-load map for US06 transient test cycle
Figure 3.4	Test sequence consisting of various transient test cycles
Figure 4.1	Location of temperture sensors
Figure 4.2	Diesel particulate filter inlet-outlet temperatures for healthy, fault 1 and fault
	4 type failed filter on FTP75 test cycle run after filter regeneration 28
Figure 4.3	Diesel particulate filter inlet-outlet temperatures for healthy and fault 4 type
	failed filter on FTP75 test cycles for different initial conditions
Figure 4.4	DPF inlet and outlet temperature trend depending on type of filter failure . 32
Figure 4.5	Cross-correlation of upstream and downstream temperature signals for
	healthy and failed filter cases for FTP75, LA92 and US06 tests of cycle 1 33
Figure 4.6	Attempt to achieve common magnitude for cross-correlation function for
	FTP75, LA92 and US06 tests of cycle 1 on healthy filter by normalizing by
	various parameters
Figure 4.7	Hypothetical temperature signals before and after DPF for healthy and failed
	filter conditions
Figure 4.8	(a) Raw pre and post DPF temperature signals for healthy filter test cycle 1
	(b) Filtered, windowed and mean value subtracted temperature signals for
	healthy filter test cycle 1

Figure	Pa	ıge
Figure 4.9	(a) Raw pre and post DPF temperature signals for type 4 failed filter test	
	cycle 1 (b) Filtered, windowed and mean value subtracted temperature	
	signals for type 4 failed filter test cycle 1	38
Figure 5.1	Correlating pressure signals to determine DPF transfer function	
	characteristics	42
Figure 5.2	Finding transfer function characteristics	42
Figure 5.3	Flow diagram for finding characteristics of DPF transfer function	44
Figure 5.4	Speed map for FTP75 test cycle	45
Figure 5.5	Raw upstream pressure data for FTP75 test cycle 1 on healthy filter and it	S
	magnified image for 0.5 seconds	46
Figure 5.6	Absolute Discrete Fourier Transform of upstream pressure signal for FTP?	75
	cycle 1	48
Figure 5.7	Energy spectral density of upstream pressure signal for FTP75 cycle 1	49
Figure 5.8	Energy per hertz bin	50
Figure 5.9	Energy per hertz bin of upstream and downstream pressure signals	50
Figure 5.10	Ratio of energy/Hz bin of P2 to ratio of energy/Hz bin of P1 for FTP75 tes	st
	from cycle 1 for healthy filter case	51
Figure 5.11	Frequency range detection - Energy/Hz bin of upstream and downstream	
	pressure signal for 5 transient cycles on healthy filter	53
Figure 5.12	Transfer function characteristics comparison for FTP75 cycle 1	54
Figure 5.13	Energy content – upstream and downstream pressure signals for the FTP7:	5
	cycle 1	55
Figure 5.14	Transfer function characteristics comparison for LA92 cycle 1 and Energy	,
	content of upstream and downstream pressure signals	56
Figure 5.15	Transfer function characteristics comparison for US06 cycle 1 and Energy	
	content of upstream and downstream pressure signals	56
Figure 6.1	Soot load trend of energy ratio plot for healthy filter on all the transient tes	st
	cycles	58

Figure	Page
Figure 6.2	Energy ratio peak trend for healthy filter
Figure 6.3	Energy ratio peak trend of 5-point average for healthy and failed filter
	conditions 60
Figure 6.4	Energy ratio areas under the curve trend for healthy and failed filter
	conditions 62
Figure 6.5	Fixed threshold concept
Figure 6.6	Fixed threshold – false pass
Figure 6.7	Flow chart for filter failure detection algorithm
Figure 6.8	Difference in 5-point average peak of healthy and failed filters 67
Figure 6.9	Healthy filter soot loading trend crossing the variable threshold due to partia
	regenerations 68
Figure 6.10	Effect of additional sensor noise error on energy ratio plot on healthy filter
	FTP75 test for cycle 1
Figure 6.11	5% additional sensor noise effect on energy ratio 5-point average peak trend
	compared against logarithmic trend line fitted to nominal healthy filter data
Figure 6.12	10% additional sensor noise effect on energy ratio 5-point average peak
	trend compared against logarithmic trend line fitted to nominal healthy filter
	data
Figure 6.13	5% additional sensor noise effect on area under the curve of energy ratio plo
	compared against logarithmic trend line fitted to nominal healthy filter data
Figure 6.14	10% additional sensor noise effect on area under the curve of energy ratio
	plot compared against logarithmic trend line fitted to nominal healthy filter
	data
Appendix F	igure
Figure A.1 l	Energy ratio plots for FTP75-cycle 1 for all filter cases
Figure A.2 l	Energy ratio plots for all LA92-cycle 1 for all filter cases

Appendix Figure	Page
Figure A.3 Energy ratio plots for US06-cycle 1 for all filter cases	84
Figure A.4 Energy ratio plots for FTP75-cycle 2 for all filter cases	85
Figure A.5 Energy ratio plots for all LA92-cycle 1 for all filter cases	85

ABBREVIATIONS

DFT Discrete Fourier Transform

DOC Diesel Oxidation Catalyst

DPF Diesel Particulate Filter

ECM Electronic Control Module

EGR Exhaust Gas Recirculation

EPA Environmental Protection Agency

FFT Fast Fourier Transform

Kn Knudsen Number

NAC NO_X Adsorption Catalyst

PAH Polycyclic Aromatic Hydrocarbons

Pe Peclet Number

PM Particulate Matter

SCF Stoke-Cunningham Factor

SOF Soluble Organic Fraction

VGT Variable Geometry Turbocharger

SYMBOLS

 A_f DPF Filtration Area

 C_{xx} Auto-covariance Function of Signal x

 c_{xy} Cross-covariance Function of Signals x and y

 c_{yy} Auto-covariance Function of Signal y

 $d_{aggregate}$ Mean Soot Particle Aggregate Diameter

 d_p Primary Soot Particle Diameter

D_p Particulate Diffusion Coefficient

 d_{pore} Pore diameter of DPF Porous Substrate

F Firing Frequency in Hertz

 $|H|^2$ Represents Magnitude Square of DPF Transfer Function Characteristics

 $k_{\scriptscriptstyle B}$ Boltzmann's Constant

 $k_{continuum}$ Theoretical Porous Media Continuum Permeability

 k_p Particulate Cake Layer Permeability

 k_s Clean Porous Wall Permeability

 $k_{\it slip-flow}$ Slip Flow Corrected Porous Media Permeability

M Exhaust Gas Molecular Weight

 m_p Particulate Load in DPF

Number of Samples In Given Data Set

 N_{y} Noise Added to Pressure Signal

 P_0 Reference Exhaust Pressure

 P_1 Pressure Upstream of DPF

 P_2 Pressure Downstream of DPF

P_{exh} Exhaust Pressure

R Universal Gas Constant

S Engine Speed in rpm

 $S_{N_{V}N_{V}}$ Energy Spectral Density of N_{V}

 S_{xx} Energy Spectral Density of pre-DPF Pressure Signal

 $S_{Y_{mY_m}}$ Energy Spectral Density of post-DPF Measured Pressure Signal

 T_{exh} Exhaust Temperature

 W_s Porous Wall (Substrate) Thickness

 Y_m Downstream Measured Pressure Signal

 β Forchheimer Coefficient

 ΔP Pressure Drop Across DPF

 ΔP_p Particulate Layer Pressure Drop

 ΔP_s Ceramic Substrate Pressure Drop

V Superficial Wall Flow Velocity in DPF

 λ Gas Mean Free Path

 $\lambda_{\rm ref}$ Gas Mean Free Path at a Specified Reference Condition

 μ Exhaust Gas Viscosity

E Wall (Substrate) Porosity

 ρ_p Particulate Cake Layer Density

 ho_{solid} Density of Solid Carbon

 ρ_{xy} Normalized Cross-correlation Function of Signals x and y

ABSTRACT

Surve, Pranati Ramdas. M.S.E.C.E., Purdue University, August 2008. Diesel Particulate Filter Diagnostics Using Correlation and Spectral Analysis. Major Professors: Peter H. Meckl and Venkataramanan Balakrishnan.

Diesel Particulate Filters (DPF) are used to trap the harmful particulate matter (PM) present in the exhaust of diesel engines. The particulate matter is trapped in and on a porous ceramic substrate to keep PM emissions low. The onboard diagnostics requirements enforced by Environmental Protection Agency (EPA) require that the DPF perform well to keep emissions below certain specified levels. Further, should the DPF fail in any way, resulting in higher emission levels, this event must be detected by the engine control module. The objective of this work is to "detect failed DPF condition". The temperature and pressure signals from transducers inserted into the inlet and outlet of the DPF are analyzed. The approach is to correlate the pre-DPF and post-DPF temperature and pressure signals and define the transfer function characteristics for nominal DPF behavior. Determining how these characteristics change as a result of filter failure forms the basis of a DPF fault detection algorithm. It is observed from the test data that for the pressure signal, other than the mean value signal (i.e., at zero frequency), most of the energy content is concentrated at the firing frequency of the engine. The dynamic pressure signals are used to determine the magnitude squared of the transfer function characteristics of DPF by energy spectral analysis. This approach can achieve a failure detection of lightly failed DPF which is not possible by current algorithms based on mean value pressure drop. The most significant contribution of this research is the extension of dynamic pressure signal analysis from steady-state engine operation to transient operating conditions.

1. INTRODUCTION

Diesel engine vehicles are widely used primarily due to their high efficiency, good fuel economy and durability, but the drawback is that they emit high particulate matter (PM) and NO_X . To reduce particulate matter from diesel exhaust, aftertreatment of the exhaust emissions, using a diesel particulate filter (DPF), is considered the most effective countermeasure. However, over time, these filters can suffer irreversible decrease in trapping efficiencies as the filter develops cracks due to extremely high temperatures during uncontrolled filter regeneration. Regeneration is a means by which the soot accumulated in the filter is burned off. Loss in trapping efficiency may lead to increased particulate matter emission well above the regulated limit. Filter failure causing such increase in PM needs to be detected by the engine control module. This research attempts to focus primarily on filter failure detection based on two types of signals – temperature and pressure measured pre and post-DPF. Time domain analysis of temperature signals and frequency domain analysis of pressure signals are presented for transient engine operation. A filter failure detection algorithm based on these pressure signals is also developed.

Some background on the need for diesel particulate filter implementation, its operation, and causes of filter failure is discussed next.

1.1. Motivation for Diesel Particulate Filter Implementation

Meeting existing and upcoming legislation for reduced emission standards is a major challenge faced by engine manufacturers. One of the components emitted by diesel engines is particulate matter, which is known to have harmful effects on human health.

The gradual reduction in statutory limits has caused emission control technology to change direction every few years. Earlier, tailpipe limits were met by enhancements to fuel metering and ignition systems. But, starting from year 2007, diesel particulate filters are necessary to meet the stringent emission standards [1, 2].

1.1.1. Particulate Matter Composition and Health Hazards

Particulate matter (PM) is extremely complex chemically [1]. It is normally thought of as consisting of 3 components –

- 1. The insoluble fraction This is the PM originally emitted by the engine. It is in the solid phase and composed primarily of carbon, but includes also a small amount of incombustible ash. This ash is derived mostly from the lubricant, with trace contributions from fuel additives.
- 2. Sulphates (SO_4^{2-}) These are derived from sulphur compounds in the fuel and to a lesser extent in the oil. Sulphates are emitted from the engine as sulphur dioxide (SO_2) along with smaller amounts of sulphur trioxide (SO_3) . SO_2 is not a problem by itself, but since it is readily oxidized to form SO_3 , it can become a contributor to the PM indirectly.
- 3. The soluble fraction, also called Soluble Organic Fraction (SOF) This is high molecular weight organic compounds derived from both the fuel and lubricant. The major groupings are unburned hydrocarbons, oxygenated hydrocarbons and polycyclic-aromatic hydrocarbons (PAH).

Particulate matter spans a very wide range of sizes [1, 3]. The upper limit is normally considered to be 10 μ m. More than 90% of the particles fall between a few tens of nanometers and a couple of micrometers, with the largest number of particulates concentrated around 100 nm or 200 nm. Size distribution is described as bimodal, with a smaller "nuclei" mode (\sim 30 nm), and a large "accumulation" mode (\sim 200 nm), as shown in Figure 1.1.

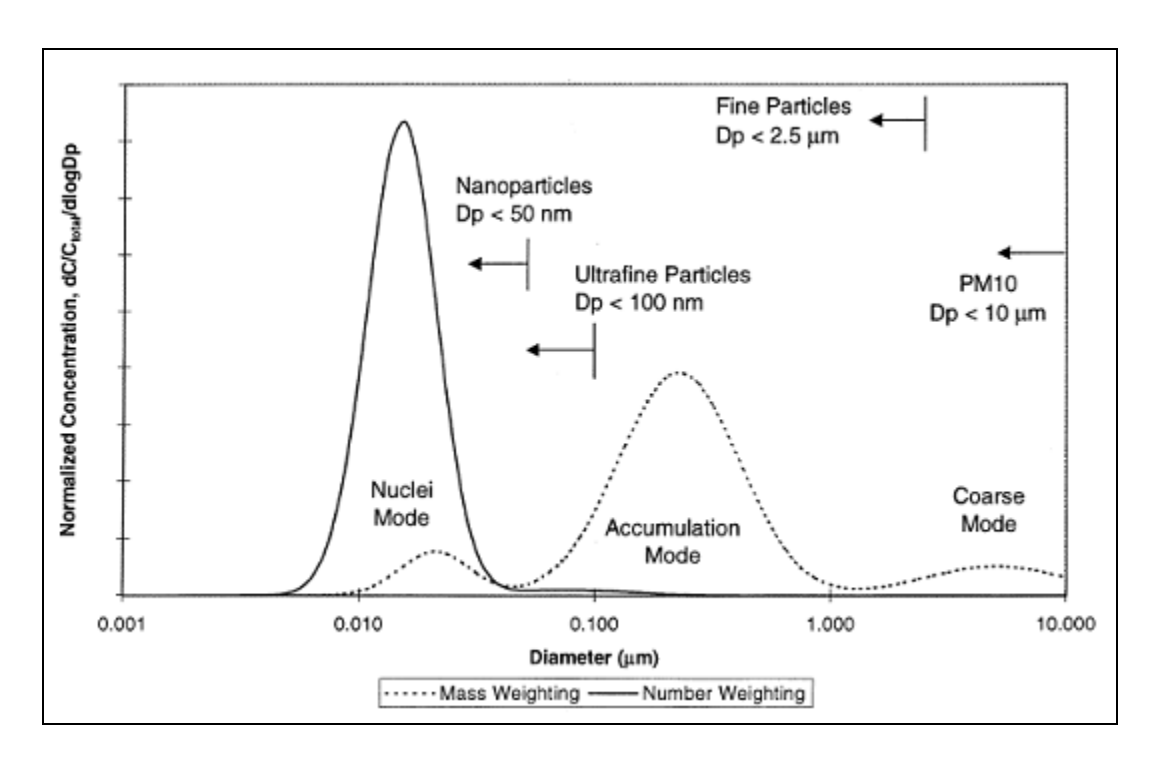


Figure 1.1 Diesel exhaust particulate size distribution – mass and number weightings. [Figure from reference 4]

Diesel PM is known to have significant implications on health. Both composition and size variation are responsible for this. "Health concerns have traditionally focused on PAH and their derivatives, nitro-PAH, some of which are known to be carcinogenic or mutagenic" [1]. The fine particulate matter can penetrate deep into the lungs and pose serious health risks, including lung damage, and premature death. They can also aggravate conditions such as asthma and bronchitis [5]. In addition, diesel exhaust is a likely human carcinogen. Diesel exhaust also has environmental impacts. "PM from diesel engine exhaust contributes to haze, which restricts visibility" [6]. Stringent regulations are a product of adverse health and environmental effects of particulate matter.

1.1.2. EPA Regulations

In 1985, EPA promulgated diesel particulate emission standards for heavy-duty diesel engines. As shown in Table 1.1, these regulations took effect in model year 1988 and became increasingly stringent. 90% reduction in particulate matter emissions was expected in 2007 compared to the 1994 standards. Though the PM emission regulations do not change from the year 2007 to 2010, regulation standards of other components such as NO_X become more stringent.

Table 1.1 Heavy Duty US EPA diesel particulate matter regulation [7]

Year	PM (g/bhp-hr)
<1988	Unregulated
1988	0.60
1991	0.25
1994	0.10
2007	0.01
2010	0.01

These standards are required to be tested on the transient Federal Test Procedure (FTP) engine dynamometer cycle. Additional emission testing requirements, first introduced in 1998, include Supplemental Emission Test (SET) and Not-to-Exceed (NTE) testing. Federal regulations require the supplemental testing from all engine manufacturers effective from year 2007. In California, the tests are required for all engines effective model year 2005.

The European Union (EU) emission standards came into effect from 1992. Table 2 lists the subsequent evolution. PM emission regulations from Euro IV to Euro V are the same, but other emission regulations become stricter.

Tier	Year	PM (g/bhp-hr)
Euro I	1992 < 85 KW	0.612
	1992 > 85 KW	0.36
Euro II	1996	0.25
	1998	0.15
Euro III	1999 EEVs only ^a	0.02
	2000	0.10
	2000	0.13*
Euro IV	2005	0.02
Euro V	2008	0.02

Table 1.2 Heavy Duty EU diesel particulate matter regulation [7]

Emission standards of United States and Europe are the most stringent. Emission regulations of other countries can be found in [7].

Concurrent with decreasing allowable particulate levels, the regulated level of NO_X emissions is also decreasing. This makes in-engine control of particulate emissions especially difficult because of the inherent interrelationship between particulate and NO_X control in the engine combustion process [1]. Hence the use of a diesel particulate filter is necessary to check the particulate matter emission.

1.2. DPF Background

A diesel particulate filter (DPF) is an afterteatment device used to trap the particulate matter coming out from the exhaust of a diesel engine. It consists of a ceramic monolith with axial channels having porous partition walls. The entrances and exits of neighboring channels are alternately blocked and so form a checkerboard pattern. A channel itself has just one open end so that the exhaust entering through the inlet of a channel cannot exit

^a Enhanced Environmentally Friendly Vehicles

^{*} For engines < 0.75 dm³ swept volume per cylinder and a rated power speed > 3000 rpm

through the same channel as its other end is closed. The exhaust gas is forced to pass through the porous wall in order to exit the DPF through the adjacent channel. In this process, the particulate matter gets trapped in and on the porous walls. Larger particles get trapped simply because they are larger than the pores in the wall. But other processes such as diffusion and thermophoresis also play a role in trapping the particulate matter [1, 8]. This structure of the diesel particulate filter is shown in Figure 1.2.

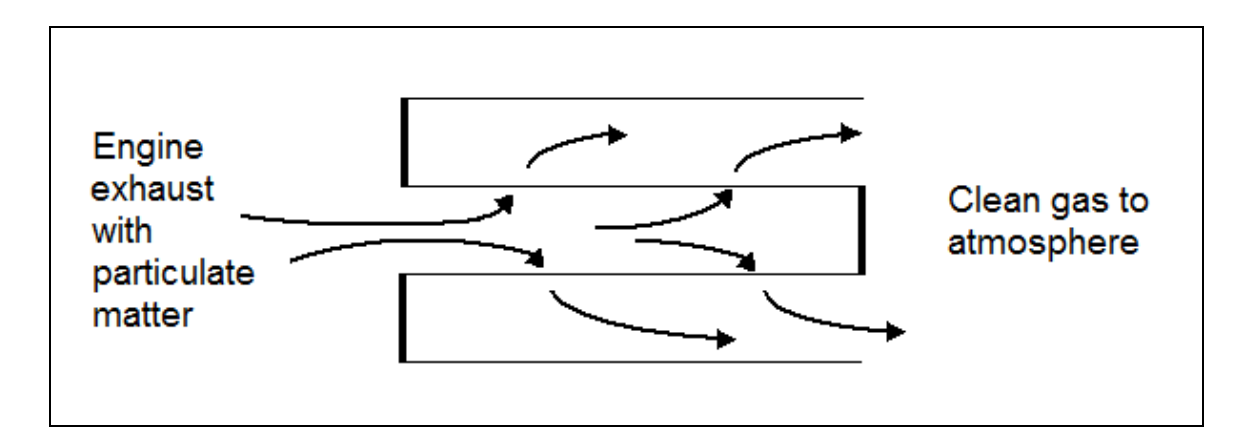


Figure 1.2 Wall flow diesel particulate filter structure

Efficient DPFs can quickly accumulate significant amounts of particulates in very little time. This leads to an increased resistance for the flow through the DPF and, therefore, increased backpressure on the engine. Filter backpressure increases fuel consumption and reduces available torque [9]. Thus, it is necessary to clean the filter periodically by burning off the collected particulate matter. This process is known as filter regeneration. Successful regeneration of DPF should achieve fast, reliable and cost effective conversion of the accumulated particulate mass, i.e., mainly carbon particles, to carbon dioxide before the filter backpressure rises to unacceptably high levels.

Numerous regeneration techniques are mentioned in the literature. These techniques can be classified as active or passive. Active regeneration schemes employ external or engine means. External means include use of fuel burners, electric heating, microwave heating, injection of combustibles (e.g., fuel) in the exhaust, and injection of catalytic and reactive

species in the exhaust [2]. Regeneration by engine means include schemes such as post injection of fuel and injection timing retard. Passive regeneration is carried out typically through catalytic means. This includes regeneration by means of fuel-borne catalysts, catalytic filter coatings (help in conversion from carbon to carbon dioxide) and reactive species generation (e.g., conversion from nitrogen oxide to nitrogen dioxide) [2].

The regeneration process can also be classified depending on the type of oxidation. It could be oxidation of particulate matter by oxygen molecules (O_2) or by nitrogen dioxide (NO_2) . In both these cases, the respective species react with carbon to form carbon dioxide. The main difference is in the temperatures at which these reactions take place. Though O_2 is available in the exhaust stream itself, O_2 -based regeneration requires temperatures of around 600 °C. NO_2 -based regenerations occur at lower temperatures, starting from 300 °C [10]. However, NO_2 concentration in the raw diesel engine exhaust, of the order of 10% of total NO_X emissions, is too low to be sufficient for filter regeneration. One way to increase NO_2 concentration in the filter is to place an oxidation catalyst upstream, converting part of the engine-out NO to NO_2 . Filter regeneration technology basically aims at increasing the reactivity of the accumulated carbonaceous particles by raising the exhaust gas temperature, or by making the particulates and/or the environment in the filter intrinsically more reactive, or both [2].

For filters with catalytic coating, regenerations occur when the temperatures are high enough for burning off the collected soot. Such filters are also referred to as continuously regenerating traps. Most such real-world regenerations of DPFs are likely to be partial, leaving some amount of soot in the filter. This is called partial regeneration.

As mentioned earlier, particulate matter also contains small amounts of incombustible ash. Origin of ash is the lubricating oil additives and fuel containing additives for regeneration promotion. Ash accumulation after repeated regenerations is a critical factor

that affects the expected lifetime of DPFs [2]. It eventually increases the backpressure and the filter needs to be cleaned to remove ash as per the maintenance schedule.

A filter failure or breakdown of any sort may render the DPF useless. Various causes leading to filter failure are described in the next section.

1.3. Causes of DPF Failure

Regeneration is the main cause of filter failure. The soot burn-off usually begins locally. Then it spreads radially and axially through the filter, if sufficient oxygen is available for combustion. Local temperature spikes can occur during burn-off, depending on the prevailing temperature, soot mass, oxygen content and thermal conductivity [11]. The temperature spikes cause high thermo-mechanical stresses that result in cracking. The crack propagation velocity of ceramic materials is exceptionally high. The crack can spread rapidly through the entire filter. The filter does not immediately fragment because the crack has released the stress. But high leakage begins immediately and the filter becomes ineffective.

High amount of soot may be accumulated in the passive regeneration mode. For extreme low load applications, prolonged operating phases can occur during which the exhaust temperature conditions are insufficient to trigger regeneration [11]. The oxidation rate may get high enough, during soot burn-off, to cause an uncontrolled temperature excursion. The resulting heat can destroy the filter [12].

Partial regenerations also play a significant role in filter damage. After a partial regeneration, the soot remaining in the filter may not be evenly distributed in the channels. The maximum radial thermal gradient is not only a function of initial soot loading but also a strong function of soot loading distribution [13]. Large thermal gradients in the (porous) solid portions of the DPF can cause it to fail mechanically [14, 12].

The filter may suffer failure when being cleansed from ash at regular intervals. The cleaning process consists of putting the filter into an oven to make it free of combustible residues and then passing pressure pulses through it to blow out the ash. The burn-off in the oven subjects the filter to thermal stresses [11], which can cause the external surface of the filter to crack.

Another reason for filter failure is excessive vibration and mechanical stress. The ceramic filter is mounted in proximity to the engine to facilitate filter regeneration. Thus the filter is exposed not only to vehicle vibrations but also suffers very high engine-induced vibrations. This may lead to damage of the brittle filter material [11].

The importance of the DPF is in reducing particulate matter in the exhaust of diesel engines to meet stringent emission regulations. But if the DPF cracks, or breaks down in any way (also referred to as filter failure or filter fault), then the particulate matter can still find its way to the atmosphere. This loss in trapping efficiency of the filter may result in increased particulate matter emissions well above the regulated limit. In such cases, the purpose of the DPF is defeated. A failed DPF needs to be detected and replaced as soon as possible. This provides motivation for this research, which focuses on DPF failure detection methods.

1.4. Document Organization

Chapter 2 provides the relevant literature survey of the various methods used currently for detecting filter failure. Data for this research was acquired from a Cummins ISB 6.7 series medium-range diesel engine. Chapter 3 describes the data sets analyzed in this research. It also describes the types of filter failures tested. Chapter 4 focuses on filter failure diagnostic methods based on pre and post-DPF temperature measurements. Spectral analysis of pre and post-DPF pressure signals is presented in chapter 5. Chapter 6 presents a diagnostic algorithm to detect failed filter condition using energy correlation

of pre and post-DPF pressure signals. Conclusions drawn from this research and ideas for future work are mentioned in chapter 7.

2. LITERATURE REVIEW

In this chapter, the literature related to diesel particulate filter (DPF) diagnostics is reviewed. If diesel particulate filters accumulate heavy soot load, then high temperatures may be reached during regeneration. This can cause uncontrolled regenerations leading to filter break down as described in section 1.3. A conservative approach to avoid filter failure would be to request additional soot regenerations to eliminate soot that may get missed under presently available regeneration schemes [12]. A systematic approach to enhancing soot filter protection by detecting and labeling a filter regeneration event is described in [12, 15]. This results in a major fuel penalty and does not guarantee complete filter protection. Also, this preventive approach provides no means of detecting a failed filter condition. Various techniques for detecting DPF failure are surveyed next.

Fault is an unacceptable functional departure of a component from its nominal behavior, leading to failure of the component. The effects of failure can be observed through symptoms. Thus, faults cause symptoms. A single fault can cause multiple symptoms. Fault detection is finding the size and time of occurrence of a fault through symptoms [16]. Detecting diesel particulate filter failures is of interest for this study. Various approaches taken so far for this purpose are examined below.

2.1. Offline Diagnostic Methods

In the offline diagnostic methods, the DPF is not diagnosed when it is mounted on the engine aftertreatment system while the engine is in operation. The DPF has to be removed from the aftertreatment system. One such way of monitoring the DPF is disclosed in [17]. The filter is examined by flowing particulates in an axial direction of

the DPF from one end surface body, catching the particulates on a gas-permeable screen intimately mounted on the other end surface to form a figure of the particulates, and checking the figure to inspect defects at internal partition walls and sealing portions of the honeycomb structural body. This offline detection scheme is helpful mainly for inspecting a DPF in the production stage.

2.2. Insertion Techniques

If a filter is in healthy operating condition, it has a very good trapping efficiency, typically more than 90% [18]. However, in the event that a DPF becomes cracked or otherwise damaged, some of the soot in the exhaust gas may find its way to the environment. This principle is used in [19, 20] to come up with a filter failure monitor. A particulate sensor, downstream of the DPF, for sensing the presence of particulates in a gas flow stream is disclosed in [19]. The particulate sensor includes a housing having a flow driver, two flow paths, two filters, two temperature sensors, a heater and a control device. The apparatus is configured in such a way that equal temperature measurements are observed in the two flow paths when there is no soot in the exhaust gas flow, and different temperature measurements are observed in the presence of soot content in the exhaust gas flow, thereby enabling a means for sensing the presence of soot in the gas flow. The control device is configured to provide an onboard diagnostic signal in response to a temperature differential sensed by the two temperature sensors exceeding a defined threshold.

A different method using only soot sensors having a temperature measurement is described in [21]. Filter in the soot sensors are, preferably, made of the same material as the particulate filter. The soot sensors are periodically regenerated or cleaned. The amount of heat generated to burn off the soot is monitored. For the upstream sensor, this heat generation amount is correlated to soot accumulation in the filter since only a part of the soot goes into the first sensor. When the heat generated is greater than the threshold for the downstream soot sensor, it indicates a failed filter condition. Though these

techniques seem to be good, they require the housing of the soot sensor, which itself requires a lot of hardware, inside the exhaust pipe, and hence can prove to be expensive.

Another insertion technique disclosed in [20] includes an insertable chamber and gas sensors for determining the concentration of at least one component of exhaust gas, preferably oxygen. This chamber also consists of a filter. Its clogging, which corresponds to DPF failure, is detected by oxygen concentration fluctuations inside and outside this chamber. The frequency spectrum of these sensor signals corresponds to the frequency spectrum of a low-pass filter and its cut-off frequency depends on the degree to which the filter to be monitored is loaded with soot. A filter failure is detected by determining the limit frequency of the sensor provided in the chamber. The above mentioned methods are suitable for mass application in vehicles and allow measurement of leaks and cracks in the soot filter during operation. But these methods are expensive on account of extra hardware and additional sensors.

2.3. Engine and DPF Sensor Signal Based Methods

Diagnostic methods based on the information available from the engine and standard pressure and temperature sensors mounted pre and post-DPF, have also been developed.

[22]

One such method is described in [23]. Here, the particulate filter temperature is maintained using engine speed to ensure that an uncontrolled regeneration of the filter does not take place. A regeneration parameter is then determined based on differential pressure measurement across the filter and volumetric flow rate estimation made from other engine parameter values. Based on this regeneration parameter, estimates of the health of the filter are made. Higher differential pressure indicates a plugged filter and extremely low differential pressure indicates a failed filter state. For differential pressures in between these thresholds, the filter is considered to be healthy. There is a possibility of not detecting a failed filter here. If a filter soot loads to some extent and then fails, so that

its differential pressure decreases as compared to a healthy soot-loaded filter case, but is still more than the low differential pressure threshold, then it is declared to be in a good state. This drawback can be overcome by setting a variable threshold as is done in the method described next.

Parameter values correlated with a flow of exhaust gas of the engine are determined, and the differential pressure between upstream and downstream sides of the particulate filter is determined. The ratio of a variation rate of the parameter values correlated with the exhaust flow to a variation rate of the differential pressure is compared with a predetermined threshold value during transitional operation of the engine to determine the state of the particulate filter [24]. The idea of variable threshold as filter soot loads and/or for ash accumulation is valuable. It allows for DPF failure detection even after it has soot loaded to some extent. Detecting such failures is difficult with fixed thresholds as this condition could be falsely indicated as a healthy filter, as explained above. Thus implementing variable threshold prevents misjudging the failed filters as healthy. The main drawback of this method is that this algorithm works only during acceleration or deceleration of the engine and hence cannot be used for any other transient engine operation.

DPF soot load models can be used for DPF diagnostics. A DPF can be recognized as failed when the difference between predicted and actual soot load in the DPF increases beyond some predetermined threshold. One such soot load model is developed in [25]. The effect of DPF load on the flow through the exhaust pipe is modeled as a valve which is slowly closing. The model requires pre and post-DPF pressure, pre-DPF temperature, fuel flow and air mass flow for effective area which is considered to be a function of particulate load in the DPF.

A virtual soot sensor is developed by Konstandopoulos et. al. in [26]. A filter loading model primarily based on mean value pressure drop is developed and is used to solve the so-called inverse problem of estimating the accumulated soot mass inside the filter. The

solution requires knowledge of the filter geometry, the filter pressure drop, the exhaust gas temperature, the engine operating conditions as well as the micro-structural properties of the soot.

Most of these methodologies for determining the filter's state are based on measuring the mean value pressure drop across the filter. The pressure drop across a filter increases as the filter soot load increases. At some pre-determined pressure drop, the filter is run through a regeneration cycle. This methodology has drawbacks. Non-uniform soot distribution in the DPF and particulate micro-structural variability influences the pressure drop behavior such that the filter may appear to be in need of regeneration later or sooner than necessary [27]. Also, a breakdown or burn-through of the substrate leads to a low pressure drop, which may be interpreted as a clean filter and would result in significant loss of filtering capability [27]. The above-mentioned drawbacks are described in detail in the following sub-sections.

2.3.1. Drawback of Mean Value Pressure Drop Approach - Particulate Microstructural Variability

To solve the inverse problem of determining the state of the filter based on the measurements of exhaust gas flow rate, the DPF temperature and back pressure, pressure drop modeling is required. Many such models are present in the literature. They assume constant wall and soot permeability. This assumption proves unable to predict the influence of the gas temperature on the pressure drop. The permeability actually changes with soot loading. This micro-structural variability is discussed here.

The total pressure drop across the filter is assumed to be the sum of the ceramic substrate pressure drop and the particulate layer pressure drop [28]

$$\Delta P = \Delta P_s + \Delta P_p$$
 Eq. 2.1

For ceramic substrate and the particulate layer, Darcy's law is assumed to be valid. Hence,

$$\Delta P = \frac{\mu v w_s}{k_s} + \frac{\mu v w_p}{k_p}$$
 Eq. 2.2

where μ is the exhaust viscosity, ν is the wall flow velocity (perpendicular to the porous wall), w_s is the thickness of the porous wall, w_p is the thickness of the particulate layer, k_s is the permeability of the porous substrate, and k_p is the permeability of the particulate cake layer. By using the concept of effective thickness of the particulate layer, and including the Forchheimer correction term for high exhaust flow rates,

$$\Delta P = \frac{\mu v w_s}{k_s} + \frac{\mu v m_p}{A_f \cdot (\rho_p k_p)} + \frac{\beta v^2 m_p}{A_f}$$
 Eq. 2.3

where ρ_p is the bulk density of the deposit layer, A_f denotes filtration surface area and β is the Forchheimer coefficient, which depends on the porous medium. The above equation fails due to the slip conditions present when the gas flows through the small passages of low porosity medium. The slip phenomenon is related to the Knudsen number, which is the ratio of the gas mean free path to the pore size in the porous medium.

$$K_n = \frac{\lambda}{d_{pore}}$$
 Eq. 2.4

The mean free path λ is given by

$$\lambda = \frac{\mu}{P_{exh}} \sqrt{\frac{\pi R T_{exh}}{2M}}$$
 Eq. 2.5

where M is the exhaust gas molecular weight.

The theoretical permeability values assume no-slip at the interface of gas with channels in the porous media [29]. When the pore diameter is much larger than the mean free path ($K_n << 1$), the no-slip assumption is valid. However, when the mean free path is higher than the mean pore diameter ($K_n >1$), this assumption breaks down. If the Knudsen number $K_n \approx 10^{-2}$, slip flow can be neglected, but for Knudsen number close to unity, it cannot be neglected [28]. Both factors, soot layer density and soot layer permeability are variable, and so the product $\rho_p k_p$ in equation (2.3) is widely varying [9]. Many relations of permeability to take slip flow into account are present in the literature. In [28], particulate density and permeability are considered to be proportional to mean free path,

$$\rho_p k_p = c \frac{\lambda}{\lambda_{ref}}$$
 Eq. 2.6

where c is an empirical constant and λ_{ref} is the gas mean free path at a chosen reference condition. From Equations 2.5 and 2.6, $\rho_p k_p$ is an increasing function of T_{exh} and from Equation 2.3, ΔP is inversely related to $\rho_p k_p$, and hence ΔP depends on the exhaust temperature.

In [2], the Stokes-Cunningham Factor (SCF) is employed to deal with the slip-flow effects.

$$SCF = 1 + K_n \left[1.257 + 0.4 \exp\left(\frac{-1.1}{K_n}\right) \right]$$
 Eq. 2.7

$$k_{slipflow} = SCF \cdot k_{continuum}$$
 Eq. 2.8

In [31], the following empirical relation expressing the dependency of soot permeability on local temperature and pressure is used.

$$k_p = k_0 \left[1 + C_4 \frac{P_0}{P_{exh}} \mu \sqrt{\frac{T_{exh}}{M}} \right]$$
 Eq. 2.9

The constants k_0 and C_4 have to be estimated experimentally.

Peclet number, P_e and SCF are used to relate permeability and density to temperature [18, 30, 8]. Soot packing density can be expressed in terms of the soot layer porosity as

$$\rho_p = \rho_{solid} \cdot (1 - \varepsilon),$$
Eq. 2.10

where ε is the wall porosity. The porosity relation is described by

$$\varepsilon = A \cdot P_e^B + C, Eq. 2.11$$

where A, B and C are constants that depend on the morphology of the deposition surface and P_e is the Peclet number given by,

$$P_e = \frac{vd_p}{D_p}$$
 Eq. 2.12

where d_p is the primary soot particle diameter and D_p is the particle diffusion coefficient, given by

$$D_p = \frac{k_B T_{exh}}{3\pi\mu d_{aggregate}} \cdot SCF ,$$
 Eq. 2.13

where k_B is the Boltzmann's constant and $d_{aggregate}$ is the mean soot aggregate size. The permeability of the soot cake micro-structure is given by [8],

$$k_p = f(\varepsilon) \cdot d_p^2 \cdot SCF$$
 Eq. 2.14

where $f(\varepsilon)$ is given by the Kuwabara function,

$$f(\varepsilon) = \frac{2}{9} \cdot \left[\frac{2 - \frac{9}{5} (1 - \varepsilon)^{\frac{1}{3}} - \varepsilon - \frac{1}{5} (1 - \varepsilon)^2}{(1 - \varepsilon)} \right]$$
 Eq. 2.15

The inclusion of pressure-dependent gas properties in the analytical expression has proven to be necessary. Hence these complex and empirical relations have to be taken into account. Neglecting this effect could yield an error on the order of 10% in terms of pressure drop predictions [31]. A diagnostic algorithm used to determine if a filter is in healthy operating condition or is damaged, may make use of the pressure drop across the DPF to make the decisions. In real world transient engine operation, it is difficult to accurately determine pressure drop and this may eventually result in false diagnostic results.

2.3.2. Drawback of Mean Value Pressure Drop Approach - Non-uniform Soot Distribution

Non-uniform soot distribution patterns are very likely to occur in random real world driving cycles. This is because the exhaust gas flow rate varies in this case, leading to radial and axial soot maldistribution in the DPF. More soot is deposited in the central channels of the DPF in the initial loading stage on account of higher flow through the central channels [9]. Also, partial regenerations are a potential cause of radial soot maldistribution. This is because the outer DPF channels are at lower temperature than the central channels, and hence do not get completely regenerated. Flow rate also affects axial soot distribution. Higher flow rate leads to more soot deposition at the end of the channels leading to axial maldistribution.

Non-uniform soot distribution causes uncertainty in accurate soot mass detection in the DPF from pressure drop measurement. The effect of soot loading non-uniformity on pressure drop was examined in [13]. As different pressure drop measurements were noted for the same amount of soot mass, it was confirmed that the pressure drop cannot be safely linked with soot mass. Thus the same amount of pressure drop could correspond to different soot mass and the same amount of soot mass could lead to different pressure drop measurements.

Thus, particulate micro-structural variability and non-uniform soot distribution cause uncertainty in safely linking pressure drop to soot mass and this is the main drawback of the diagnostic methods based on mean value pressure drop measurement.

2.4. Transfer Function Methods

Diesel particulate filters affect acoustics and also work as mufflers. To properly design exhaust systems, acoustic models for DPFs are needed. A study in this direction was first undertaken by Sabry Allam and Mats Abom. Modeling of sound transmission loss and

attenuation is presented in [32, 33]. Their work helps to understand acoustics of the DPF, but does not provide any direction for estimating soot load or DPF failure. DPF failure detection using acoustic sensing is disclosed in [34, 27]. Acoustic apparatus consisting of a 1st receiver, 2nd receiver, resonator and transmitter is used to monitor the state of the particulate filter [34]. The type of sound waves transmitted by the transmitter may be selectively adjusted by the electronic control module (ECM) in terms of their frequency, intensity, wavelength, amplitude and other properties based upon the characteristics of the IC engine, particulate filter, particulate matter, and/or the working environment. The acoustic emissions from the filter may be compared to a known filter state to determine the present filter state. As the soot loading of the particulate filter increases, the transmission loss of a sound wave detected across the filter also increases. This relationship may be preprogrammed into the electronic control module and the acoustic apparatus can also be used to detect soot loading of the particulate filter. Here the nominal behavior of the DPF is determined in terms of sound waves and any departure from that is recorded as DPF failure. The sound waves are analyzed in the frequency domain. This method becomes expensive due to the extra hardware involved.

Another patent [27] discusses monitoring of DPF using acoustic sensing. This technique analyzes acoustic emissions from the engine. An acoustic transfer function is determined and the frequency resulting therefrom is compared to a known filter state or the determined transfer function is compared to one or more reference transfer function characteristics of various preselected filter states such as loading, full, empty, or failed. This principle is based on the fact that, depending on the state of the filter, variations in the acoustic transfer function could appear in engine sounds that pass through it. The idea of using a transfer function for regeneration management based on pulsating pressure signals provided with temperature correction is disclosed in [35]. The DPF failure method developed in present research work, discussed later in this document, also consists of characterizing the nominal behavior of the DPF. But it involves analyses of pre-DPF and post-DPF pressure signals only and hence is more cost-effective.

3. TEST PROCEDURES

The data used for the purpose of this study was provided by Cummins, Inc. The testing was performed on a 6.7L diesel engine with a cooled exhaust gas recirculation (EGR) system and a variable geometry turbocharger (VGT) in a test cell with a dynamometer capable of running transient speed-load maps. The engine was fully equipped with aftertreatment devices for particulate matter and NOx (oxides of nitrogen). With NOx adsorption catalyst (NAC) and diesel oxidation catalyst (DOC) in place, the DPF was truly tested for real-world conditions. Thus, a state of the art system was used for testing. This section describes the test cycles and modes of filter failure that were tested.

3.1. Type of Filter Failure

For the purpose of diagnosing filter failure, real-world and artificially failed filters as well as healthy filters were tested. "Healthy filter" refers to an undamaged filter. Two real-world filter failure cases were tested. The more failed filter is called the "fat failed" and the less failed filter is called the "thin failed" filter. Four types of artificially failed filter cases were tested. Particulate filters were artificially failed by drilling a hole through the central channels of the substrate parallel to the direction of exhaust flow. This failure case is referred to as parallel filter failure. The extent of filter failure is characterized by the size of the hole drilled. The different types of filter cases and the names by which they are referred for the rest of this document are summarized in Table 3.1. Failed filters were simulated by artificially failing particulate filters by drilling through holes since this is the most repeatable way of failing filters known so far. A realistic simulated failure by causing the filter damage chemically is possible, but repeatability of such type of failure could be an issue.

Table 3.1 Types of damaged and undamaged filter cases tested

Case Number	Filter Type	Name Used
1	Good or undamaged filter	Healthy filter
2	Artificially failed filter – smallest hole	Type 1 failed filter
3	Artificially failed filter – bigger hole	Type 2 failed filter
4	Artificially failed filter – even bigger hole	Type 3 failed filter
5	Artificially failed filter – biggest hole	Type 4 failed filter
6	Real-world failed filter – thin failure	Real pr1
7	Real-world failed filter – fat failure	Real pr2

3.2. Test cycle

All the test cycles considered were transient test cycles, meaning that the engine speed and load were constantly changing. Standard transient driving cycles for emission testing were used. Specifically, the Federal Test Procedure (FTP), LA92 and US06 cycles were run. These are environmental protection agency (EPA) certified test cycles. They simulate urban routes with frequent stops and are mainly used for emission certification testing of cars and light and heavy duty trucks in the USA [7]. The speed-torque maps for each of the 3 transient test cycles are as shown in Figures 3.1, 3.2 and 3.3.

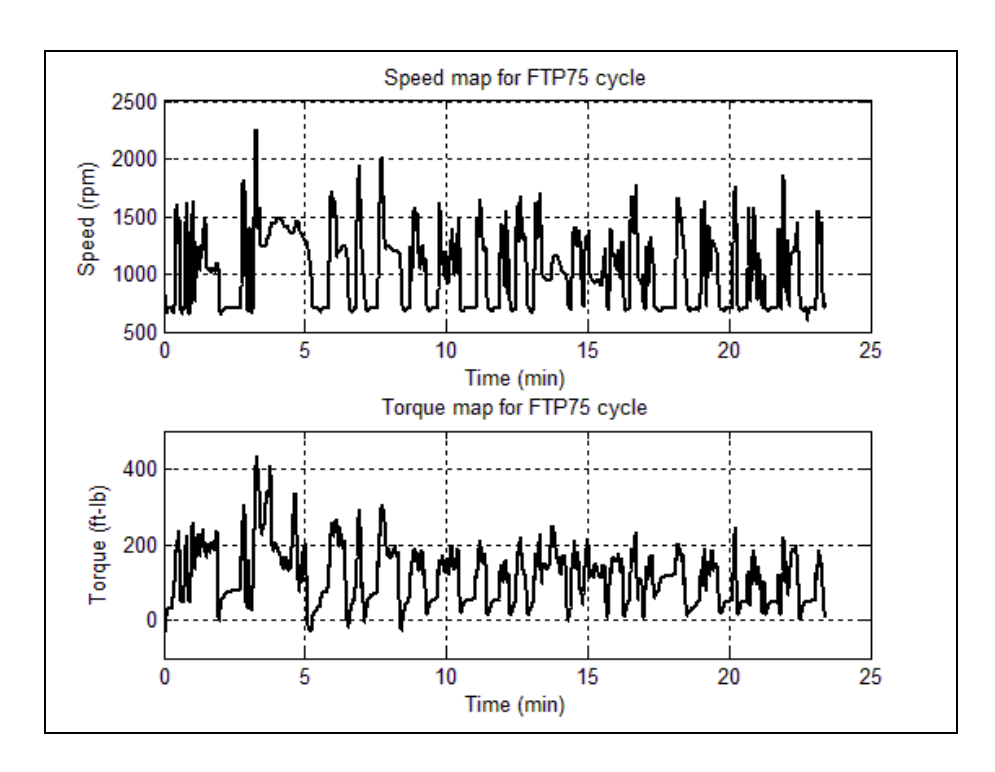


Figure 3.1 Speed-load map for FTP75 transient test cycle

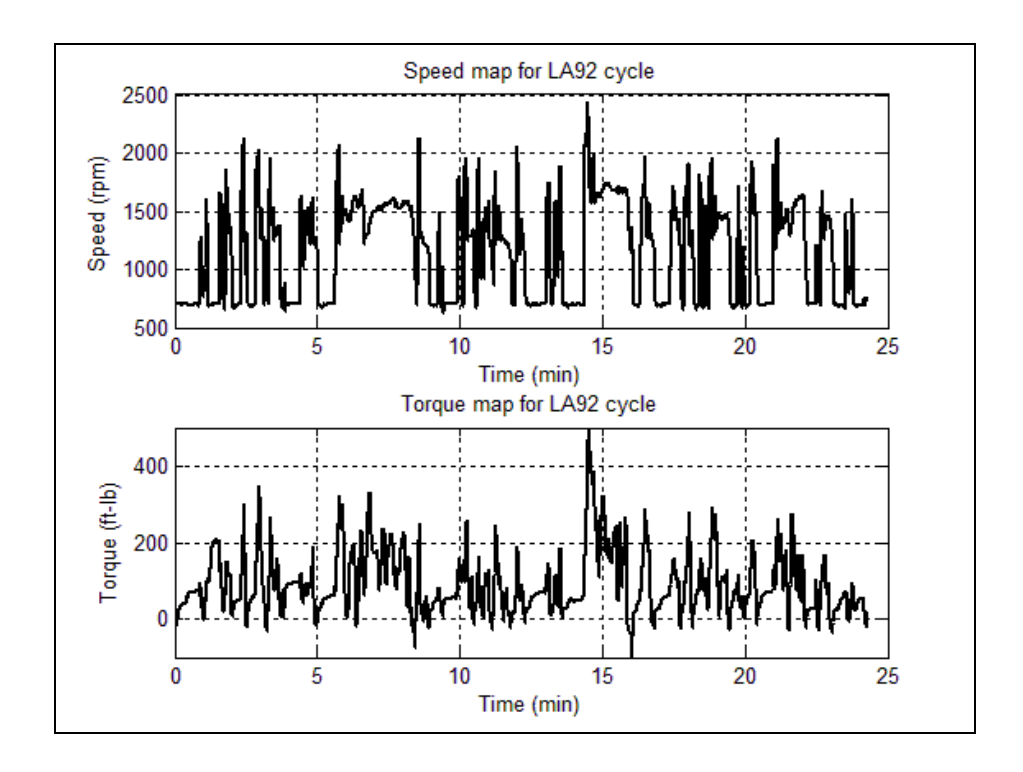


Figure 3.2 Speed-load map for LA92 transient test cycle

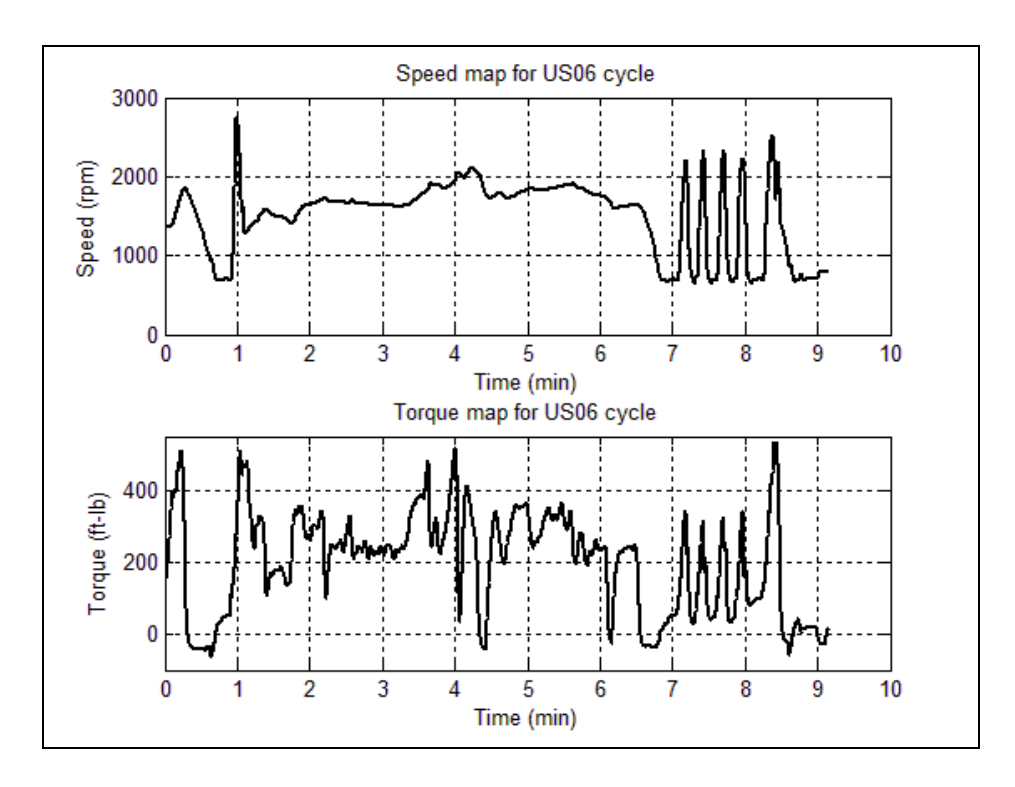


Figure 3.3 Speed-load map for US06 transient test cycle

The sequence of tests followed in the test procedure for testing filters is described in Figure 3.4

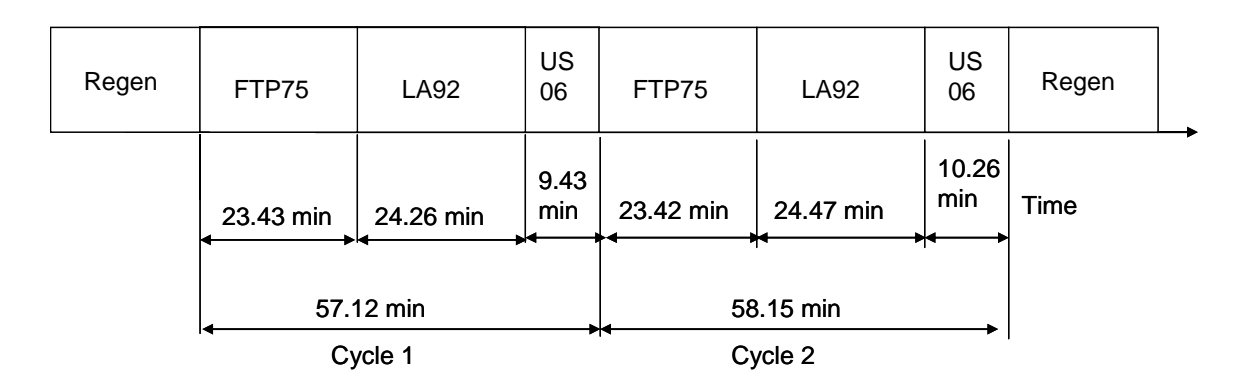


Figure 3.4 Test sequence consisting of various transient test cycles

The filter was first regenerated to ensure that it was free of any soot. This freshly regenerated filter was then weighed, following which cycle 1 consisting of FTP75, LA92

and US06 tests was run. Without regenerating the DPF, the same set of tests consisting of FTP75, LA92 and US06 was run again. This set will be referred to as cycle 2. Cycle 1 represents the tests run on freshly regenerated DPF, which can be considered as clean or free of soot. Cycle 2 represents the same tests performed on a soot loaded condition of the DPF. This sequence gives the opportunity to test the DPF behavior for the same test cycle, for example on FTP75, when the DPF is clean and when it is soot loaded. The particulate filter is weighed at the end of cycle 2 and then regenerated. This sequence of tests is repeated for all the 7 filter cases described in the previous section.

3.3. Data Recording

As mentioned earlier, a state of the art engine and aftertreatment system was used. No sensors other than the ones that are available on a production engine of this series have been used in this study. All the engine sensor data and ECM variables, including the pre and post particulate filter temperature sensor signals, were logged at the sampling rate of 10 Hz. These variables were recorded for the entire duration of the test. Three pressure sensors were mounted near the DPF. Upstream pressure sensor (P1), downstream pressure sensor (P2) and differential pressure sensor (Δ P) signals were logged at the sampling rate of 1500 Hz. This data was also recorded for the entire duration of the test. Two separate logging systems were used to record the data at these two different frequencies.

4. TEMPERATURE SIGNALS – TIME DOMAIN ANALYSIS

4.1. Introduction

Historically, pressure signals have been used as primary diagnostic signals to detect diesel particulate filter failure. But temperature is another available signal that could be used to improve the failure detection ability and could be used in conjunction with pressure monitoring. The usefulness of the temperature signal as a filter failure detection parameter is investigated in this chapter.

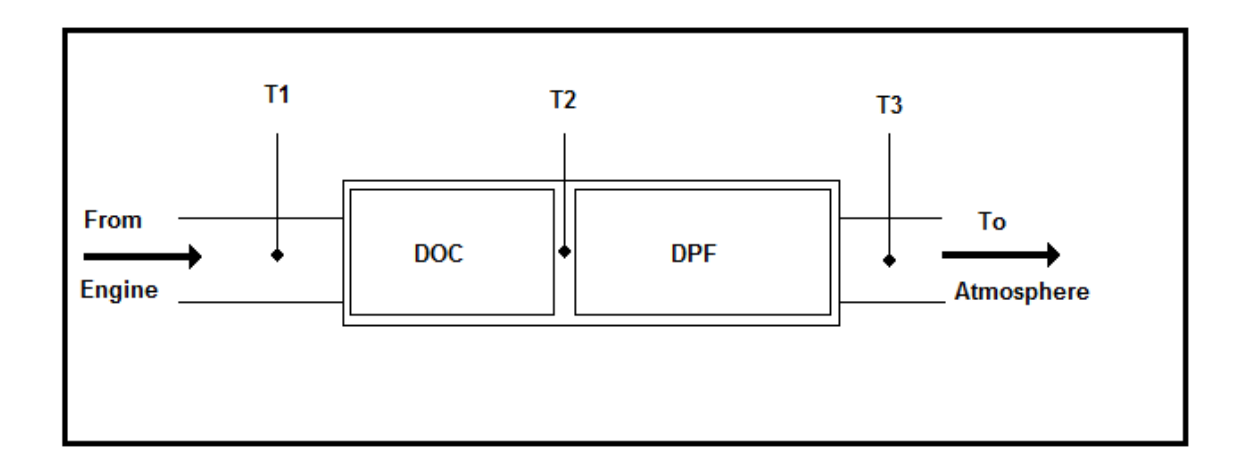


Figure 4.1 Location of temperature sensors

Figure 4.1 shows a part of a diesel engine exhaust aftertreatment system. Specifically, the locations of temperature sensors around the DPF are shown. T1 is the temperature sensor upstream of the Diesel Oxidation Catalyst (DOC). T2 and T3 are the temperature sensors upstream and downstream of the DPF respectively. This nomenclature has been used for this study and will be referred to for the remainder of this document.

4.2. Magnitude Difference

The temperature at the inlet of the DPF is higher as it is closer to the engine than that at the outlet of the DPF, which is comparatively low on account of heat transfer from the hot exhaust gas to the substrate, metal casing, and surroundings.

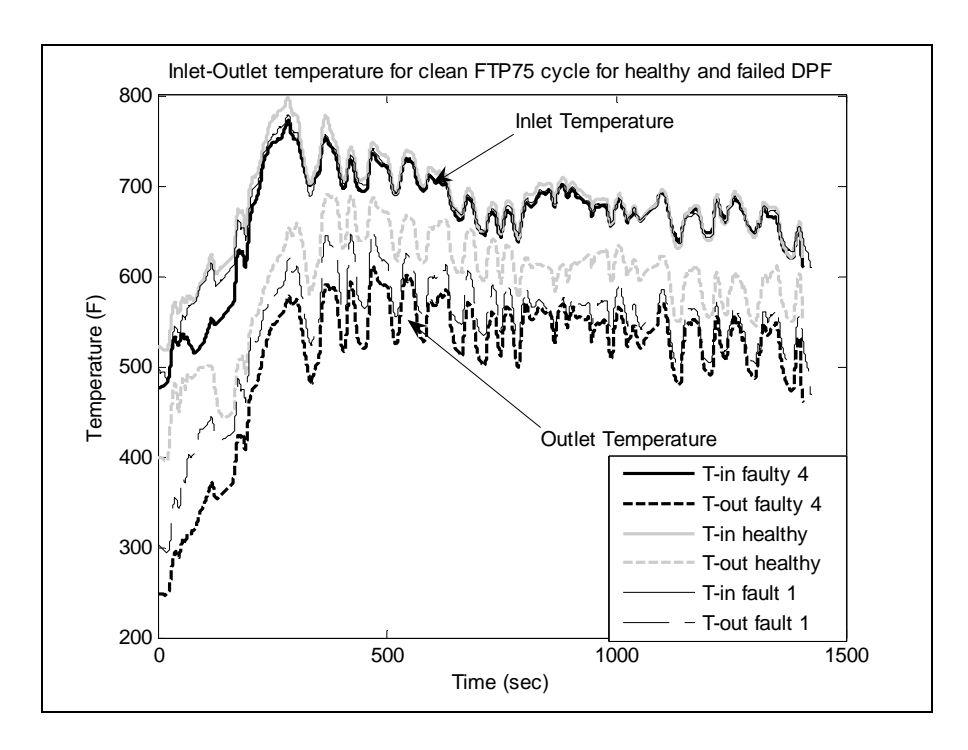


Figure 4.2 Diesel particulate filter inlet-outlet temperatures for healthy, fault 1 and fault 4 type failed filter on FTP75 test cycle run after filter regeneration

Figure 4.2 shows the inlet and outlet temperatures of the diesel particulate filter for healthy, fault 1 and fault 4 type failed filters on FTP75 test cycle run on a clean filter, i.e., after filter regeneration. It can be seen from the figure that the inlet temperatures, represented by solid lines, in all the cases follow the same trend. This does not come as a surprise as it is expected that the pre-DPF temperature will be the same for the engine run through the same speed-load conditions regardless of the filter condition. The dashed lines show the post-DPF temperatures. It is observed that the DPF outlet temperature of the healthy filter is higher than the DPF outlet temperatures of faulty filters. It can also be

seen that the differential temperature between the diesel particulate filter inlet and outlet increases as the filter fails further.

The above explained trend of pre and post filter temperatures is observed even when the initial filter conditions are different. This is shown in Figure 4.3

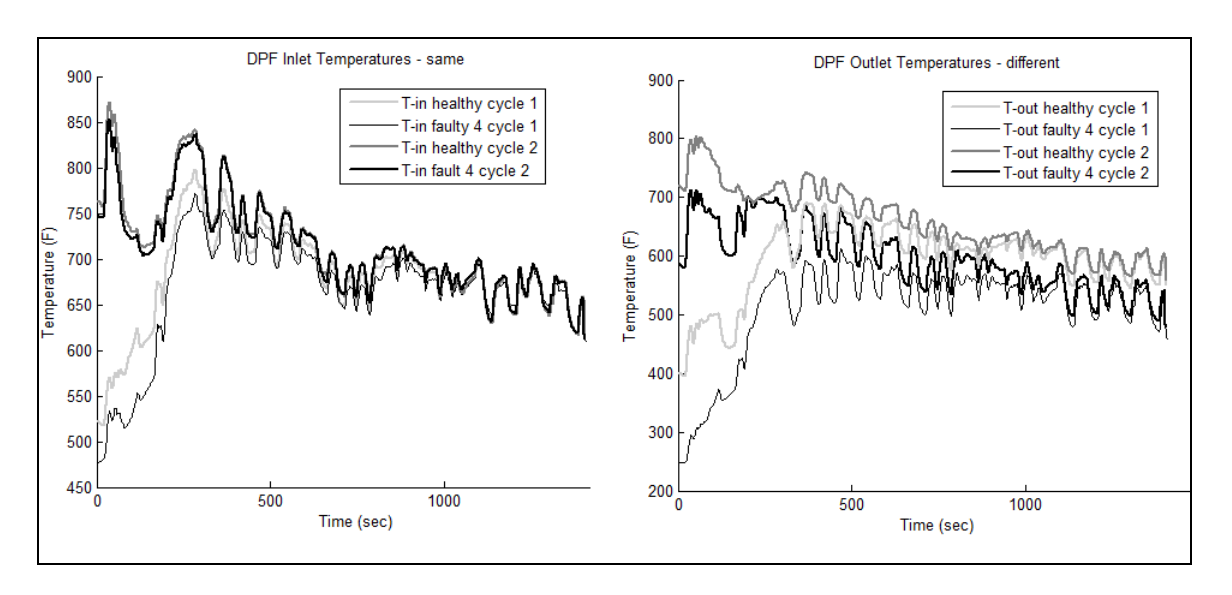


Figure 4.3 Diesel particulate filter inlet-outlet temperatures for healthy and fault 4 type failed filter on FTP75 test cycles for different initial conditions

Cycle 1 was the test cycle run after regeneration and hence the filter was clean. The engine and DPF were cooled after regeneration before starting cycle 1 resulting in lower T-in and T-out temperatures for cycle 1 as seen in Figure 4.3. Cycle 2 was run after cycle 1 without any regeneration. Hence soot loaded DPF is the initial condition for cycle 2. As this was a continuation of cycle 1 without any cool down, T-in and T-out temperatures are higher, as seen in Figure 4.3. It can be seen from the graph of inlet temperatures that, although the starting temperature of T-in is different for different cycles, they converge as time passes and are almost indistinguishable by the end of FTP75 cycle. This reiterates the point that DPF inlet temperature is only dependent on engine test cycle.

The DPF was warmer at the start of cycle 2 and comparatively cooler at the start of cycle 1. This results in higher T-out for cycle 2 than that for cycle 1 for both healthy and fault 4 type failed filter. The temperature trends of cycle 1 and cycle 2 of healthy filter converge by the end of FTP75 test. This is also true for fault 4 type failed filter and its temperature trends for cycle 1 and cycle 2 converge. Hence, although T-out at the start of the test cycle depends on the DPF initial condition, the later part of Tout as the cycle progresses is dependent on the filter's condition. T-out of the failed filter is lower than that for the healthy filter. Thus, the difference in magnitude of T-out can be used to build a filter failure detection algorithm. As T-in is the same in all cases, the differential temperature magnitude between the inlet and outlet of the filter can be used as a property to build a filter failure detection algorithm.

4.3. Cross-correlation Method

In signal processing, covariance is a measure of similarity between two signals, commonly used to find features of an unknown signal by comparing it to a known one. If x(n) and y(n) are two sequences with finite energy, each of length N, then their covariance function is mathematically defined as follows

$$c_{xy}(k) = \frac{1}{N} \sum_{n=1}^{N-k} (x(n) - \bar{x}) \cdot (y(n+k) - \bar{y})$$
 Eq. 4.1

where N = Number of samples of x(n) and y(n), and y(n)

$$\overline{x} = \frac{1}{N} \sum_{n=1}^{N} x(n).$$

The amplitudes of x(n) and y(n) will influence the amplitudes of $c_{xy}(k)$. Thus, it is not accurate to compare the degree of correlation of two different signals by using only their

covariance function amplitudes. To avoid the amplitude influence on the degree of correlation, the covariance function must be normalized. The dimensionless normalized cross-correlation function is given by

$$\rho_{xy}(k) = \frac{c_{xy}(k)}{\sqrt{c_{xx}(0) \cdot c_{yy}(0)}},$$
Eq. 4.2

where $c_{xx}(0)$ and $c_{yy}(0)$ are autocorrelation functions of x and y at lag 0, respectively. ρ_{xy} is used to assess the degree of linear dependence between any two variables x and y on a scale from -1 to +1; ρ_{xy} = -1 simply means that the relationship between x and y is inverse rather than direct.

The cross-correlation between the upstream and downstream temperatures of the DPF has been calculated. It is hoped that this cross-correlation function for the healthy filter condition is different enough from that of the failed filter condition to be able to build a diagnostic algorithm based on it.

4.3.1. Method of Magnitude

When the DPF substrate is in healthy condition (intact substrate), the cross-correlation function will have a rather high value particularly at lower lags, indicating a good correlation between the DPF upstream and downstream temperature signals.

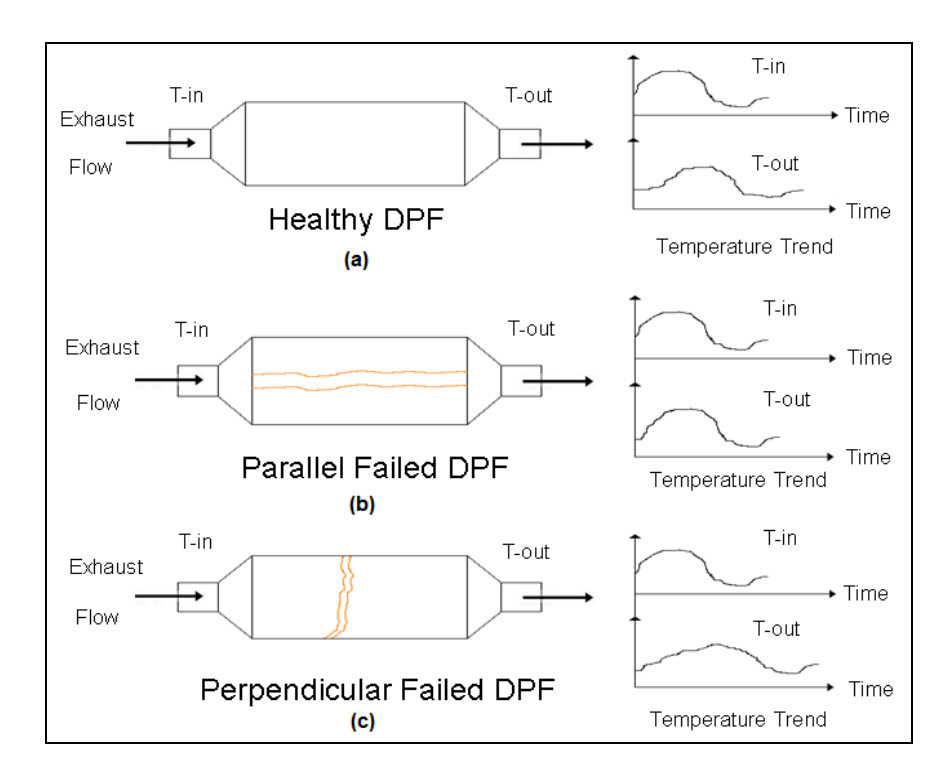


Figure 4.4 DPF inlet and outlet temperature trend depending of type of filter failure

Figure 4.4(a) shows a hypothetical temperature trend in the case of a healthy filter. It can be seen that the DPF downstream temperature follows a similar trend to the DPF upstream temperature. This similarity will give rise to a high value of the cross-correlation function.

Figure 4.4(b) shows a condition where the filter has failed on account of melting of the central channels of the DPF due to high temperatures. This melting is parallel to the exhaust flow, shown in the figure, resulting in a through hole in the DPF. This will cause the temperature at the inlet of the DPF to transmit to the outlet without much distortion, represented in the above figure, which will result in a still higher correlation compared to the healthy filter case.

Figure 4.4(c) shows a filter failure case where the filter has cracked in the direction perpendicular to the direction of exhaust flow. This kind of filter failure causes the substrate to eventually break into two parts. The DPF inlet temperature trend will be

much more distorted in this case before reaching the DPF outlet. This is shown in the last figure. This distortion will result in a lower magnitude of the cross-correlation function. By monitoring the magnitude of the cross-correlation function of the inlet and outlet DPF temperature signals, it may be possible to detect the filter condition.

A correlogram is a summary statistic for a time series that tells us the correlation coefficients at lags k (k=1,...,N, N=length of time series). Figure 4.5 shows a correlogram for 500 lag values for data recorded on the FTP75, LA92 and US06 test cycles for the clean (regenerated) filter condition. It can be seen that the magnitude of the cross-correlation is low for the healthy filter case and it increases as the fault intensity increases, for small lag values. This nature of the cross-correlation function was observed since the type of artificial filter failure used for this study was cracking the DPF substrate through the central channels, as shown in case (b) of Figure 4.4.

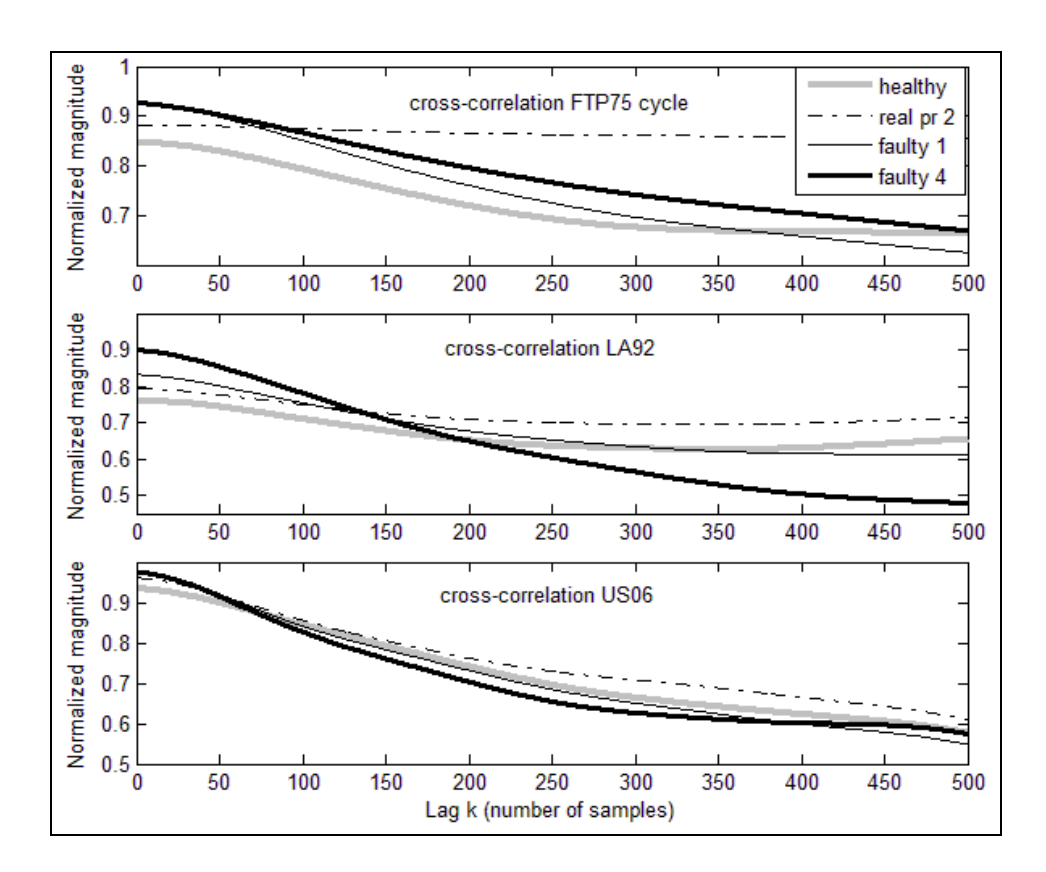


Figure 4.5 Cross-correlation of upstream and downstream temperature signals for healthy and failed filter cases for FTP75, LA92 and US06 tests of cycle 1

It is observed from Figure 4.5 that the magnitude of cross-correlation is not the same for all three test cycles for any given filter condition and seems to depend on the particular transient cycle. If a common value for the magnitude of the cross-correlation function for a healthy filter can be determined, then a filter failure detection algorithm can be developed using that common value as threshold. From Figure 4.5, it is observed that the magnitude of the cross-correlation function for a healthy filter is the highest for the US06 cycle. The speed and load were highest for this cycle as well. Therefore, normalizing the cross-correlation function with average values of speed, torque and volumetric flow rate for a given test cycle was tried. The results are as shown in Figure 4.6.

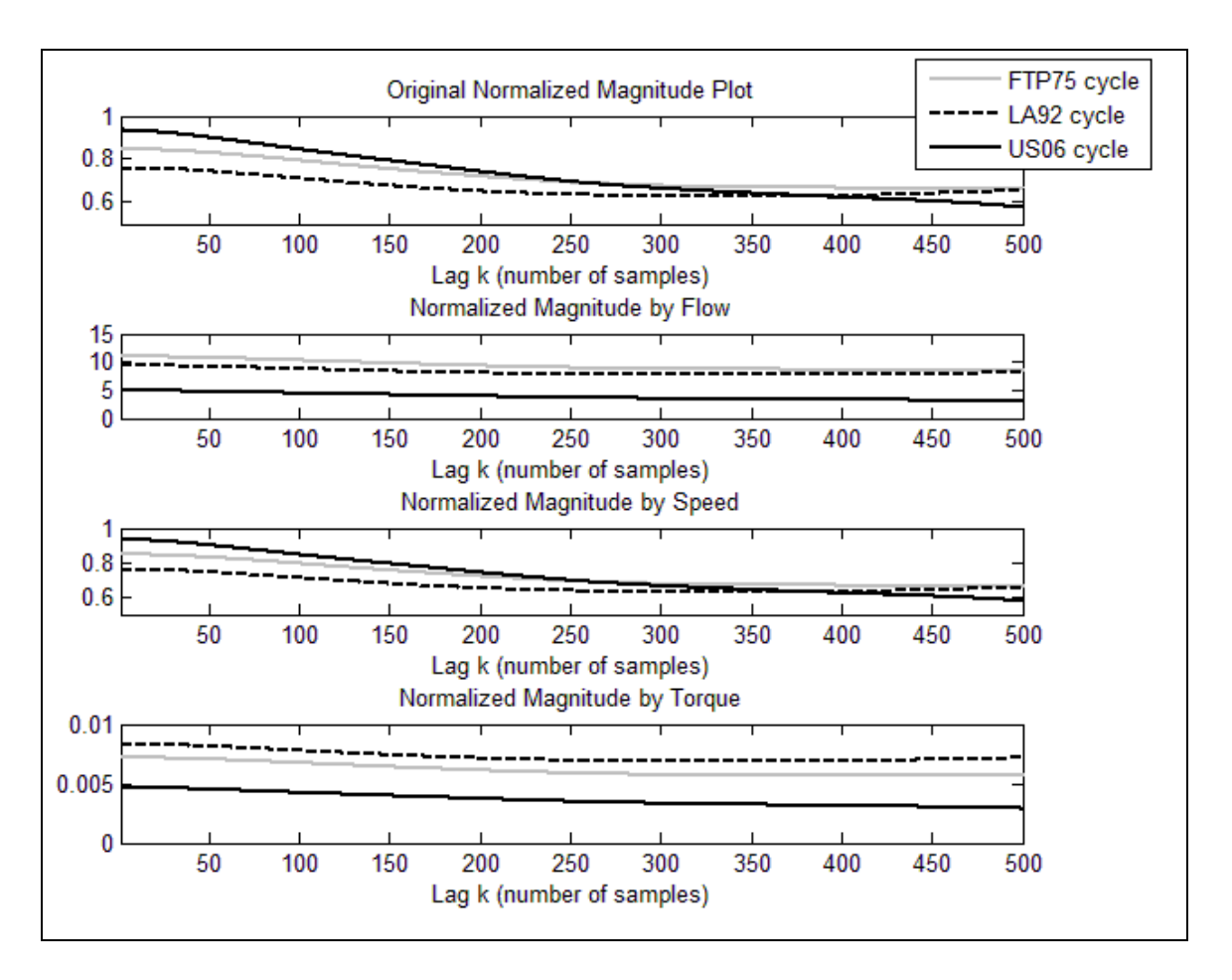


Figure 4.6 Attempt to achieve common magnitude for cross-correlation function for FTP75, LA92 and US06 tests of cycle 1 on healthy filter by normalizing by various parameters

The first subplot from Figure 4.6 is the original cross-correlation function for FTP75, LA92 and US06 transient tests of cycle 1 on a healthy filter. The subsequent subplots show the cross-correlation functions after normalizing by parameters such as average transient cycle volumetric flow rate, average transient cycle speed and average transient cycle torque. It is observed that normalizing by any of these parameters does not yield a common value of magnitude in the cross-correlation function for the three transient cycles under consideration.

However, from Figure 4.5, it is observed that the trend followed by the cross-correlation function is the same for all the transient test cycles for all the filter cases. Hence, if data on a healthy regenerated filter for a given test cycle is available, it may be possible to use its magnitude for lower lag values as a threshold for detecting another filter's condition tested on the same test cycle.

4.3.2. Time Delay Detection

It is observed that as the temperature wave passes through the DPF, the DPF outlet temperature signal is attenuated and it appears to be a time shifted version of the DPF inlet temperature. Hence, the DPF seems to dampen and delay the temperature signal as it passes through it. This tendency for time delay can be used for DPF diagnostics.

If the diesel particulate filter fails or cracks in a fashion shown in Figure 4.4(b), producing a through hole which is parallel to the direction of the exhaust flow, then the time delay between the temperatures upstream and downstream decreases, i.e., the temperature signal will take less time to transmit from the DPF inlet to the DPF outlet through a failed DPF than through a healthy filter. This situation is explained in Figure 4.7. Consider a hypothetical temperature signal. The temperature signal will experience a higher time delay while passing through a healthy filter and a lower time delay passing through a failed filter.

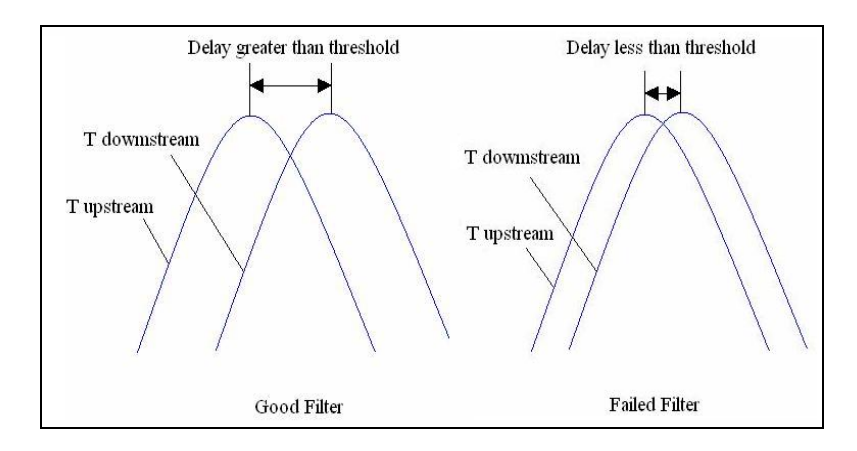


Figure 4.7 Hypothetical temperature signals before and after DPF for healthy and failed filter conditions

By setting a threshold on this delay, it is possible to recognize the failed filter condition. The cross-correlation technique is used to find the relative delay between the upstream and downstream temperature signals.

Equation 4.2 is used to find the cross-correlation between the pre and post DPF temperature signals at various lag values. The lag k, where the maximum magnitude of cross-correlation function is achieved, is noted as the delay count. This is the time delay in the units of the sampling time that the output temperature signal appears after the input temperature signal. For example, if the largest cross-correlation magnitude appears at lag value k=73, for a sampling rate of 10 Hz, it corresponds to 7.3 seconds time delay. This implies that the output temperature signal correlates best with the input temperature signal starting at the 73rd sample, or at 7.3 seconds. In other words, the temperature signal appears at the DPF output 7.3 seconds after it is recorded at the DPF input.

The signal conditioning is done as follows:

To find the correlation between the temperature signals, we are interested in the overall trend of the signals and not the local fluctuations taking place. Thus the higher frequency components are not of much interest here. Hence the temperature signals are filtered

through a zero-phase-lag low-pass filter. A 70 Hz zero-phase-lag low-pass filter is used for the purpose of this study, but it may vary and is a parameter that can be calibrated.

The DPF pre and post temperatures are continuously recorded when the engine is in operation. The length of signal to be used for the purpose of analysis is also a parameter that can be calibrated. If the DPF is in the cooled condition when the engine starts, a steep temperature rise is observed and it remains more or less continuously fluctuating around some mean value if higher regeneration temperature is not reached. This trend is observed in FTP75 test cycle data as it is the first engine cycle. This steep temperature rise is ignored and data is windowed from 10000th sample up to the end of the signal.

Figures 4.8 (a) and 4.9 (a) show the actual raw temperature data recorded for healthy and fault 4 type failed filter. Figures 4.8 (b) and 4.9 (b) show the corresponding zero mean (i.e., subtracting the mean value from raw data to signal), zero-phase-lag low-pass filtered and windowed temperature signals.

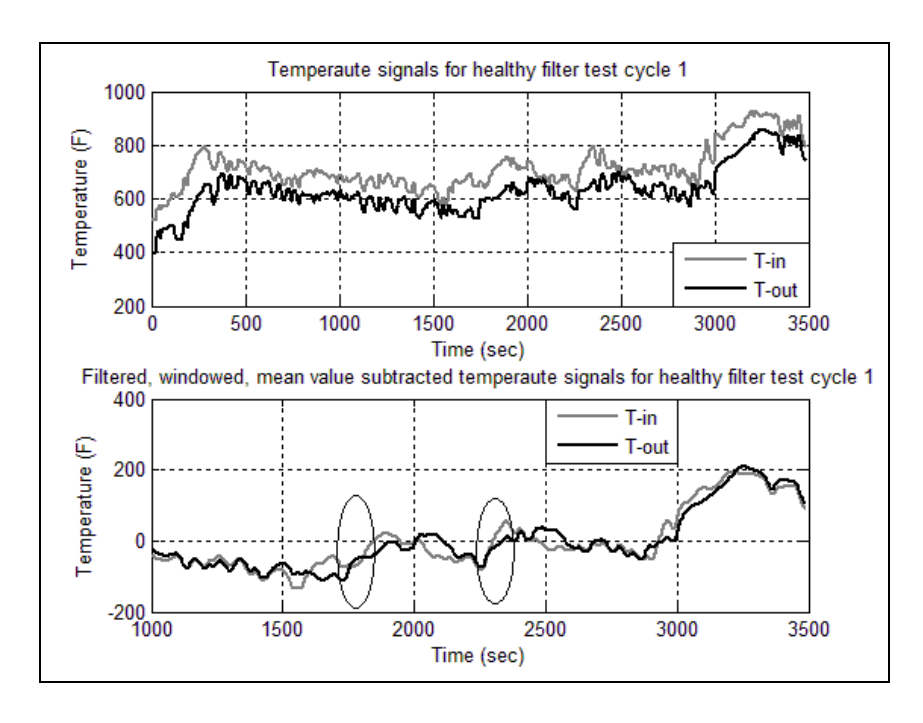


Figure 4.8 (a) Raw pre and post DPF temperature signals for healthy filter test cycle 1 (b) Filtered, windowed and mean value subtracted temperature signals for healthy filter test cycle 1

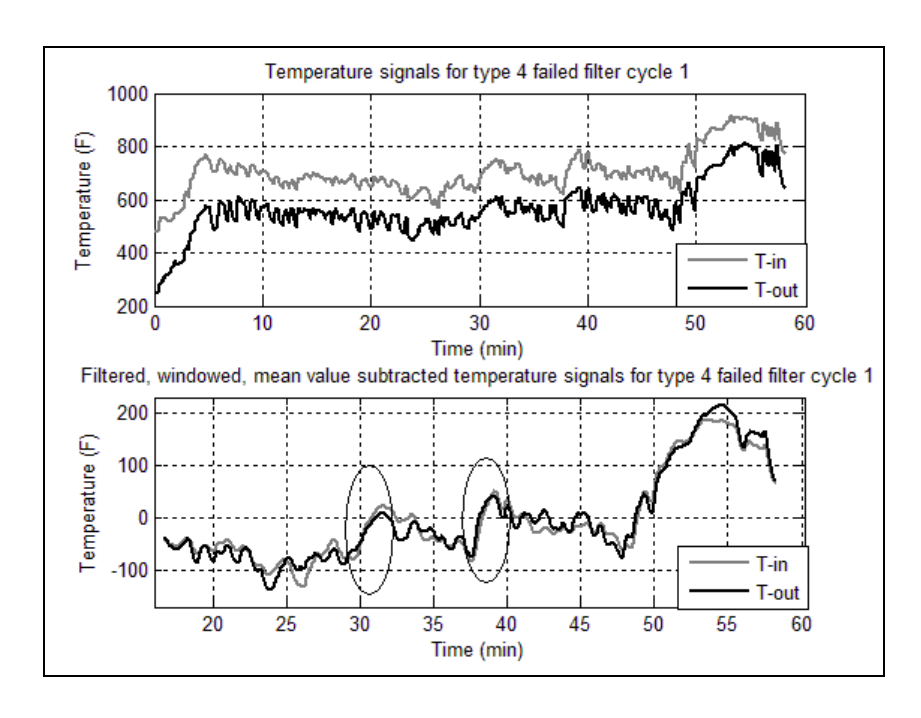


Figure 4.9 (a) Raw pre and post DPF temperature signals for type 4 failed filter test cycle

1 (b) Filtered, windowed and mean value subtracted temperature signals for type 4
failed filter test cycle 1

The time lag (shift in signals) can be noticed for a steep temperature rise (marked by an ellipse in these figures). The time lag seems to be more for the good filter and almost zero for the failed filter.

The above procedure, which includes signal conditioning of temperature data, windowing, filtering and subtracting the mean value from raw data, and then calculating the maximum magnitude of cross-correlation function, is applied to various filter types for cycle 1 and 2 temperature data. The results obtained are summarized in Table 4.1.

Table 4.1 Summary of delay count between pre and post-DPF temperature signals for various filter cases tested

Filter Type	Cycle number	Delay Count
Healthy filter	1	73
	2	109
Real pr1	1	26
	2	27
Real pr2	1	25
	2	34
Type 1 failed filter	1	0
	2	0
Type 2 failed filter	1	0
	2	0
Type 3 failed filter	1	0
	2	0
Type 4 failed filter	1	0
	2	0

For good filter and real world failed parts, the results are reasonable. The highest delays are observed for the good filter, delay decreases for the less failed filter and lowest delay is observed for the severely failed real world failed filter. Also the delay for cycle 2 data is more than the delay for cycle 1 data, which is expected since cycle 2 represents soot loaded condition and cycle 1 represents a clean filter. When a through hole is present (artificially failed filters), the delay count goes to 0.

Although this method can differentiate between healthy and failed filter conditions, it cannot give the true estimate of the extent of filter failure. This is because the attenuation and shift in the inlet temperature as observed at the outlet is not uniform. Many other factors are also involved. The exhaust flow rate will determine the amount of delay and it cannot be considered a constant during transient engine operation. The effect of

conductive heat transfer from the filter substrate to the metal casing and heat radiation to the surroundings also play a role and may not be uniform throughout the length of the filter. Events such as partial regeneration or localized temperature variation will also affect the temperature trend. The DPF may treat different frequency components of the temperature signals differently.

The various methods of finding differences between temperature trends of healthy and failed filters could be used to build a filter failure detection algorithm. This can be a stand-alone technique or can be used along with a technique based on pressure signals. The pressure signal analysis for filter diagnosis is the subject of the next chapter.

5. PRESSURE SIGNALS – FREQUENCY DOMAIN ANALYSIS

5.1. Introduction

Empirical correlations between dynamic pressure signal features are studied in this chapter for diesel particulate filter fault diagnostic purposes. Relationship between upstream and downstream pressure signals across the DPF is studied. Specifically, the energy content of each signal at different frequencies is correlated with the health of the filter

Dynamic pressure signal features and their correlations with particulate load in the diesel particulate filter have been presented [36]. These dynamic pressure features clearly show pulsations at the engine's firing frequency [36]. This work has been done in steady state, meaning at constant engine speed and load condition. These correlations demonstrate the potential use of the dynamic pressure signals for DPF monitoring and control.

The work described here is focused on transient engine operation and the emphasis of this research is more on DPF failure diagnostics than on measuring soot load. Dynamic pressure signals are measured at 1500 Hz upstream, downstream and across the DPF throughout the duration of the test. The test cycles 1 and 2 consist of FTP75, LA92 and US06 cycles each as described in Chapter 3.

5.2. Approach

Frequency domain analysis of upstream and downstream pressure signals is performed. These pressure signals are correlated to understand the characteristics of the diesel particulate filter transfer function. Once the method to correlate the pressure signals is fixed, the characteristics of the transfer function of the DPF can be determined.

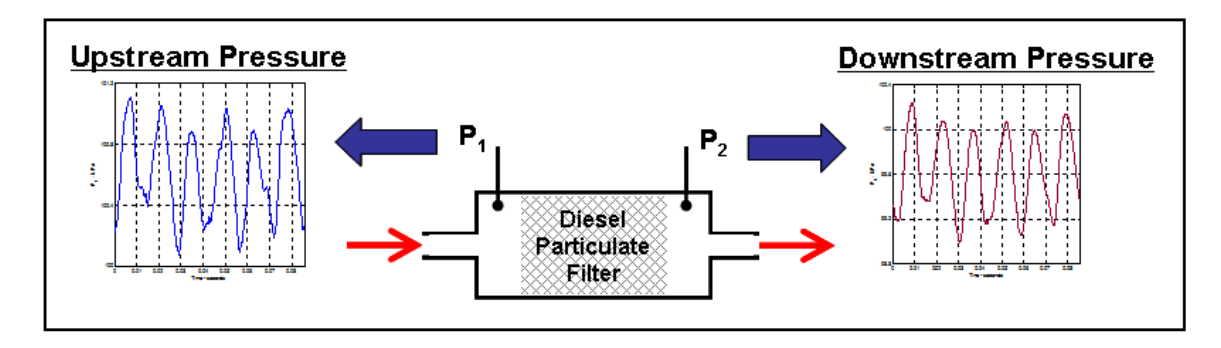


Figure 5.1 Correlating pressure signals to determine DPF transfer function characteristics

By comparing the characteristics of the transfer function of a given filter with that of a healthy filter, it is possible to comment on the health of the particulate filter under consideration.

Consider that the block H in Figure 5.2 is the transfer function of the diesel particulate filter. X represents the pressure signal upstream of the DPF and Y is the pressure signal downstream of the DPF. N_y is the noise added to this pressure signal. It could be some other signal addition, but we are not interested in it at this point, and hence, it is treated simply as noise. Y_m is the actual measured post-DPF pressure signal.

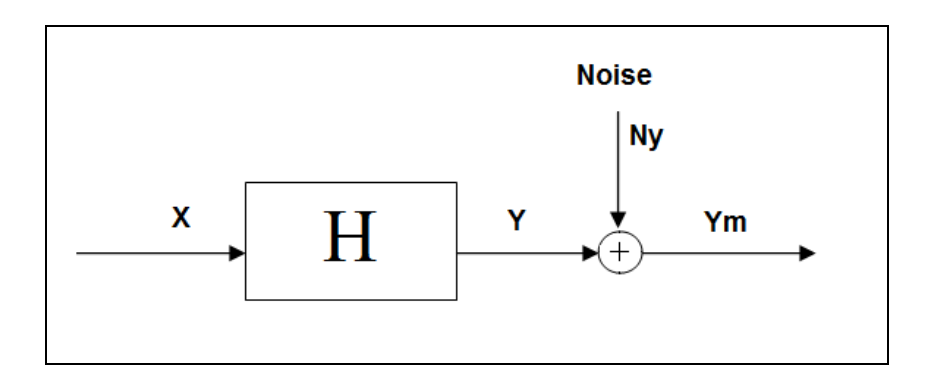


Figure 5.2 Finding transfer function characteristics

Let S_{XX} , S_{YmYm} and S_{NyNy} be the energy spectral density of X, Y_m and N_y respectively. They are related by the following equation:

$$S_{Y_{NYM}} = |H|^2 \cdot S_{XX} + S_{NyNy}$$
 Eq. 5.1

Dividing by S_{xx} gives

$$\frac{S_{YmYm}}{S_{YX}} = |H|^2 + \frac{S_{NyNy}}{S_{YY}}$$
 Eq. 5.2

If the noise term is assumed to be negligible, then the energy content of the noise can be approximated to 0. In that case, the ratio of spectral energy density of post DPF pressure to pre DPF pressure is equal to the absolute magnitude squared of H.

$$\frac{S_{YmYm}}{S_{xx}} = |H|^2$$
 Eq. 5.3

It is hoped that the values for $|H|^2$ for healthy and failed filters are different. Hence, it is possible to base a filter diagnostic algorithm on calculating $|H|^2$ of a given filter by comparing it to that of a healthy filter.

5.3. Method of Analysis

The flow diagram in Figure 5.3 explains the method used for calculating the magnitude squared characteristics of the transfer function.

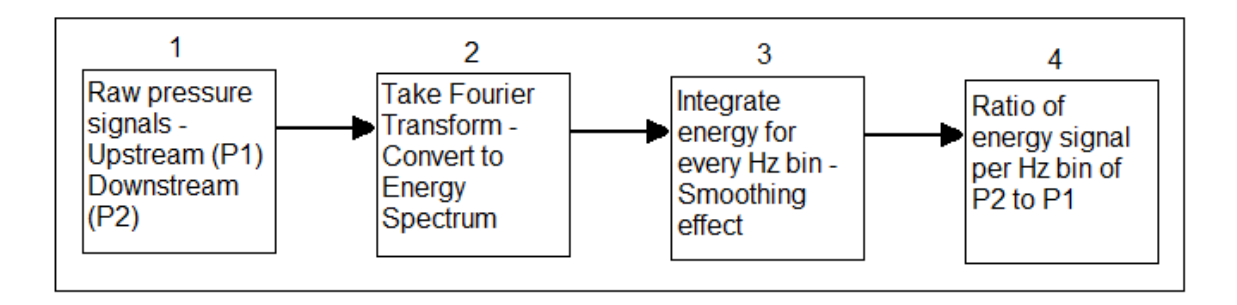


Figure 5.3 Flow diagram for finding characteristics of DPF transfer function

The number on the top of each block in the flow diagram shows the step number in the procedure for calculating the DPF transfer function. Each step of the flow diagram is described in the following sections.

5.3.1. Transient engine operation and raw pressure signals

The engine is run in transient mode in most real world applications. Hence, it is most important to build a diagnostic test for DPF fault detection not only for steady-state operation but also for transient engine operation. Transient engine tests consist of constantly changing speed and load conditions. This was achieved by running the engine through FTP75, LA92 and US06 test cycles.

Figure 5.4 shows a speed map for the FTP75 cycle. It can be seen that speed is constantly changing for the entire duration of the test. Hence, this is a truly transient engine operation.

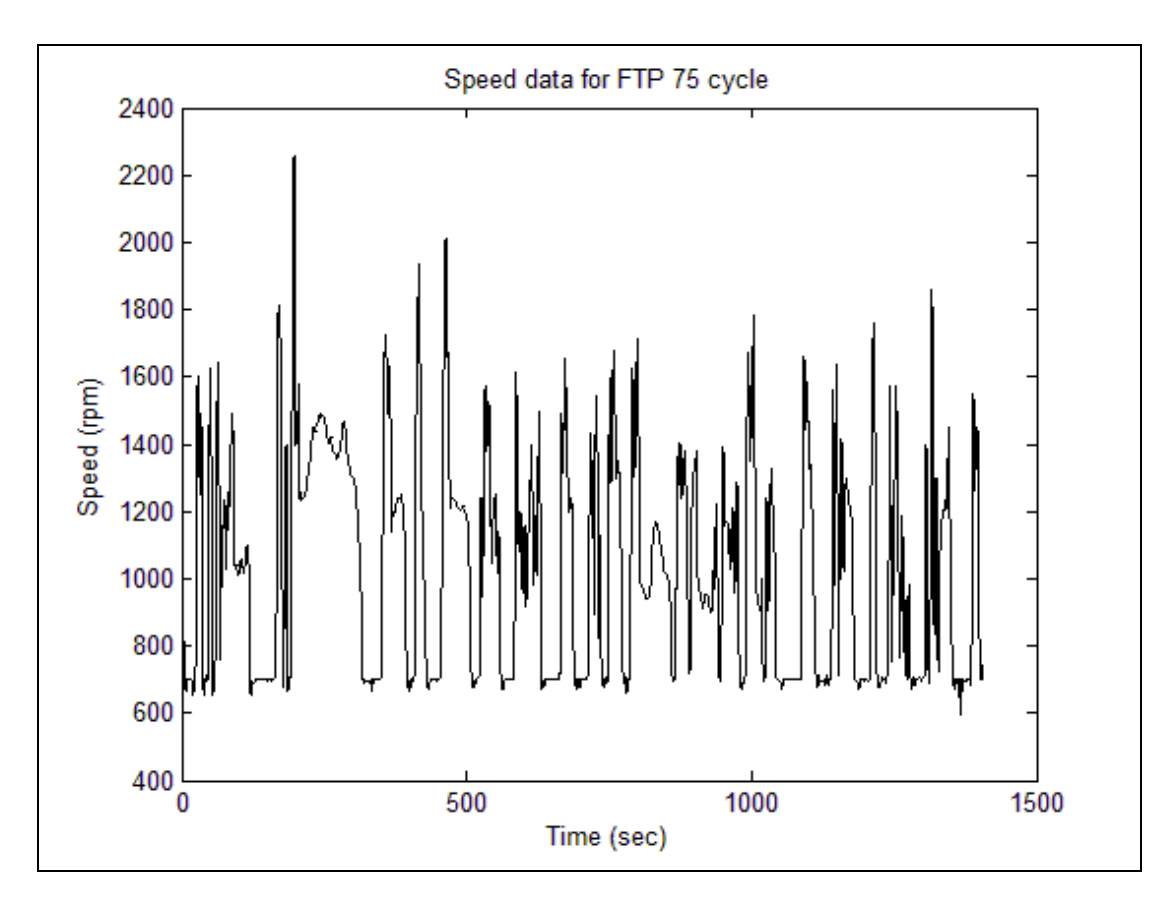


Figure 5.4 Speed map for FTP75 test cycle

Figure 5.5 shows upstream pressure data for FTP75 test cycle collected on a healthy filter. It can be seen that the pressure signal has a similar trend as the engine speed data and it is clear that the pressure signal trend depends heavily on the speed signatures. But real exhaust pressure signals are pulsating dynamic signals [36]. These pulsations can be seen in the magnified image. A portion of the raw pressure signal marked with an ellipse has been magnified for clarity. The magnified portion shows only 0.5 second of data.

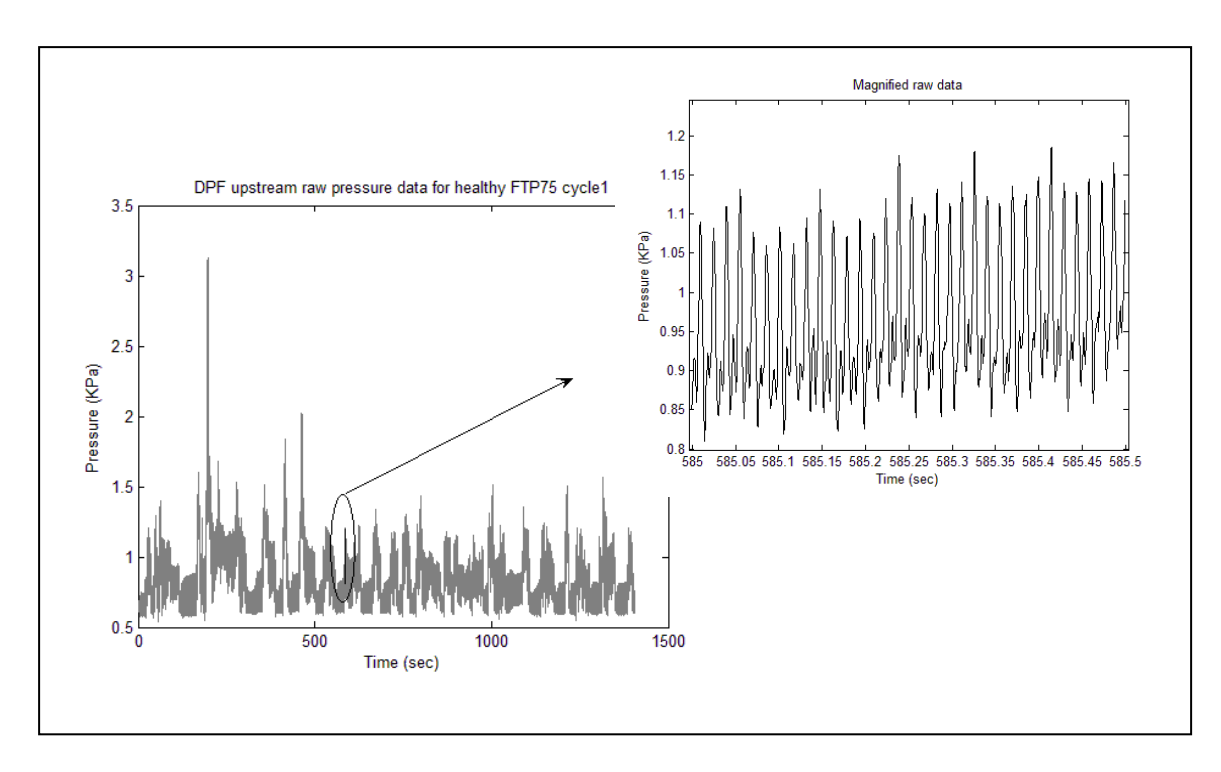


Figure 5.5 Raw upstream pressure data for FTP75 test cycle 1 on healthy filter and its magnified image for 0.5 seconds

Raw pressure data is non-stationary in nature due to transient engine operation. The firing frequency component embedded in the pressure signal changes with engine speed. The pressure signal follows the trend of speed and, if the speed is not constant, it gives rise to a time-varying pressure signal. Also, as the particulate filter gets soot loaded, the back pressure increases and hence, the magnitude of this upstream pressure signal keeps increasing until the filter is regenerated to make it free of soot.

Frequency domain analysis of this non-stationary pressure signal is studied in this work. Specifically, the energy content of the upstream pressure (P1) and downstream pressure (P2) signals are related to come up with a filter failure detection algorithm. This is a frequency domain analysis. The energy content of each signal is calculated from its Fourier coefficients. The details for calculating Fourier coefficients are described in the next section.

5.3.2. Fourier Transform and Energy Spectrum

Fourier transform representations basically involve the decomposition of the time domain signals in terms of sinusoidal (or complex exponential) components. The Fourier transform of a continuous time signal x(t) is given by

$$X(f) = \int_{-\infty}^{\infty} x(t) \cdot \exp(-j2\pi ft) \cdot dt$$
 Eq. 5.4

The Fourier transform of an aperiodic signal of length T is given by

$$X(f) = \int_{0}^{T} x(t) \cdot \exp(-j2\pi ft) \cdot dt$$
 Eq. 5.5

where the integration is done over the length of the signal instead of infinite length. In order to process the sampled signal, the Fourier transform in equation 5.2 is approximated by the discrete Fourier Transform (DFT) as,

$$X(k) = \Delta \cdot \sum_{n=0}^{n=N-1} x(n\Delta) \cdot \exp\left(-j\frac{2\pi kn}{N}\right)$$
Eq. 5.6

where Δ is the sample time, N is the number of samples of signal considered for analysis, f_s is the sampling frequency, n is the time step index and k denotes the frequency component. Since the DFT is symmetric in the frequency domain, only half of the frequency components are of real interest and need be calculated only up to N/2 instead of N-1. Fast Fourier Transform (FFT), is used as a means of calculating DFT. Figure 5.6 shows the absolute FFT components calculated for upstream pressure data of FTP75 test from cycle 1 on a healthy filter. FFT coefficients for frequencies in the range

of 30 Hz to 150 Hz are considered for all the data analysis. This is because most of the firing frequency components lie in this range for the engine speeds of the transient cycles considered for the purpose of this study for a 6-cylinder, 4-stroke diesel engine. Maximum peak at 35 Hz corresponds to 700 rpm which is the idle speed of the engine and it can be seen from the speed map for the FTP cycle in Figure 5.4 that it is dominant.

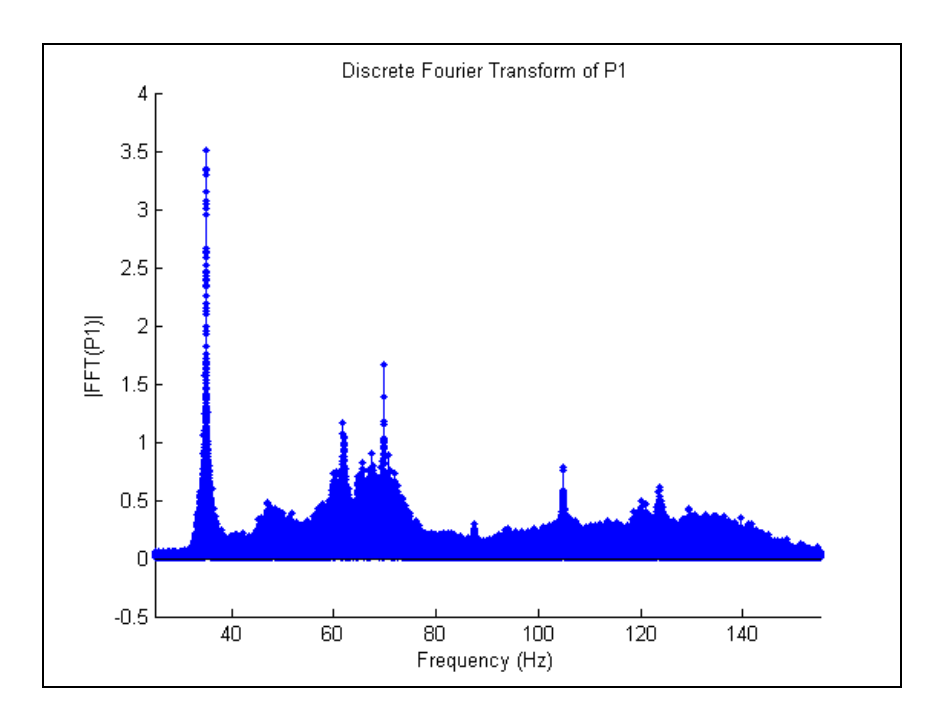


Figure 5.6 Absolute Discrete Fourier Transform of upstream pressure signal for FTP75 cycle 1

The energy spectral density of any signal x(n) is the square of the absolute value of its FFT coefficients, as shown in Equation 5.7.

Energy Spectral Density =
$$|FFT(x)|^2 = S_{XX}$$
 Eq. 5.7

Figure 5.7 shows the energy spectral density of the upstream pressure signal for FTP75 cycle 1 for the frequency range from 30 Hz to 150 Hz. Note that the higher energy

components can more prominently be seen in this plot than in the magnitude plot of FFTs in Figure 5.6.

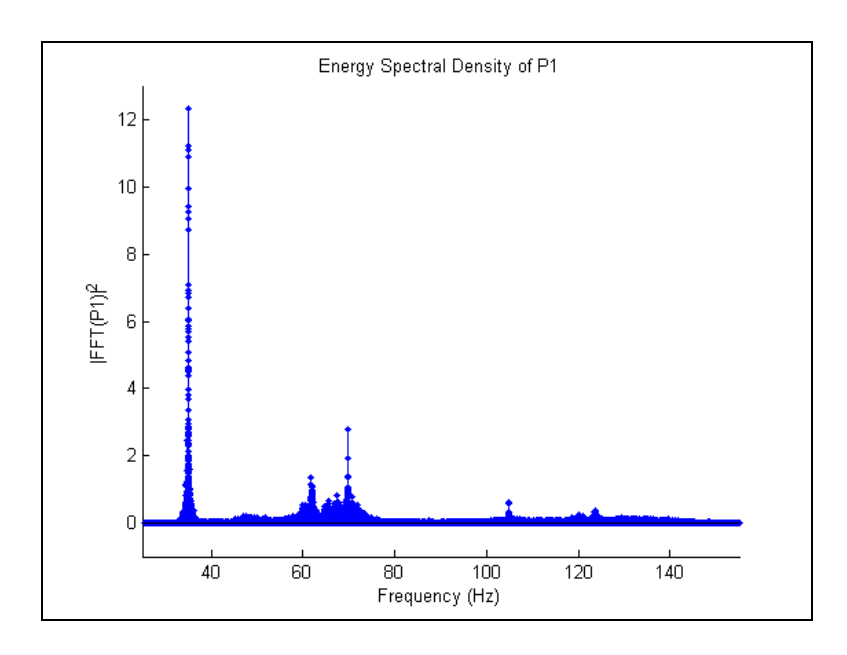


Figure 5.7 Energy spectral density of upstream pressure signal for FTP75 cycle 1

5.3.3. Integrating energy per hertz bin

The energy signal is summed for each hertz bin. For example, all the energy components between 30 Hz and 31 Hz are summed up and assigned to 30 Hz. Those components between 31 Hz and 32 Hz are summed and assigned to 31 Hz. Each hertz bin is as shown in Figure 5.8. This gives a smoothing effect. It also implies that small fluctuations occurring during 1 Hz intervals are not accounted for and hence can be treated as noise.

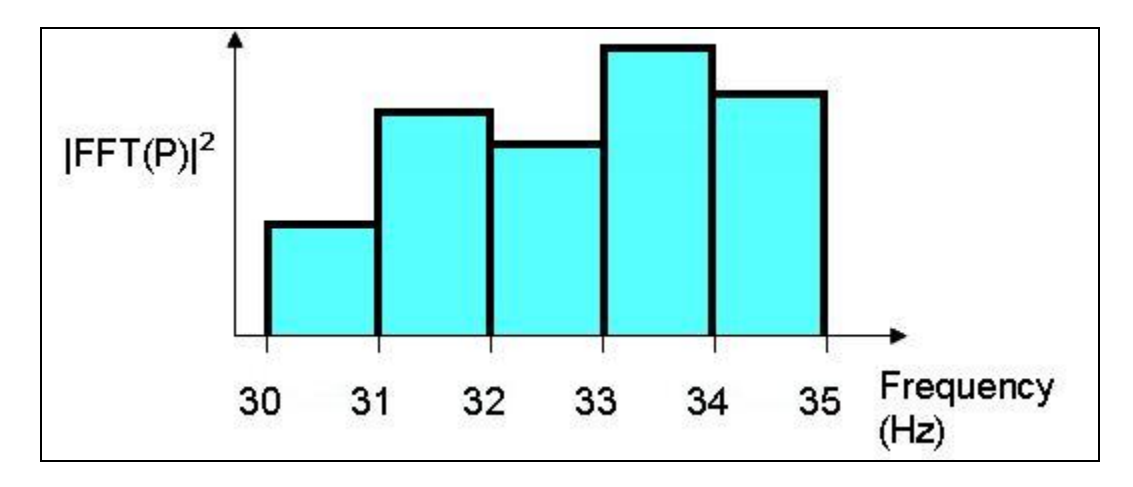


Figure 5.8 Energy per hertz bin

Figure 5.9 shows the integrated energy signals over 1 Hz for the upstream and downstream pressure signals. It is observed that the energy content of the downstream pressure signal, indicated by the dotted line in the plot, is lower than the energy content of the upstream pressure signal.

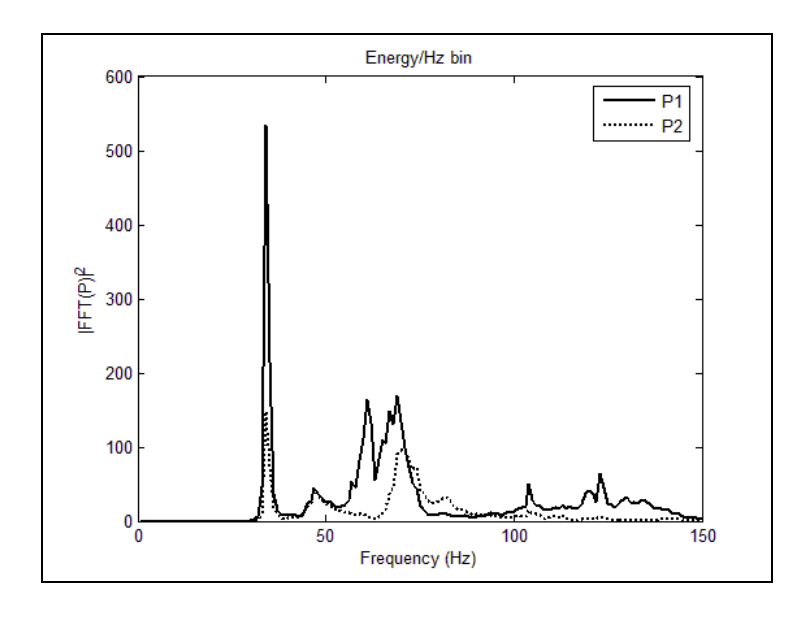


Figure 5.9 Energy per hertz bin of upstream and downstream pressure signals

5.3.4. Ratio of Energy Signals

Ratio of energy signals per hertz bin of P2 to P1 is taken. It is represented by Equation 5.8.

Ratio of energy/Hz bin =
$$\int_{f_{1}}^{f_{2}} |FFT(P_{2})|^{2} \cdot df$$

$$\int_{f_{1}}^{f_{2}} |FFT(P_{1})|^{2} \cdot df$$
Eq. 5.8

This ratio for FTP75 test from cycle 1 for healthy filter case is shown in Figure 5.10. This ratio describes the magnitude squared characteristic of the diesel particulate filter transfer function relating downstream pressure to upstream pressure. Note that taking the ratio of energy signals eliminates the effect of delay.

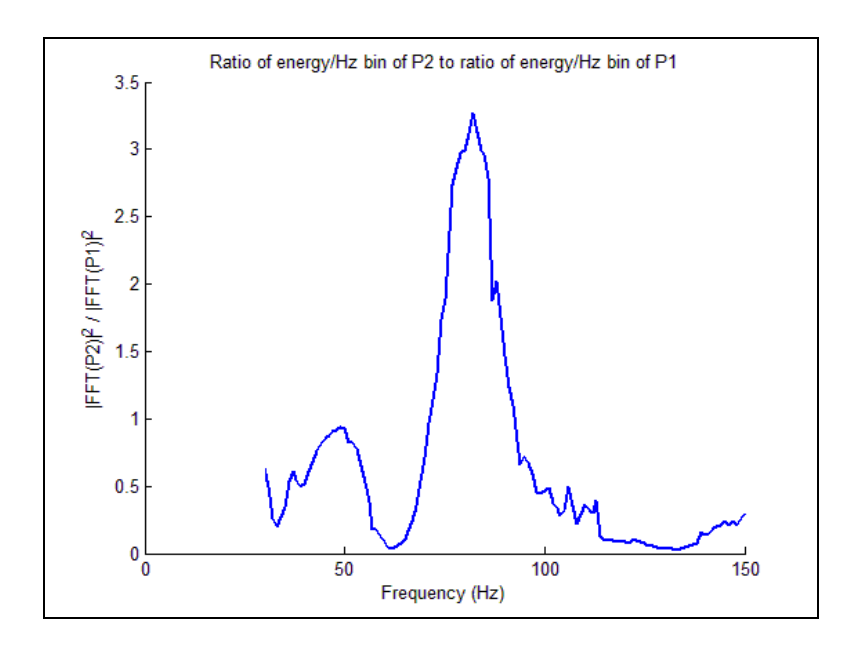


Figure 5.10 Ratio of energy/Hz bin of P2 to ratio of energy/Hz bin of P1 for FTP75 test from cycle 1 for healthy filter case

As mentioned in section 5.2, the above plot describes $|H|^2$ for the healthy filter case for FTP75 test from cycle 1. Characteristic ratios for failed filter cases are calculated and their plots are compared to that of the healthy filter case in the following sections.

5.4. Frequency Range Selection

To compare the plots of $|H|^2$ for healthy and failed filter cases, a frequency range needs to be defined within which the comparison can be made. The frequency range selected in this study is 30 Hz to 150 Hz. As mentioned earlier, the energy content of the upstream and downstream pressure signals is concentrated at the firing frequency, which depends heavily on the engine speed. For a 6-cylinder, 4-stroke engine, the relation is as given by equation 5.9 below,

$$F = \frac{S \cdot 6}{60 \cdot 2}$$
 Eq. 5.9

where F is the firing frequency in Hertz and S is the engine speed in rpm. From Figure 5.4, the engine speed map for FTP75 cycle, speed varies from 700 rpm to 3000 rpm, which would correspond to 35 to 150 Hz firing frequency range.

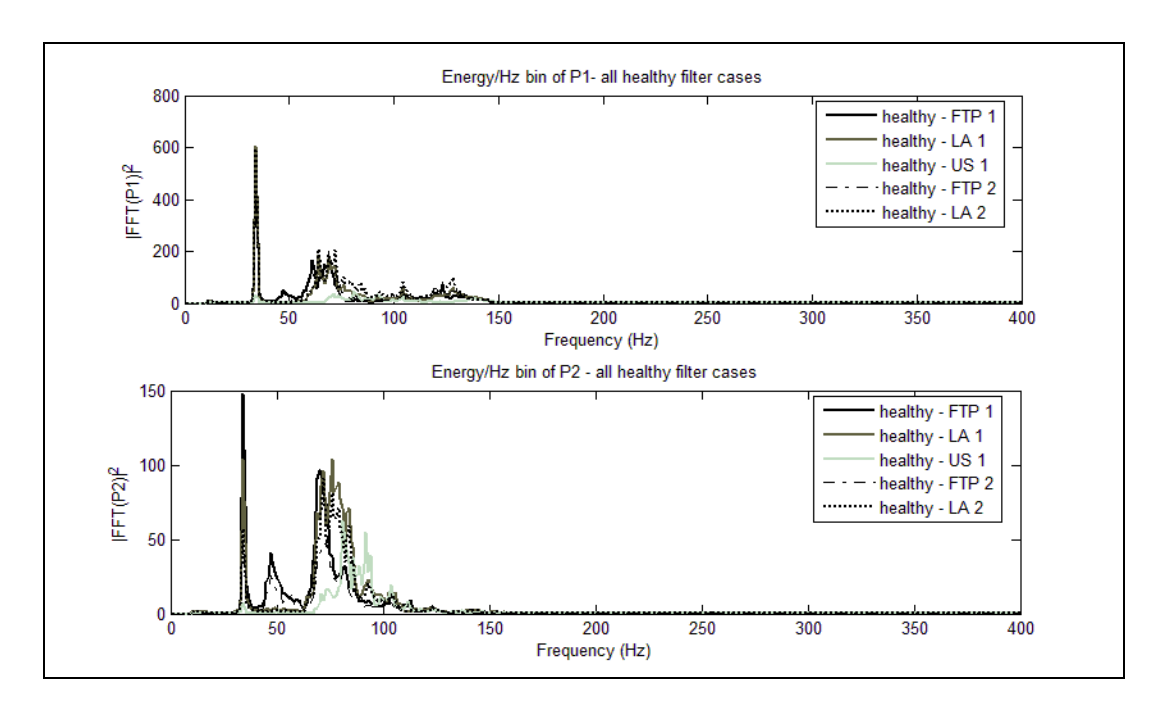


Figure 5.11 Frequency range detection - Energy/Hz bin of upstream and downstream pressure signal for 5 transient cycles on healthy filter

Figure 5.11 shows the energy / Hz bin of the upstream and downstream pressure signals for a healthy filter for the first 5 transient cycles consisting of cycle 1 - FTP75, LA92, US 06 and cycle 2 – FTP75, LA92 plotted from 10 Hz to 400 Hz. The speed maps for LA92 and US06 cycles are given in the Appendix and it can be seen that the speed for these cycles also varies in the range of 700 rpm to 3000 rpm. It can be observed from Figure 5.11 that most of the energy of the upstream and downstream pressure signals is concentrated in the 30 Hz to 150 Hz frequency range. Hence, comparing the $|H|^2$ in this range would be most valuable and hence is tested only in this range. It is important to note here that $|H|^2$ will not be zero for the rest of the frequencies although the energy content of P1 and P2 is almost zero. $|H|^2$ will show some nonzero values for the remaining frequencies as it will be a ratio of two small numbers there, but it will not give any useful information. Hence the 30 Hz to 150 Hz frequency range is selected for all the comparisons shown in the following section.

5.5. Detecting Filter Condition

The $|H|^2$ is compared for various filter conditions in the 30 Hz to 150 Hz frequency range for various transient cycles. Figure 5.12 shows a comparison of transfer function characteristics for healthy filter, real world failure and two failed filter cases.

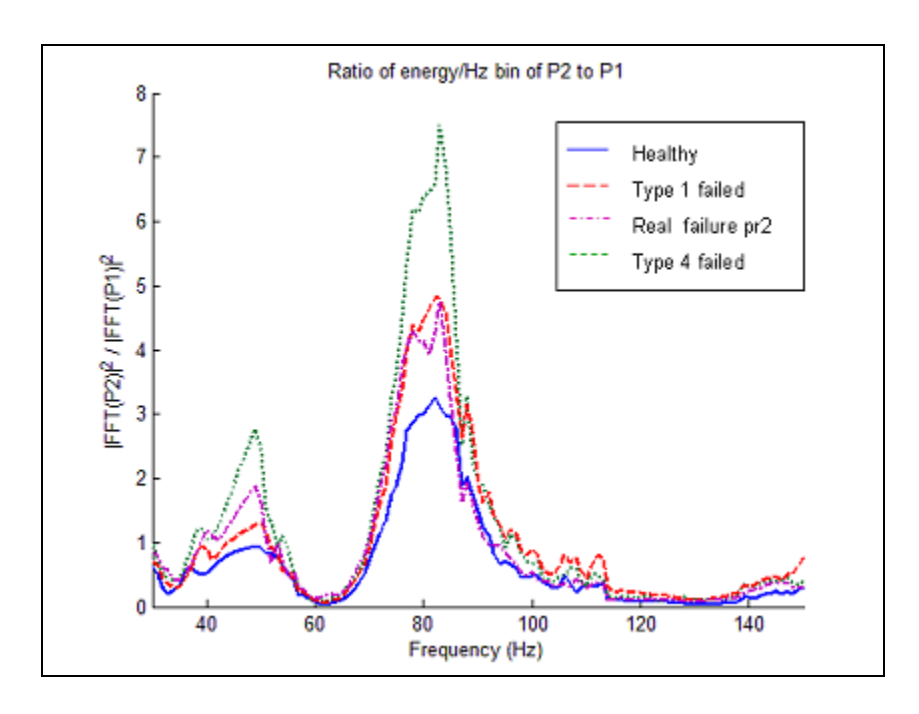


Figure 5.12 Transfer function characteristics comparison for FTP75 cycle 1

A clear difference is visible between the healthy and failed filter cases. It is observed that the peak in $|H|^2$ increases as the intensity of the filter failure increases. The reason for this trend lies in the energy content of individual P1 and P2 pressure signals. Figure 5.13 shows the energy content of upstream and downstream pressure signals for healthy and type 4 failed filter cases for FTP75 cycle 1.

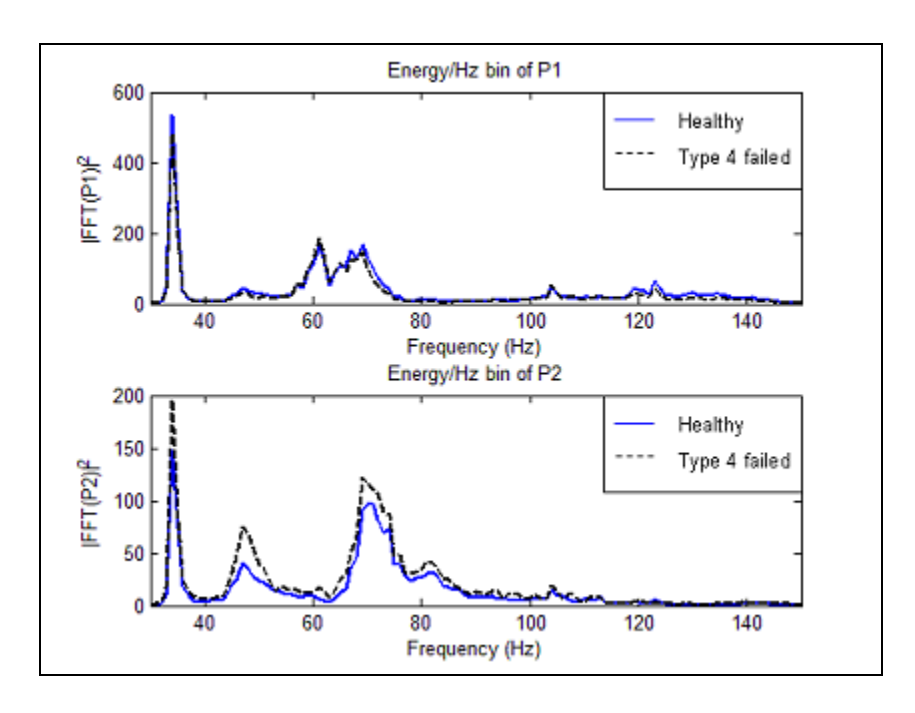


Figure 5.13 Energy content – upstream and downstream pressure signals for the FTP75 cycle 1

The energy content of P1 is almost the same for healthy and type 4 failed filter cases for FTP75 cycle 1. The energy content of downstream pressure signal for these cases varies. It is higher for type 4 failed filter case than the healthy filter case. Only two filter cases are shown here for clarity.

Figures 5.14 and 5.15 show $|H|^2$ characteristics and P1 and P2 energy content for LA92 and US06 cycles for run 1, respectively. These plots also follow the same trend as that for FTP75 transient cycle. Here also a clear distinction between healthy and failed filter cases is visible in the magnitude squared transfer function characteristics.

The energy ratio plots showing the magnitude square of the transfer function characteristics for all the transient cycles for all the filter cases tested is shown in Appendix A.

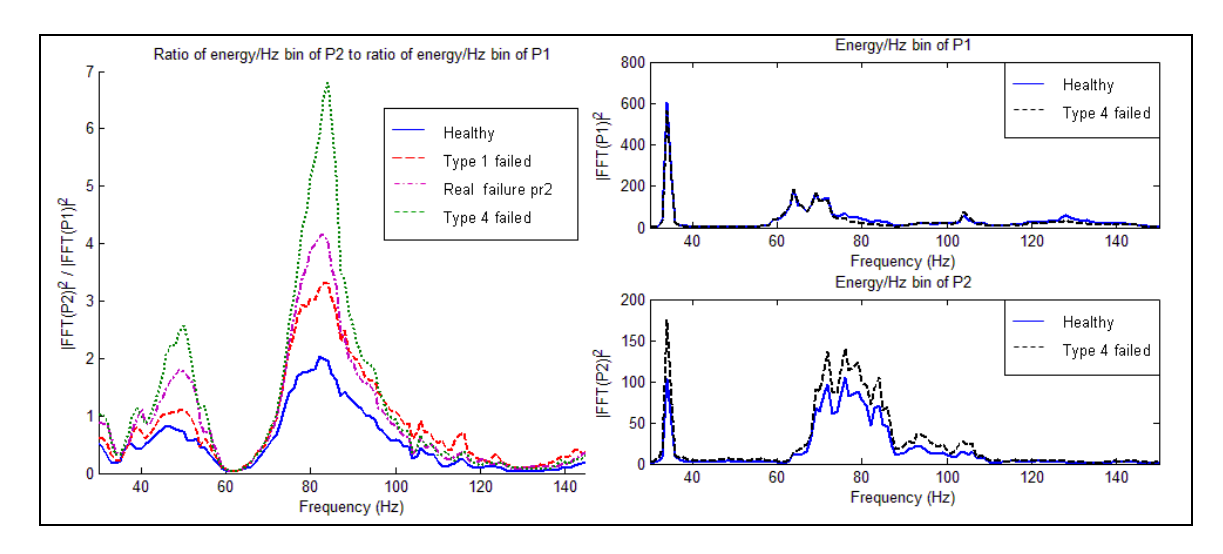


Figure 5.14 Transfer function characteristics comparison for LA92 cycle 1 and Energy content of upstream and downstream pressure signals

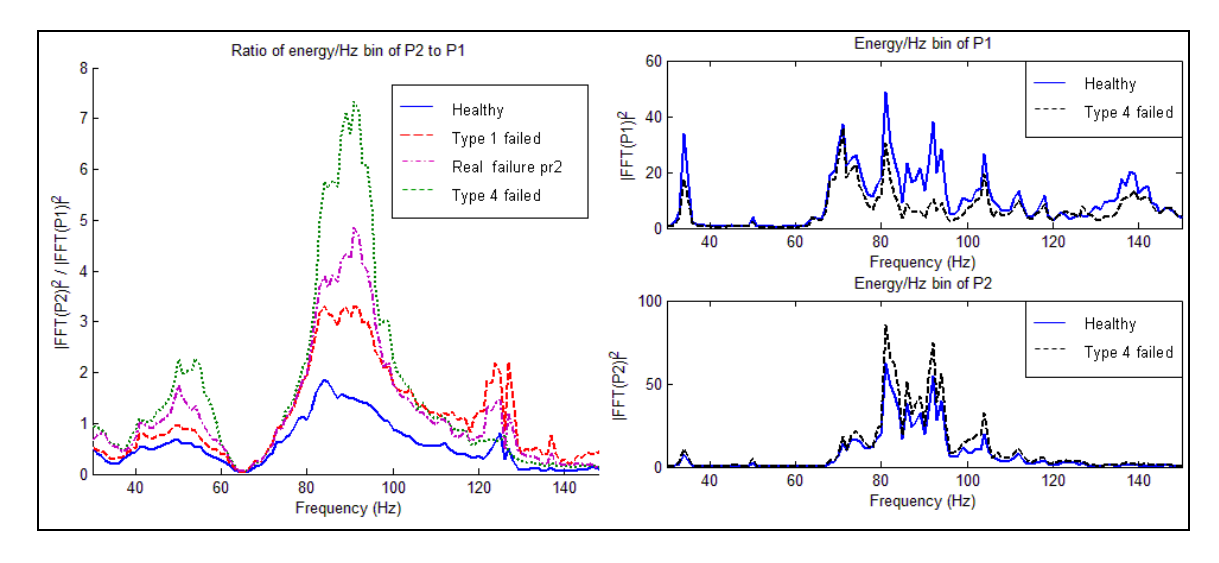


Figure 5.15 Transfer function characteristics comparison for US06 cycle 1 and Energy content of upstream and downstream pressure signals

An algorithm to detect filter failure can be built using the differences between magnitude square of transfer function characteristics for healthy and failed filters as explained above. The filter failure detection algorithm is developed in the next chapter.

6. DPF FAILURE DETECTION ALGORITHM

The technique described in the previous chapter of correlating the energy content of upstream and downstream pressure signals at different frequencies to the health of the diesel particulate filter is used to develop a filter failure diagnostic algorithm. This chapter explains the algorithm. Before describing the actual algorithm, it would be worthwhile to discuss the filter transfer function characteristics with regard to the DPF's operation. This is discussed next.

It is concluded from the previous chapter that the peak of the ratio of energy / Hz bin of P2 to energy / Hz bin of P1, for any transient test cycle, continues to increase as the intensity of filter failure increases (refer to Figures 5.12, 5.14 and 5.15). Such characteristic plots of filter transfer function magnitude squared, represented as ratios of energy / Hz bin of P2 to energy / Hz bin of P1, will be referred to as 'energy ratio plots' for the purpose of this study. The frequency range considered for this analysis is 30 Hz to 150 Hz because P1 and P2 have their highest energy content in this range of frequencies, as is explained earlier in section 5.4. Some energy is lost when the pressure pulses travel through the filter substrate of the DPF from inlet to outlet. It is argued that this energy loss is a function of filter condition, meaning that more energy is lost in a healthy filter substrate than in a cracked filter substrate. This is true since the healthy filter substrate provides more restriction to the pressure pulses than the cracked filter substrate. The lower energy loss in the case of a failed filter is the reason for higher energy content in the downstream pressure signal in failed filters than healthy filters (refer to Figures 5.13, 5.14 and 5.15).

As the filter gets soot loaded, it accumulates more particulate matter, leading to increased restriction. As the filter restriction continues to increase, the pressure signal energy loss increases as well. This will cause the peak in energy ratio plot to decrease as the filter accumulates soot. This trend for the healthy filter's magnitude squared transfer function characteristics is as shown in Figure 6.1. The sequence of transient test cycles is shown again for reference.

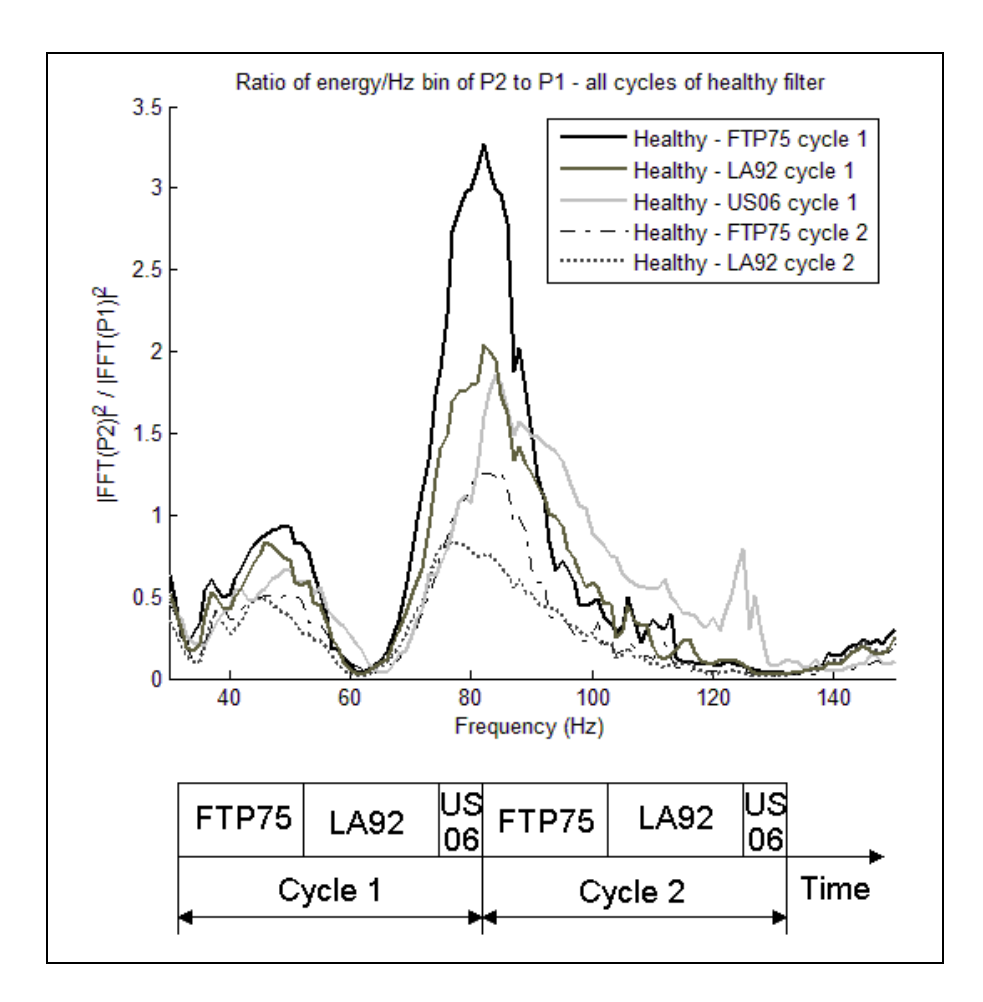


Figure 6.1 Soot load trend of energy ratio plot for healthy filter on all the transient trest cycles

From the soot load trend of energy ratio plots, it is observed that, along with reduction in the peak, the area under the energy ratio curve also seems to decrease. This fact is used later for the analysis.

6.1. Approach

Any algorithm developed for filter failure detection should be independent of test cycle. The discussion so far was based on transient test cycles and the whole test cycle data was analyzed and presented up to this point. The approach taken here to analyze the data independent of particular test cycle considers 5-minute data samples at a time. Since all 6 transient tests consisting of cycles 1 and 2 of 3 transient tests each were run continuously without removing the DPF or regenerating it intentionally, the data from all the test cycles together can be considered as 1 engine run. This data is divided into intervals of 5 minute duration and the peak in the energy ratio plot and the area under the curve of energy ratio plot are calculated for each interval. A five-point average scheme around the peak is employed. Five-point average is used for robustness so as to minimize sensitivity of the algorithm to outliers. Figure 6.2 shows the peak of energy ratio plots for each 5-minute duration intervals. It can be seen from this graph that the trend for five-point average around the peak shows less fluctuations than the single point peak.

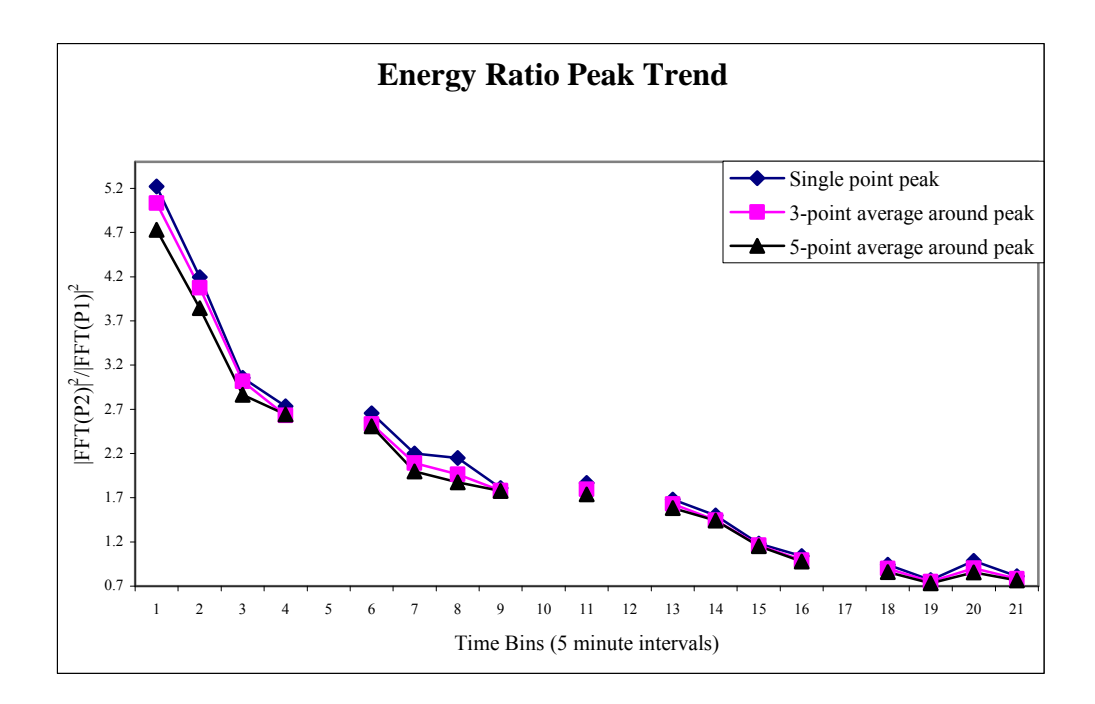


Figure 6.2 Energy ratio peak trend for healthy filter

The transient tests were run continuously, in the order shown in Figure 6.1, but the data for each test was recorded separately. Hence to calculate the energy ratio peak for 5-minute intervals, each test cycle data had to be considered separately. The FTP75 test is of 23.4 minutes, hence the first 20 minutes could be easily divided into four 5-minute intervals. The remaining 3.4 minutes worth of data from the FTP75 test and the initial 1.6 minutes of data from the LA92 cycle were not included in the analysis. This corresponds to one 5-minute interval. The remaining part of the LA92 cycle was divided into 5-minute intervals and again the 5 minutes worth of data comprising of its last part and the starting portion of the US06 cycle was not analyzed. This procedure was repeated for all the cycles. As 5 minutes worth of data was not considered for analysis purposes between two individual tests, the trend in Figure 6.2 is not continuous and gaps corresponding to the ending of a test cycle and starting of another test cycle are observed.

Figure 6.3 shows the energy ratio peak trend of 5-point average around the peak for healthy and failed filter conditions. A logarithmic trend line is fitted to the data obtained for all the filter conditions.

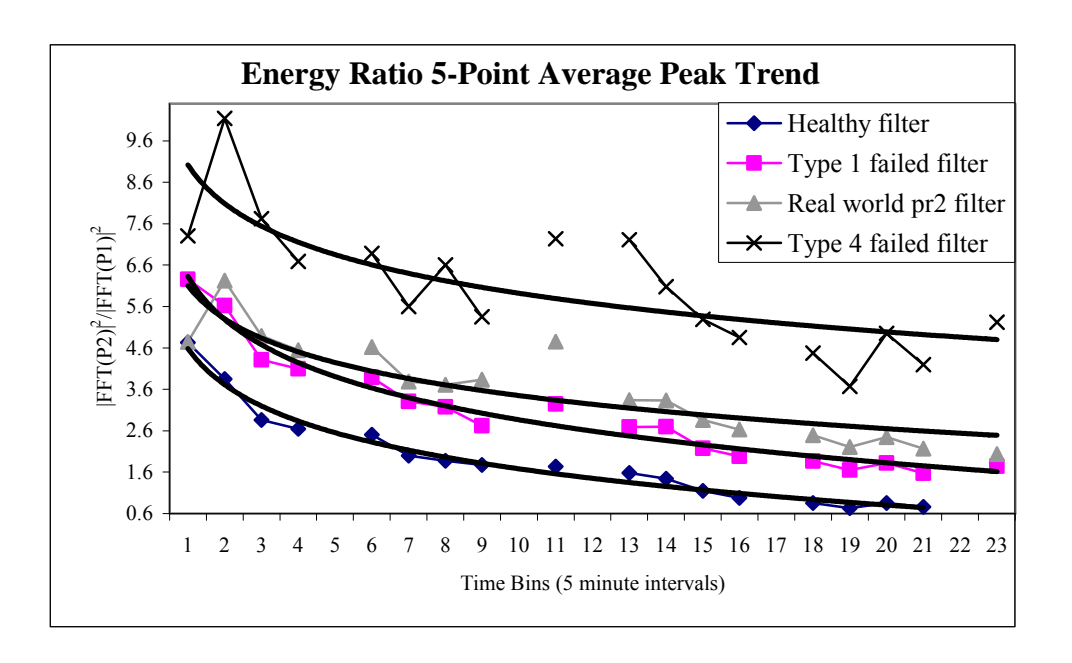


Figure 6.3 Energy ratio peak trend of 5-point average for healthy and failed filter conditions

It is observed that for the healthy filter case, the trend for energy ratio of 5-point average peak follows the logarithmic trend very well. Energy ratio point is not obtained for US06 transient test in cycle 2 for healthy filter as data for this test was unavailable. Since the data for healthy filter seems to follow a smooth decaying curve, it may be concluded that this effect is because of soot loading and that it does not depend on the transient test cycle run. If this assumption is correct, then a method to test filter condition independent of specific transient test cycle can be developed.

The equation for the logarithmic function fitted to the data obtained on each of the filter cases tested is shown in Table 6.1.

Table 6.1 Logarithmic function fitted to the 5-point average peak trend data of energy ratio plot for various filter cases tested

Filter Type	Equation for logarithmic trend line for energy ratio 5-point average peak trend
Healthy filter	$y = -1.2614\ln(x) + 4.5844$
Type 1 failed filter	$y = -1.503\ln(x) + 6.3272$
Real world pr2	$y = -1.1513\ln(x) + 6.1004$
Type 4 failed filter	$y = -1.345\ln(x) + 9.0177$

It is observed from Figure 6.3 that as the filter failure intensity increases, the 5-point average peak of the energy ratio plot lies above that of the healthy filter case for all time periods. This is depicted as higher intercept for failed filter cases in the equation of logarithmic trend line in Table 6.1 than the healthy filter case. In addition to this, the energy ratio 5-point average peak fluctuations around the logarithmic trend line are observed to increase with filter failure.

As mentioned earlier, the area under the energy ratio plots can also be used for analysis. Figure 6.4 shows the area under the curve for energy ratio plots for 5 minute time

intervals for healthy and failed filter conditions. A logarithmic trend line is fitted to the data obtained for all the filter conditions. The equation for the logarithmic trend line fitted to the data is shown in Table 6.2.

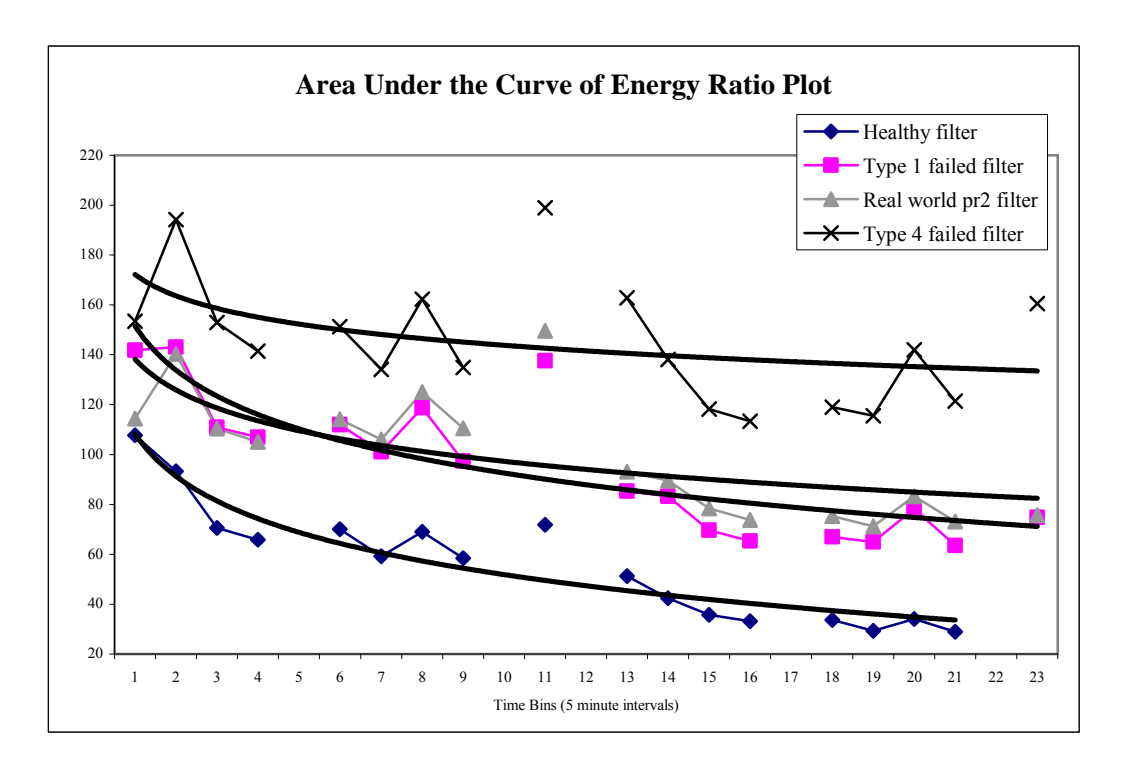


Figure 6.4 Energy ratio areas under the curve trend for healthy and failed filter conditions

Table 6.2 Logarithmic function fitted to the area under the curve trend data of energy ratio plot for various filter cases tested

Filter Type	Equation for logarithmic trend line for area under the curve of energy ratio plot
Healthy filter	$y = -24.51\ln(x) + 108.31$
Type 1 failed filter	$y = -25.646\ln(x) + 151.64$
Real world pr2	$y = -17.789 \ln(x) + 138.25$
Type 4 failed filter	$y = -12.327 \ln(x) + 172.2$

It is observed from Figure 6.4 that as the filter failure intensity increases, the area under the curve of the energy ratio area plot lies above that of the healthy filter case for all time periods which is represented by increasing intercept value of the logarithmic function equation in Table 6.2. But the data does not seem to follow a logarithmic trend exactly. The out-of-trend points at time intervals 11 and 23 are above the average trend followed by the rest of the points. These points correspond to the area under the energy ratio plot for US06 tests for cycles 1 and 2, respectively. Thus, this parameter of area under the curve seems to depend on transient test cycle run. This data may need a speed correction in order for it to follow a smoothly decaying trend. For this reason, the 5-point average parameter is used to develop the failed filter diagnostic algorithm.

6.2. Algorithm

The magnitude for the energy ratio peak of the 5-point average for a healthy filter is less than that for the failed filter case, as can be seen from Figure 6.3. A constant threshold value can be determined and filter state can be found based on which region the 5-point average peak falls in. This is illustrated in Figure 6.5.

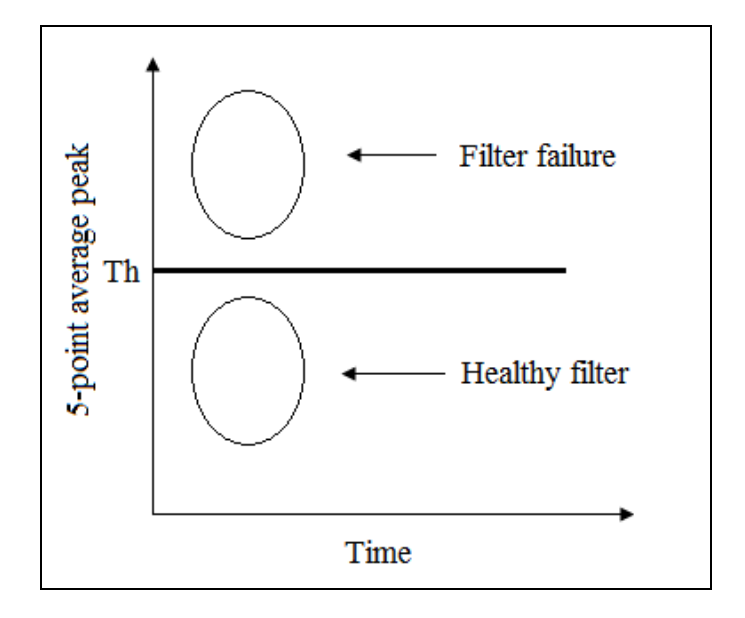


Figure 6.5 Fixed threshold concept

But this strategy will not work for the entire duration of filter operation between the 2 regeneration events. As seen from Figure 6.3, the 5-point average magnitude decreases as the filter soot loads, and this is true in the case of failed filters also. Hence a failed, soot loaded filter can be misjudged as a healthy filter, when a fixed threshold is considered. This is explained in Figure 6.6. The time when the magnitude of the 5-point average peak of a failed filter crosses the fixed threshold 'Th' depends on the intensity of the filter failure. It may cross 'Th' some time after regeneration for a less failed filter and after a very long time period for a heavily failed filter.

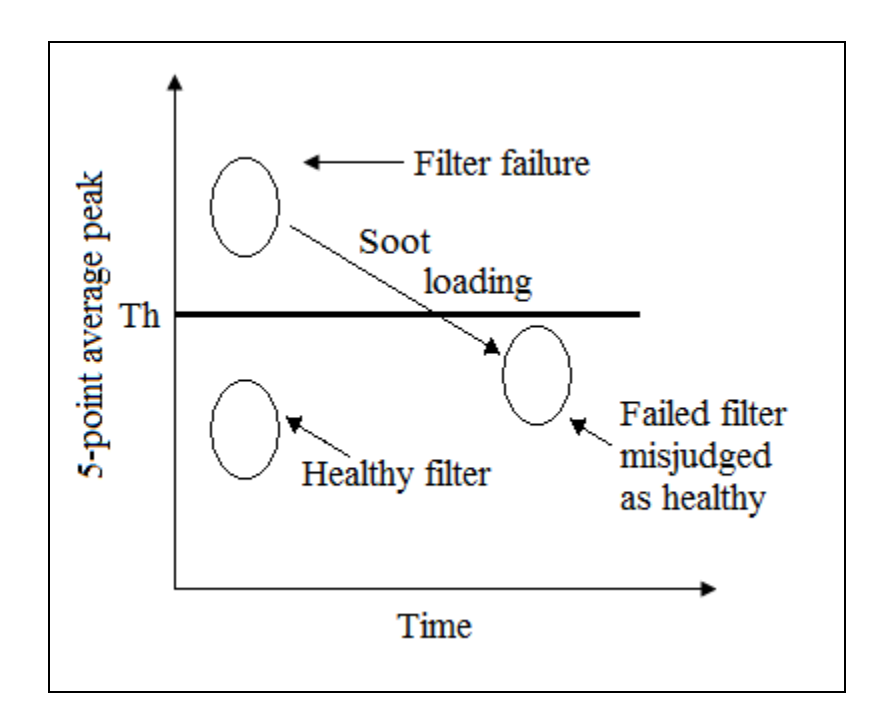


Figure 6.6 Fixed threshold – false pass

In order to avoid this false passing of the failed filters, a strategy involving testing of the filter condition for only a limited fixed time period can be used, but this leads to another problem. If the filter is in a healthy condition at the time of testing, but fails soon after that time period, then this failed condition will not be determined until the end of the next regeneration cycle when the filter is tested again. To overcome these drawbacks, and to

be able to test the filter throughout its operating period, excluding the regeneration cycles, a variable threshold concept can be used, which is explained next.

As seen from Figure 6.3, for nominal filter behavior, the trend of the 5-point average peak is a smooth decaying curve which does not seem to depend on the transient test cycle conditions. If this conclusion can be validated with the help of more transient test data, then a firm relation between the 5-point average peak and soot loading can be established. This decaying trend can be used as a variable threshold to enable continuous monitoring of the filter condition.

A filter failure detection algorithm using the variable threshold concept is described here. The variable decaying threshold to be used depends on engine type and DPF size. This variable threshold curve is stored in the form of a lookup table in the electronic control module or separate hardware may be used for this purpose. It is assumed that the time when the controlled regeneration process ends can be identified. Time after regeneration needs to be logged continuously until the start of the next controlled regeneration cycle. After the controlled regeneration process is over, a timer clock is reset. The upstream and downstream pressure signals are logged for 5 minutes with a sampling frequency of at least 400 Hz. This sampling frequency enables frequency domain analysis up to 200 Hz frequency range. The timer count 'C' is noted. The collected data is processed to find the 5-point average peak. The value of threshold at time 'C' is retrieved from the lookup table stored in the memory. The calculated 5-point average peak value is compared to this threshold and if it is found to be greater than the threshold, then the malfunction indicator lamp (MIL) is lit to signal the failed filter condition to the operator. If it is found to be lower than the threshold, then the filter is considered to be in normal operation. If the next cycle of controlled regeneration has not started yet, then the raw pressure data is collected to test the filter condition, and this process continues. The flowchart of this algorithm is shown in Figure 6.7.

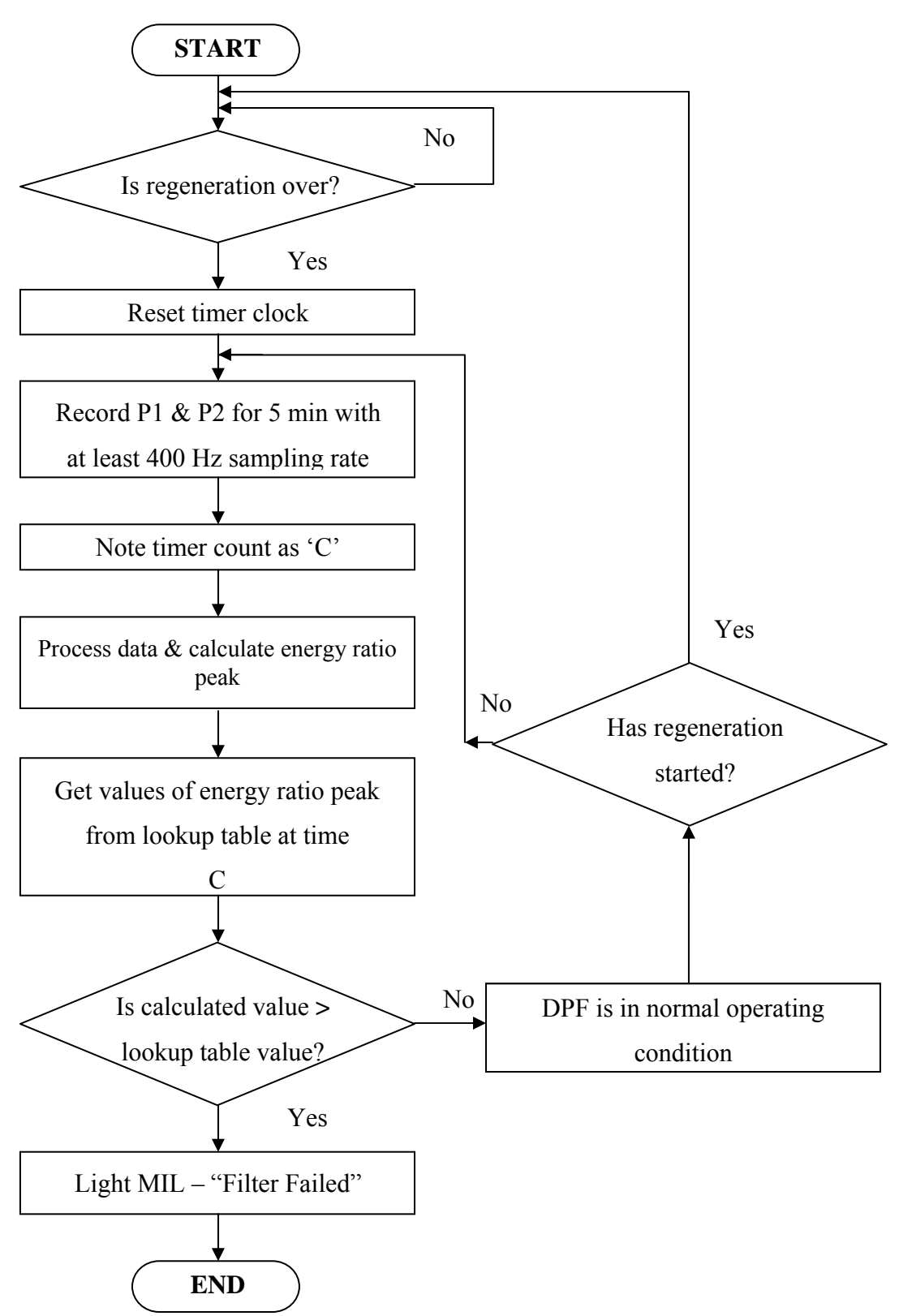


Figure 6.7 Flow chart for filter failure detection algorithm

To analyze any decision-making algorithm, it is important to know the advantages and also the risks involved. The above described algorithm operates for the entire period of DPF operation excluding the DPF controlled regeneration time. The 5-point average peak value for any specific time is compared to the threshold value at that time. As the time after regeneration increases, the difference between the 5-point average peak value for healthy and failed filter continues to increase. This can be seen from Figure 6.8, where absolute percentage differences are plotted. The reason for this increasing difference is that the failed filter accumulates soot at a lower rate than that of a healthy filter. If the variable threshold is set parallel to and above the nominal filter soot load trend so that the difference between these two lines is constant at all times, then it is possible to increase confidence in the algorithm's decision. In this case, the difference between the failed filter 5-point average peak and threshold will also increase as time passes.

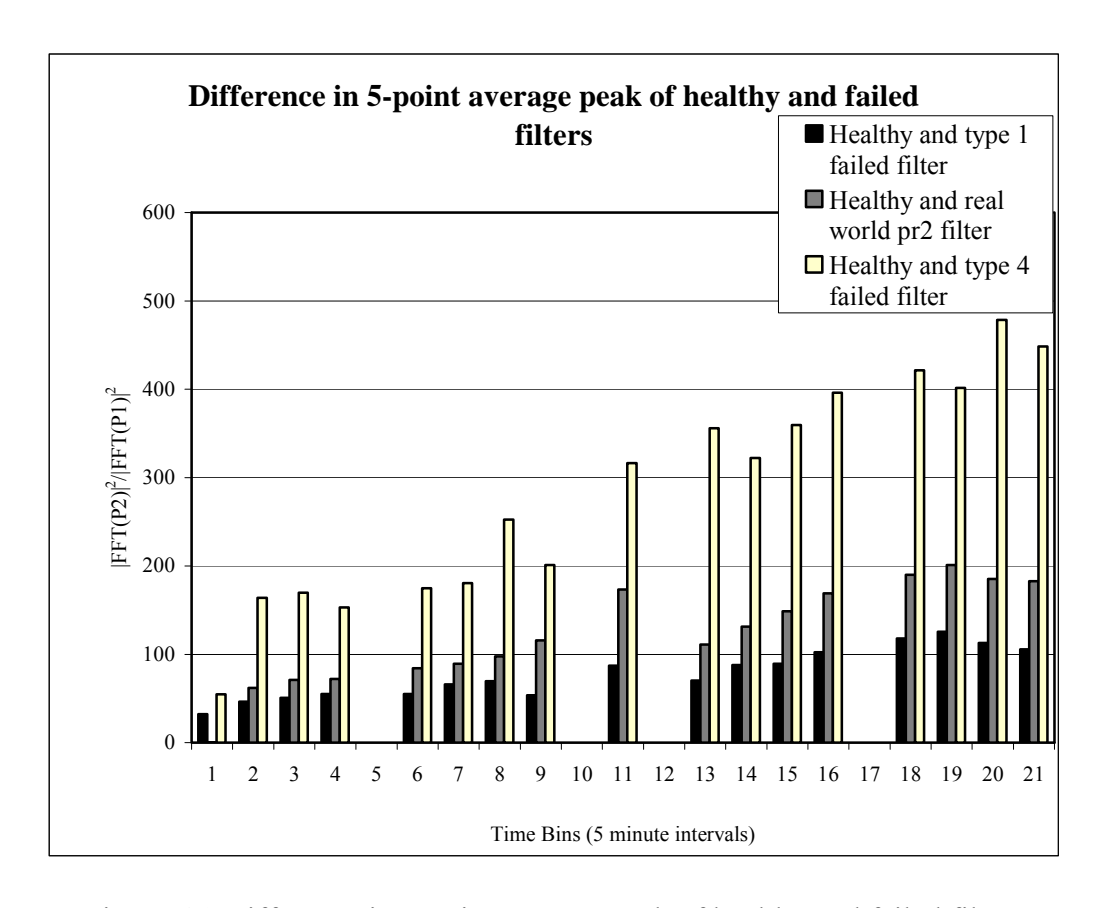


Figure 6.8 Difference in 5-point average peak of healthy and failed filters

If the DPF undergoes partial regeneration in between two controlled regeneration cycles, then the magnitude of the 5-point average peak will increase. For the failed filter case, this will mean that its difference from the threshold further increases, which is good. A failed filter will not be misjudged as a healthy filter even in case of partial regenerations.

The problem may arise for a healthy filter undergoing partial regenerations. There is a possibility that the partial regenerations may increase the magnitude of the 5-point average peak so much that it crosses the variable threshold and can be misjudged as a failed filter. This situation is illustrated in Figure 6.9. This hypothetical example shows two partial regeneration instances. The filter starts soot loading after every partial regeneration event. The first instance does not cause the 5-point average peak to cross the variable threshold, but the second instance of partial regeneration does.

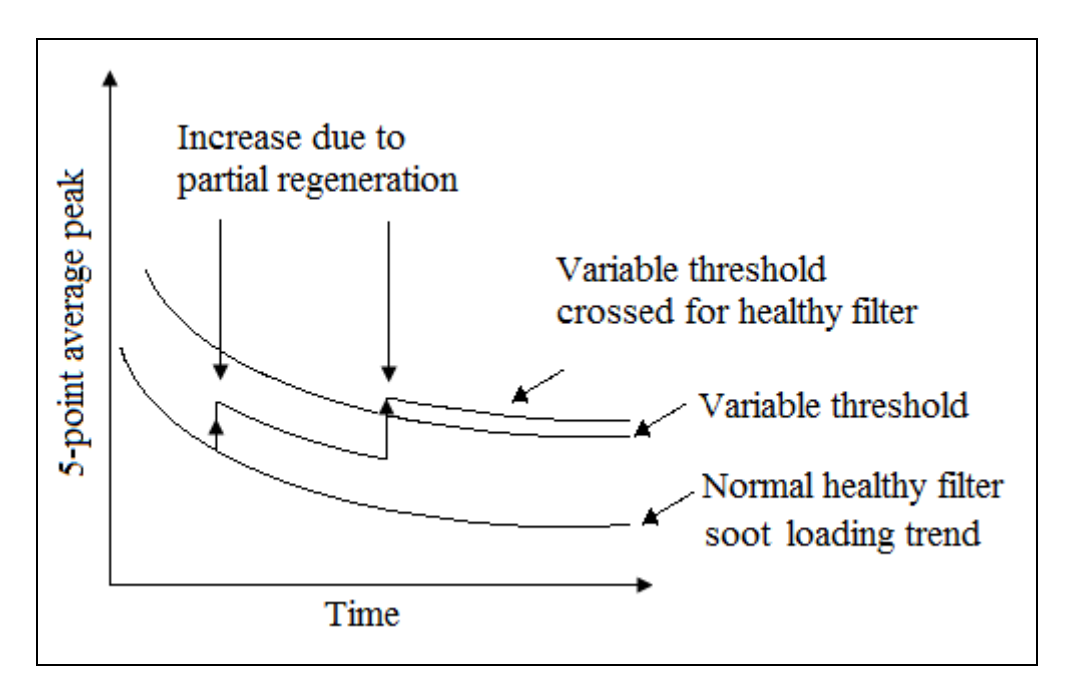


Figure 6.9 Healthy filter soot loading trend crossing the variable threshold due to partial regenerations

Partial regenerations are actually helpful as they reduce the backpressure and postpone the controlled regeneration, which improves fuel economy. Monitoring the occurrence of partial regeneration events is necessary for successful implementation of the abovementioned algorithm in light of the explained disadvantages of unnoticed partial regenerations. The DPF temperature could be monitored and if a sudden increase in energy ratio peak is observed, and is accompanied by a rise in temperature, then this situation could indicate occurrence of partial regeneration. If some such technique to account for the partial regenerations can be devised, then this variable threshold method to detect filter failure can be implemented successfully.

6.3. Computational Burden

The algorithm described here processes pressure signals in the frequency domain and hence needs high-speed sampling of these upstream and downstream pressure signals. This will increase the computational burden and the engine's electronic control module may not be able to handle the sampling and processing of the pressure signals in real time. A separate hardware may be used to sample the pressure signals with at least 400 Hz sampling frequency with a timer as indicated in the flowchart in Figure 6.7. The actual processing of the data does not seem to be computationally intensive once the data is sampled at high enough sampling rate. For computing the 5-point average peak and area under the curve of four 5 minute time intervals of the 1500 Hz sampled data, it took only 12.7 seconds on a 1 GHz processor for the Matlab program.

6.4. Sensitivity to Sensor Error

The above described algorithm relies on the 5-point average peak in the energy ratio graph, which is a function of upstream and downstream pressure signals and is therefore sensitive to measurement error in these signals. The algorithm is built on the test data collected, and hence already consists of sensor noise. In this section, robustness of the algorithm to additional noise is checked. If 5% or 10% white Gaussian noise, corresponding to a signal to noise ratio of 20 and 10 respectively, is assumed to be added

to each pressure signal at the time of measurement, then a shifted energy ratio plot is obtained. Figure 6.10 shows the shift in energy ratio plot for FTP75 test cycle on healthy filter for cycle 1 when 5% and 10% additional white Gaussian noise is added to both upstream and downstream pressure signals.

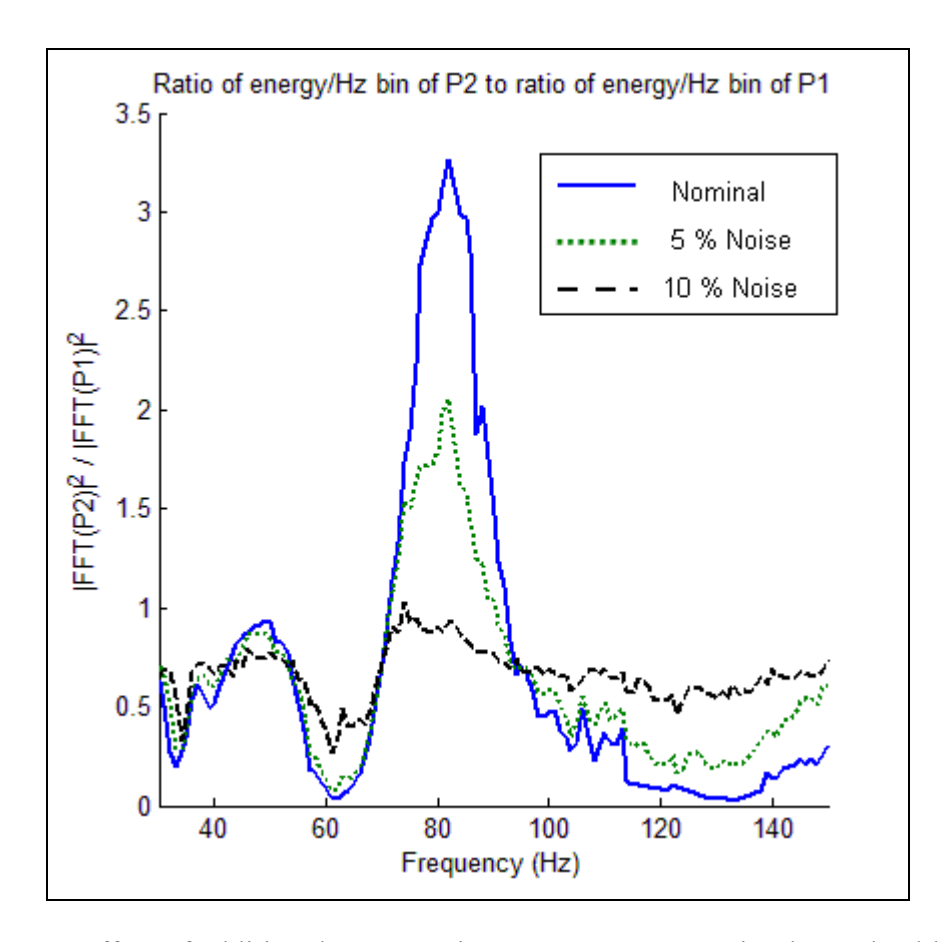


Figure 6.10 Effect of additional sensor noise error on energy ratio plot on healthy filter FTP75 test for cycle 1

It is observed that the peak in the energy ratio plot decreases with increase in noise on the raw pressure signals. This will reduce the detected 5-point average peak in the energy ratio plot. This reduction in the 5-point average peak can be misleading and may be interpreted as soot-loaded DPF state since the 5-point average peak also decreases due to soot loading of the DPF.

Another drawback of error due to sensor noise is difficulty in differentiating a failed filter from a healthy filter condition. The 5-point average peak in the energy ratio plot will also decrease for failed filters. If this peak falls below the variable threshold decided on the basis of nominal healthy filter behavior, then the failed filter will pass as a healthy one. This situation is shown for 5% noise addition in Figure 6.11 and for 10% noise addition in Figure 6.12.

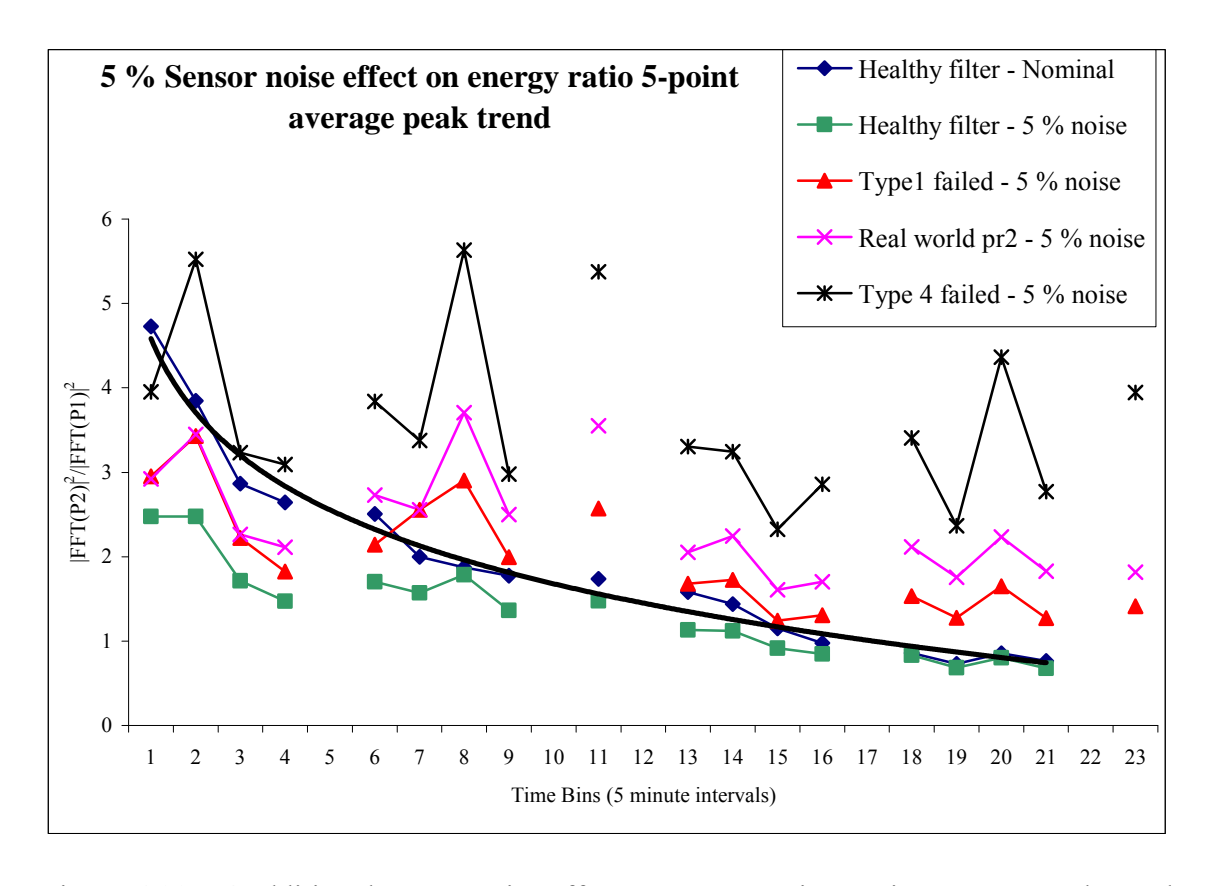


Figure 6.11 5% additional sensor noise effect on energy ratio 5-point average peak trend compared against logarithmic trend line fitted to nominal healthy filter data

The data for nominal behavior of a healthy filter is fitted with a logarithmic trend line in the above graph. The trend of the 5-point average peak in energy ratio plot after adding 5% white noise on both upstream and downstream pressure signals for healthy and failed filter cases is also shown. It is observed that the effect of noise is most pronounced in the early soot loading stage of the DPF where the peak of the failed filter falls below the

nominal healthy filter trend. In this situation, the failed filter will be misjudged as a healthy filter. As time passes and the filter gets soot loaded, the noise seems to have a less prominent effect. The 5-point average peak of failed filters lies above the nominal healthy filter trend and can be differentiated at the soot-loaded stage.

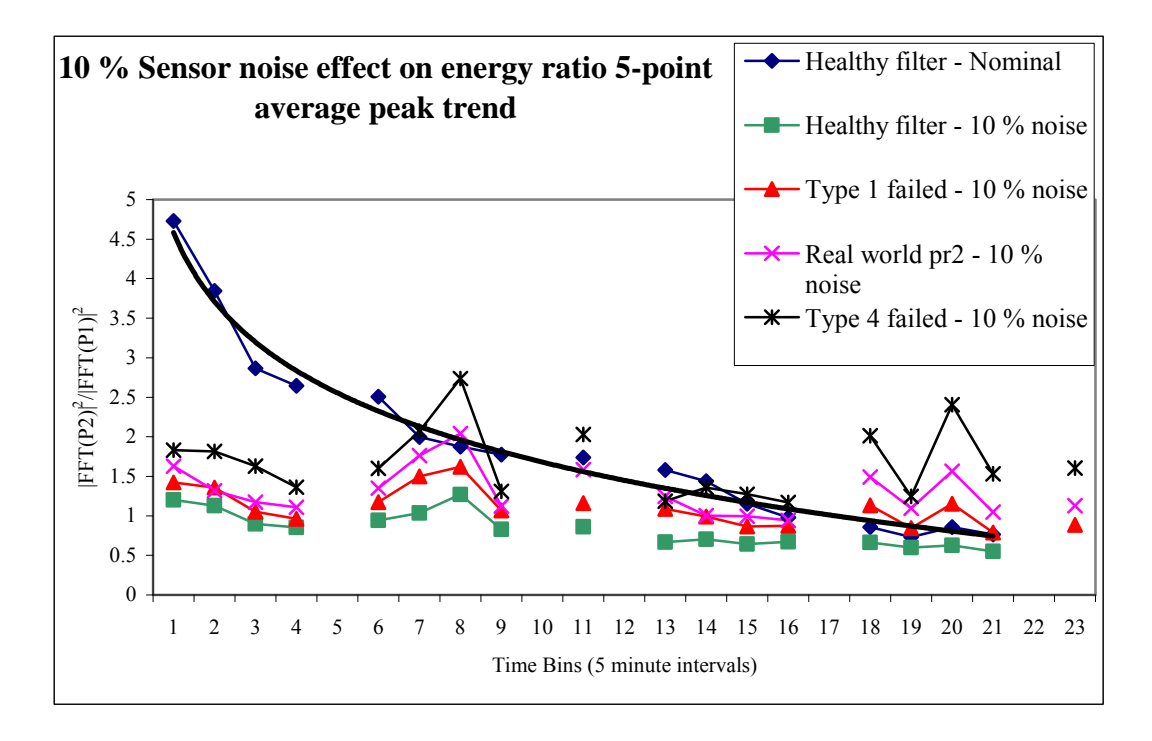


Figure 6.12 10% additional sensor noise effect on energy ratio 5-point average peak trend compared against logarithmic trend line fitted to nominal healthy filter data

As seen from Figure 6.12, the filter failure detection ability becomes even worse for 10% noise addition than for 5% noise addition. The 5-point average peak for the failed filters lies below the nominal healthy filter trend line most of the time. For such high magnitude of noise addition, the algorithm will fail to detect even the highest type 4 failed filter.

Since the addition of sensor noise shifts the energy ratio plot, as seen from Figure 6.10, the area under the curve of this plot will also change along with the 5-point average peak. Figures 6.13 and 6.14 show the effect of 5% and 10% sensor noise on the area under the curve of energy ratio plot, respectively.

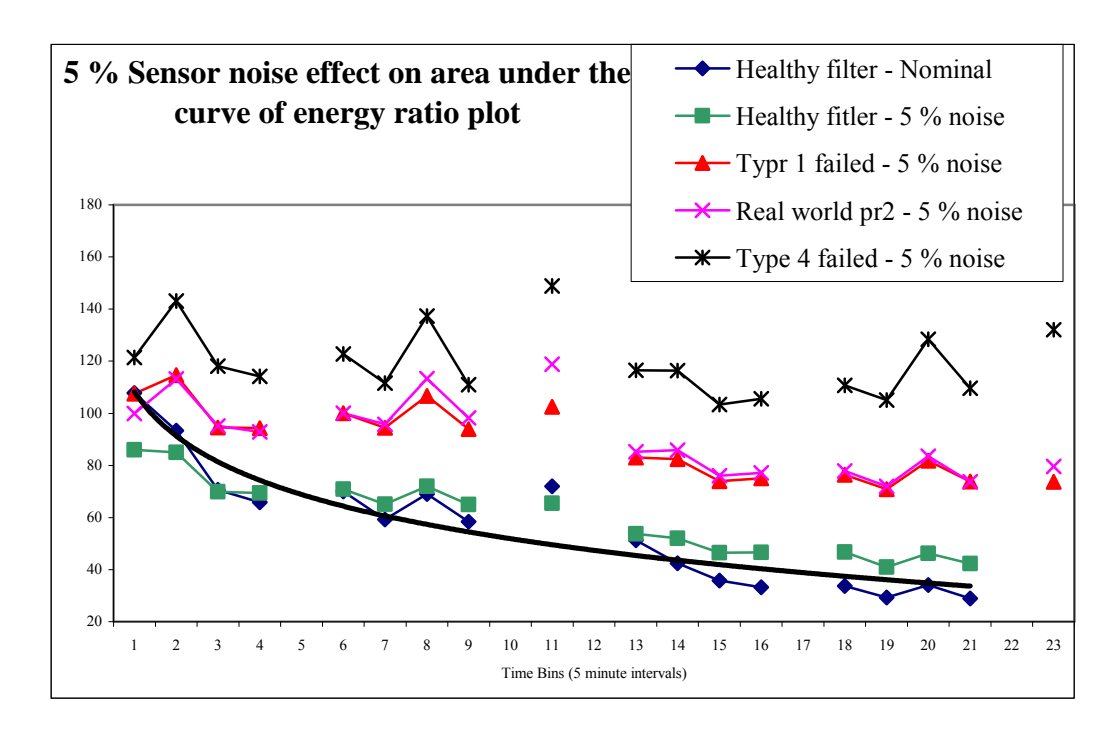


Figure 6.13 5% additional sensor noise effect on area under the curve of energy ratio plot compared against logarithmic trend line fitted to nominal healthy filter data

For the area under the curve trend plots, the nominal behavior of a healthy filter for no noise addition is fitted with a logarithmic trend. It is observed from Figure 6.13 that the 5% noise addition causes the area under the curve trend to lower for all the filter cases. Although the filter condition cannot be determined correctly for the first 5-minute time interval, the trends for all the failed filter cases lie above the nominal variable threshold line for the rest of the time intervals. Hence, if the area under the curve of energy ratio plot is used to determine the variable threshold for the filter failure detection algorithm, then such algorithm seems to be more robust than the 5-point average peak detection algorithm for 5% sensor noise addition. The 5% noise added trend for a healthy filter seems to cross the nominal behavior trend line and lies above it, but it is very close to the actual trend line, and if sufficient tolerance is considered while deciding the variable threshold, this problem can be dealt with.

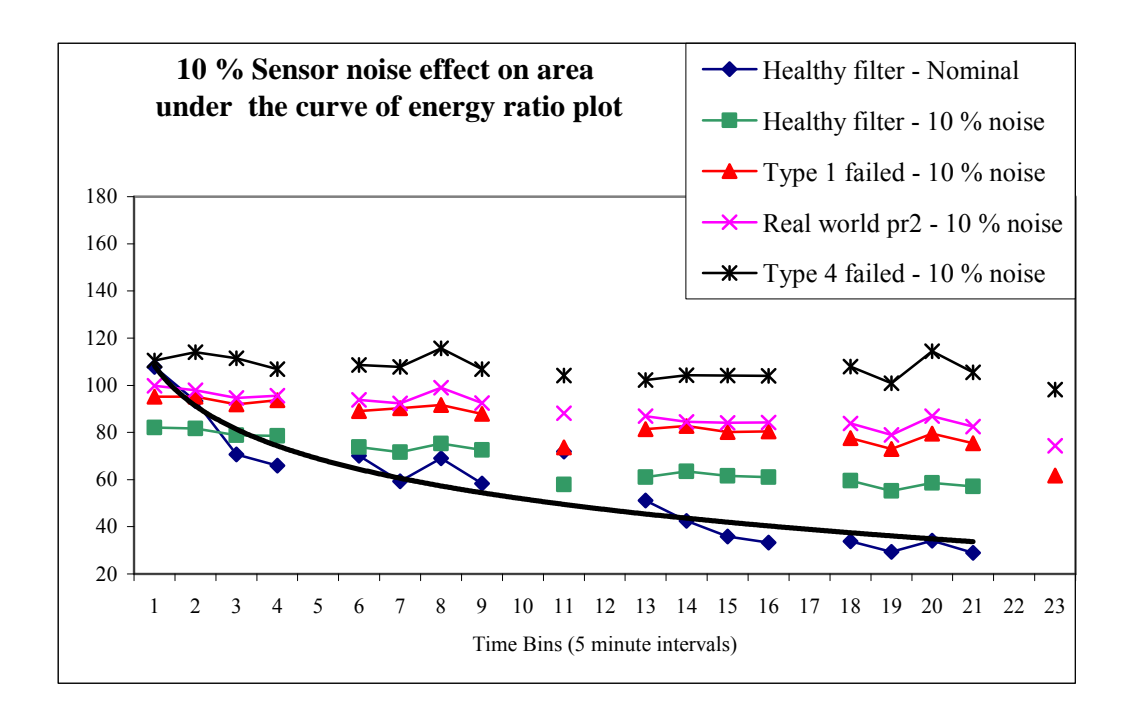


Figure 6.14 10% additional sensor noise effect on area under the curve of energy ratio plot compared against logarithmic trend line fitted to nominal healthy filter data

Figure 6.14 shows the effect on area under the curve trend for 10% noise addition. Here it can be seen that the noise added trends do not exhibit the decaying trend. The noise added trend for a healthy filter lies above the nominal healthy filter behavior trend line and can be misjudged as a failed filter. Hence sensor noise addition on the order of 10% for the algorithm that uses variable threshold based on area under the curve seems to increase the risk of false alarms.

Another type of sensor malfunction could be sensor bias error, where the sensor readings are magnitude shifted versions of actual measurements. This could be the result of sensor calibration error. This type of error will affect the average sensor reading. The pressure signal analysis method studied in this research is based on frequency domain analysis where the range of interest is 30 Hz to 150 Hz. As the magnitude shift does not affect any frequencies in this range (affects only the zero frequency component), the results of frequency domain analysis are not affected at all. Hence, this method is robust to sensor bias errors.

7. CONCLUSION AND FUTURE WORK

7.1. Conclusions

The motivation behind this work has been the stringent emission regulations and the need to monitor diesel particulate filters (DPF) for failure so that tailpipe particulate matter emissions do not exceed the stipulated emission threshold level. The temperature and pressure signals, both pre and post-DPF have been investigated for DPF failure diagnostics. Study has been performed on four artificially failed, two real world failed and one healthy operating particulate filter. All the cases were tested on the same test cycles. This research focuses on DPF diagnostics for transient engine operation and all the test cycles run were completely transient in nature.

The temperature signals were analyzed in the time domain. Various approaches were taken to study the effect of filter condition on the temperature signals. It has been observed that the differential temperature across the DPF increases as the extent of filter failure increases. The explanation for this observed trend is unclear at this point. The cross-correlation between the inlet and outlet DPF temperatures was also investigated. An encouraging trend in the cross-correlation function at 0 time lag was observed. The magnitude of cross-correlation function increases with filter failure intensity. Though this trend was observed for all transient cycles tested, the cross-correlation function itself seemed to be dependent on the nature of the test cycle. Normalizing the cross-correlation function with the transient test cycle parameters was attempted in order to make this cross-correlation function test cycle independent. The time delay methodology of cross-correlation function was also explored. The hypothesis used behind this investigation was that for the failed filter case the time delay involved between the inlet and outlet DPF

temperatures would be less than that for the healthy filter condition. The cross-correlation function was used to find the time delay between the inlet and outlet temperature signals of the DPF and an attempt was made to assess the condition of the filter based on this calculated delay. The results from this technique were of limited success. Though firm conclusions regarding the state of the filter could not be drawn from temperature signals alone, this study helped to understand the nature of the temperature signals clearly and the approaches investigated here could be applied along with some other diagnostic technique to improve the confidence of the filter diagnostic algorithm as a whole.

Pressure signals were analyzed in the frequency domain. In this approach, a relationship of the energy content of the upstream and downstream pressure signals to the state of the filter was established. The frequency range with maximum energy content was identified after neglecting frequencies near 0 Hz, and this range was used for the study. This range was determined to be from 30 Hz to 150 Hz. Identifying this frequency range would allow carrying out the same analysis even at smaller sampling rates of around 400 Hz as opposed to 1500 Hz used for the testing purpose. The identified frequency range contained the firing frequency components depending on engine speed, and hence, it was noted to have the highest energy content. The ratio of energy content of downstream pressure signal to energy content of upstream pressure signal was used to find the magnitude squared of the transfer function characteristics of the filter. A very distinct separation in these characteristics of healthy filter and failed filters was observed, which implied that these characteristics carry filter state information. The peak in the magnitude squared transfer function characteristics was observed to increase with increase in filter failure. This difference was used to build a filter failure detection algorithm. It was observed that the filter soot loading also affected these magnitude squared transfer function characteristics. The peak and the area under the curve for the magnitude squared transfer function characteristic curve were plotted as a function of time to understand their behavior with soot loading. The peak of the magnitude squared transfer function characteristic curve has a smooth decaying trend with time, i.e., the peak decreases with soot loading and hence with time. The curve of peak in magnitude squared transfer

function characteristics decays for the failed filter condition also, but it always remains above the curve for that of the healthy filter. This information was used to propose a filter failure detection algorithm. The threshold to decide whether a filter is in healthy operating condition or is failed was determined from the nominal behavior of a known healthy filter. This algorithm was analyzed with regard to fixed and variable thresholds and risks involved due to partial filter regeneration were discussed. A sensitivity analysis of this algorithm for sensor errors was performed. Sensor measurement errors were simulated by adding excess 5% and 10% Gaussian white noise to the raw upstream and downstream pressure data by setting the signal to noise ratio as 20 and 10 respectively. It was concluded that the algorithm based on detecting the peak in the magnitude squared transfer function characteristics, or measuring the area under that curve, both could be made to work even in case of 5% error, but both methods seemed to fail for 10% excess noise addition. The algorithm, which is based on the frequency domain analysis of pressure signals, was shown to be immune to any sensor bias errors.

7.2. Research Contribution

This research focused on analyzing the pre and post-DPF temperature and pressure signals separately. The analysis of temperature signals provided some interesting results. Specifically the cross-correlation of pre and post-DPF temperature signals was performed and observations regarding the magnitude and time delay between the signals were used to comment on the state of the filter. A clear connection between filter condition and energy content in pressure signals was established through the pressure signal analysis. A 4 step process for frequency domain analysis of pressure signals was devised. This consists of sampling the upstream and downstream pressure signals at high enough sampling rates, converting them to frequency domain by taking Fourier transform in the defined frequency range, squaring the Fourier components to get energy content and taking the ratio of energy / Hz bin of P2 to energy / Hz bin of P1. This frequency domain analysis of pressure signals was performed for transient engine operation. The determination of fixed frequency range to be used for analysis will make it possible to

sample the pressure signals at lower sampling rates than that used for the testing purpose. The soot loading trend of the healthy filter was observed to be more a function of time than that of the engine operation. A filter failure detection algorithm was proposed making use of a variable threshold concept. The robustness of this algorithm was checked by adding excess white noise to the raw pressure data.

7.3. Scope for Future Work

A few exciting correlations were investigated in the course of this research. Some directions in which this work can be further extended are listed below.

- Investigate the dependence of cross-correlation function of upstream and downstream temperature signals on the engine operating condition to make the cross-correlation function independent of any specific test cycle.
- Examine the dependence of the peak in the transfer function characteristics obtained from pressure signals on the filter soot load. This correlation will enable the DPF monitoring not only with respect to filter failure detection but will also enable the ECM to take regeneration decisions.
- Implement algorithm on actual engine. The specificity of the algorithm could be increased further by using both the temperature and pressure signal analysis techniques together.

LIST OF REFERENCES

- [1] P. Eastwood. Critical Topics in Exhaust Gas Aftertreatment. McGrall-Hill, New York, NY, 2000.
- [2] A. Konstandopoulos, M. Kostoglou, E. Skaperdas, E. Papaioannou, D. Zervalis, and E. Kladopoulou. Fundamental studies of diesel particulate Filters: Transient loading, regeneration, and aging. Technical Report 2000-01-1016, Society of Automotive Engineers, Warrendale, PA, 2000.
- [3] J. Heywood. Internal Combustion Engine Fundamentals. McGrall-Hill, New York, NY, 2000.
- [4] D. Kittelson. Engines and nanoparticles: A review. Journal of Aerosol Science, 29(5/6):575-588, 1998.
- [5] National Center for Environmental Assessment. Diesel engine exhaust. Health Assessment Document 600/8-90/057F, United States Environmental Protection Agency, Office of Transportation and Air Quality, Washington, DC, May 2002.
- [6] Air and Radiation, Technical Highlights EPA420-F-03-017, United States Environmental Protection Agency, Office of Transportation and Air Quality, Washington, DC, June 2003.
- [7] DieselNet. Summary of Worldwide Diesel Emissions Standards. http://www.dieselnet.com/standards, accessed June 30, 2008.
- [8] A. Konstandopoulos and J. Johnson. Wall-Flow diesel particulate Filters-their pressure drop and collection efficiency. Technical Report 890405, Society of Automotive Engineers, Warrendale, PA, 1989.
- [9] G. Stratakis and A. Stamatelos. Flow distribution effects in the loading and catalytic regeneration of wall-Flow diesel particulate Filters. Proceedings of the Institution of Mechanical Engineers, Part D: Journal of Automobile Engineering, 218(D2):203-216, 2004.

- [10] O. Haralampous, I. Kandylas, G. Koltsakis, and Z. Samaras. Diesel particulate filter pressure drop, Part 2: On-board calculation of soot loading. International Journal of Engine Research, 5(2):163-173, 2004.
- [11] A. Mayer. Typical Damages and Their Cause. Seminar on DPF Particle filter retrofitting Diesel engines, Munich, Germany, June 2007.
- [12] N. Singh and D. Wilhem. Apparatus, System, and Method for Enhancing Soot Filter Protection. Patent Application Publication, US 2008/0034738 A1, United States, February 2008.
- [13] O. Haralampous, G. Koltsakis, and Z. Samaras. Partial regeneration in diesel particulate filters. Technical Report 2003-01-1881, Society of Automotive Engineers, Warrendale, PA, 2003.
- [14] W. Wangard, A. Egelja, and H. Metwally. CFD simulation of transient soot trapping and regneration in a diesel particulate Filter. Technical Report 2004-01-2658, Society of Automotive Engineers, Warrendale, PA, 2004.
- [15] J. Wills and S. Wills. Apparatus, System, and Method for Detecting and Labeling a Filter Regeneration Event. Patent number US 7263825 B1, United States, September 2007.
- [16] A. Joshi. Strategies for Data-Based Diesel Engine Fault Diagnostics. PhD, Purdue University, West Lafayette, Indiana, USA, December 2007.
- [17] T. Hijikata, S. Yamada and R. Horie. Method of Inspecting a Honeycomb Structural Body for Purifying Exhaust Gases and Apparatus used in the Method. Patent number US 005102434A, United States, April 1992.
- [18] A. Konstandopoulos, E. Skaperdas, and M. Masoudi. Microstructural properties of soot deposits in diesel particulate traps. Technical Report 2002-01-1015, Society of Automotive Engineers, Warrendale, PA, 2002.
- [19] S. Cheng. Apparatus for Sensing Particulates in Gas Flow Stream. Patent number US 007334401 B2, United States, February 2008.
- [20] T. Schulte and B. Schumann. Device and Method for Determining a Malfunction in a Filter. Patent number US 007081154 B2, United States, July 2006.
- [21] U. Schönauer. Measuring Arrangement and Method for Monitoring the Operability of a Soot Filter. Patent number US 006432168 B2, United States, August 2002.

- [22] M. Nieuwstadt and I. Kolmanovsky. System and Method for Monitoring the Loading of a Diesel Particulate Filter. Patent number US 006397587 B1, United States, June 2002.
- [23] B. Bunting, P. Miller, B. Stoia, A. Suresh and R. Radovanovic. System for Controlling Particulate Filter Temperature. Patent number US 006910329 B2, United States, June 2005.
- [24] N. Hiroaki and W. Saitama. An Apparatus for Detecting a State of a Particulate Filter. Patent Application Publication, EP 1849972 A1. European Patent Office, October 2007.
- [25] C. Urs, V. Jo and C. Brendan. Method to Determine the Amount of Diesel Particulate Accumulated in a DPF. Patent Application Publication, EP 1081347 B1. European Patent Office, April 2003.
- [26] E. Kladopoulou and A. Konstandopoulos. A Virtual Sensor for Soot Load Estimation in Diesel Particulate Filters. Workshop of Chemical Process Engineering Research Institute, Thermi, Thessaloniki, Greece, 2004.
- [27] M. Rauchfuss, S. Cooper and N. Zayan. Diesel Particulate Filter Monitoring Using Acoustic Sensing. Patent number US 006964694 B2, United States, November 2005.
- [28] P. Versaevel, H. Colas, C. Rigaudeau, R. Noirot, G. Koltsakis, and A. Stamatelos. Some empirical observations on diesel particulate filter modeling and comparison between simulations and experiments. Technical Report 2000-01-0477, Society of Automotive Engineers, Warrendale, PA, 2000.
- [29] P. Cunningham. Monitoring Diesel Particulate Filters. PhD, Purdue University, West Lafayette, Indiana, USA, December 2006.
- [30] E. Kladopoulou, S. Yang, J. Johnson, G Parker and A. Konstandopoulos. A study describing the performance of diesel particulate filters during loading and regeneration a lumped parameter model for control applications. Technical Report 2003-01-0842, Society of Automotive Engineers, Warrendale, PA, 2000.
- [31] O. Haralampous, I. Kandylas, G. Koltsakis, and Z. Samaras. Diesel particulate filter pressure drop, Part 1: Modeling and experimental validation. International Journal of Engine Research, 5(2):149-162, 2004.
- [32] S. Allam and M. Åbom. Acoustic modeling and testing of diesel particulate filters. Journal of Sound and Vibration, 288:255-273, 2005.

- [33] S. Allam and M. Åbom. Sound propagation in an array of narrow porous channels with application to diesel particulate filters. Journal of Sound and Vibration, 291:882-901, 2006.
- [34] M. Daoud. System and Method for Monitoring a Filter. Patent Application Publication, US 2007/0199378 A1, United States, August 2007.
- [35] H. Venghaus, L. Watts, A. Mayr, C. Telford, M. Ranalli, P. Kroner, D. Herranz G. Speer, S. Schmidt and S. Walleck. Method and Apparatus for Determining Loading of an emission Trap by Use of Transfer Function Analysis. International Publication Number, WO 2007/082223 A2, Patent Cooperation Treaty, July 2007.
- [36] P. Cunningham, C. Shah, and P. Meckl. Correlating dynamic pressure signal features to diesel particulate filter load. Technical Report 2007-01-0333, Society of Automotive Engineers, Warrendale, PA, 2007.
- [37] J. Bendat and A. Piersol. Engineering Applications of Correlation and Spectral Analysis. John Wiley and Sons, Inc., New York, NY, second edition, 1993.
- [38] J. Proakis and D. Manolakis. Digital Signal Processing Principles, Algorithms, and Applications. Prentice-Hall of India, New Delhi, India, third edition, 2004.

A. DPF TRANSFER FUNCTION CHARACTERISTICS

The energy ratio plots i.e., plot of magnitude squared of transfer function characteristics of diesel particulate filter calculated in the range of 30 Hz to 150 Hz based of pressure signals are shown in appendix A. These are plotted for all the filter cases tested on five transient tests. The plots for US06 test from cycle 2 are not shown due to lack of useful data for this test.

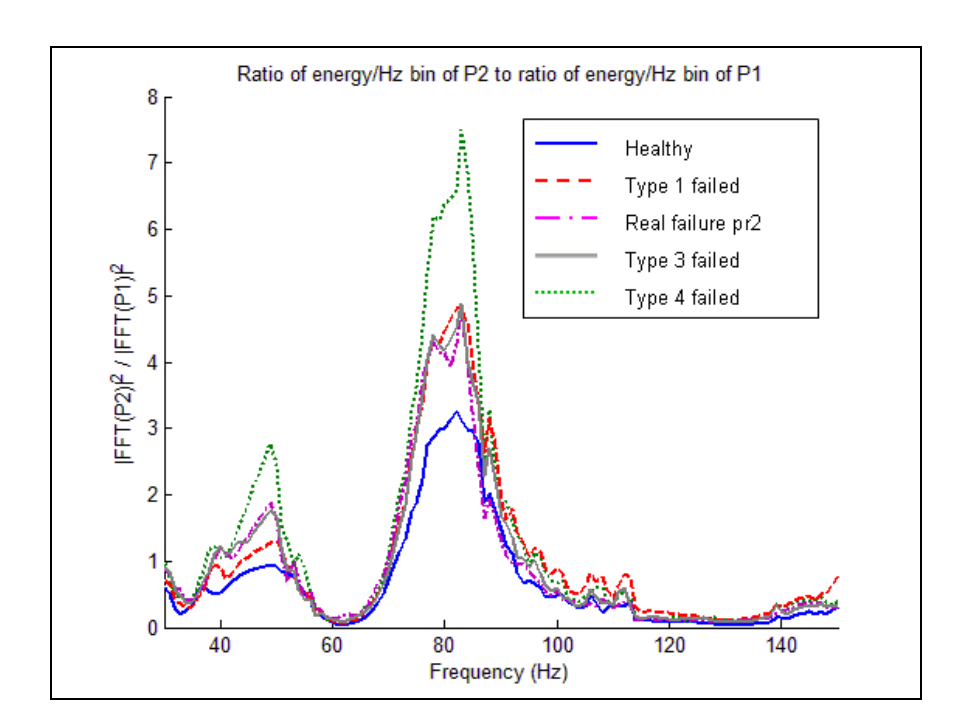


Figure A.1 Energy ratio plots for FTP75-cycle 1 for all filter cases*

* Except for Type 2 failed filter case

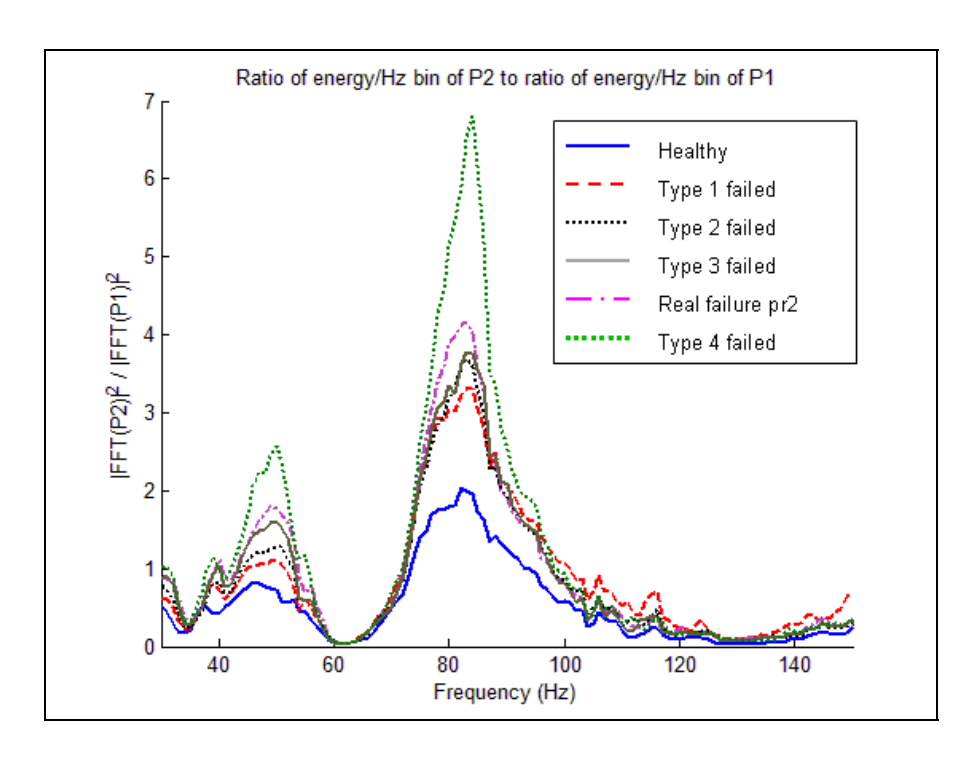


Figure A.2 Energy ratio plots for all LA92-cycle 1 for all filter cases

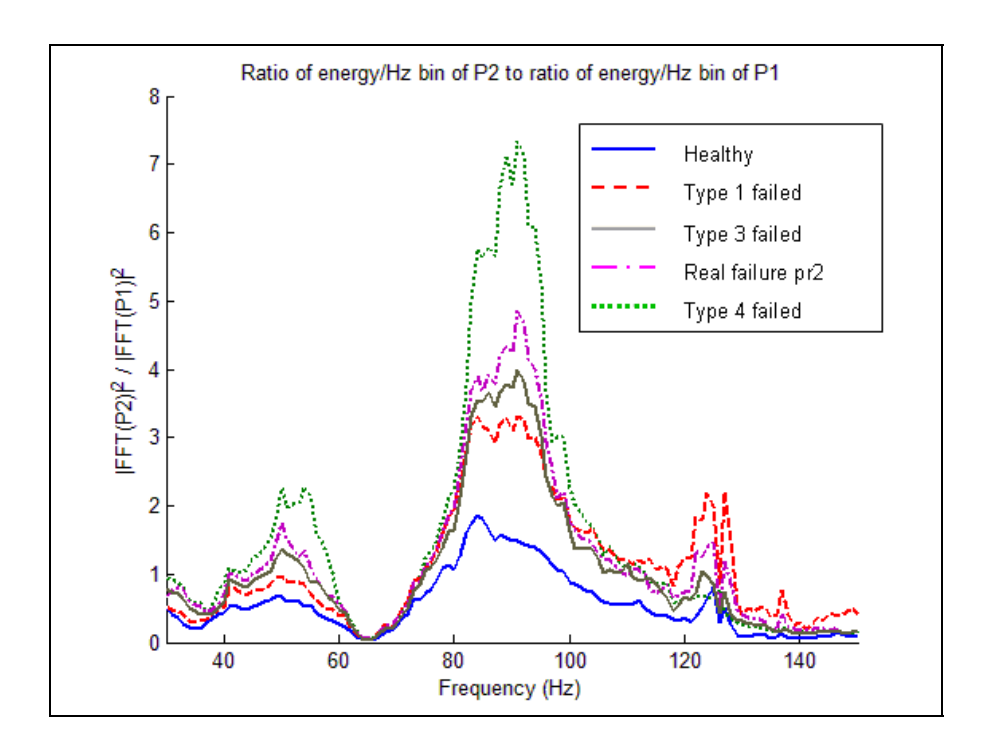


Figure A.3 Energy ratio plots for US06-cycle 1 for all filter cases*

* Except for Type 2 failed filter case

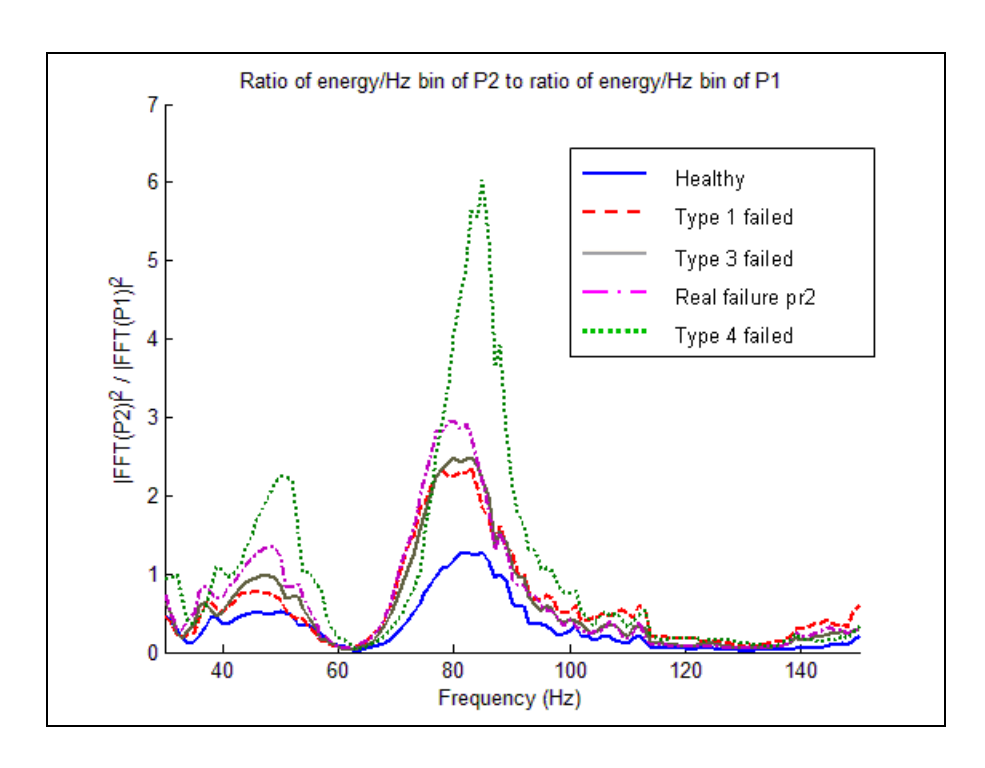


Figure A.4 Energy ratio plots for FTP75-cycle 2 for all filter cases*

* Except for Type 2 failed filter case

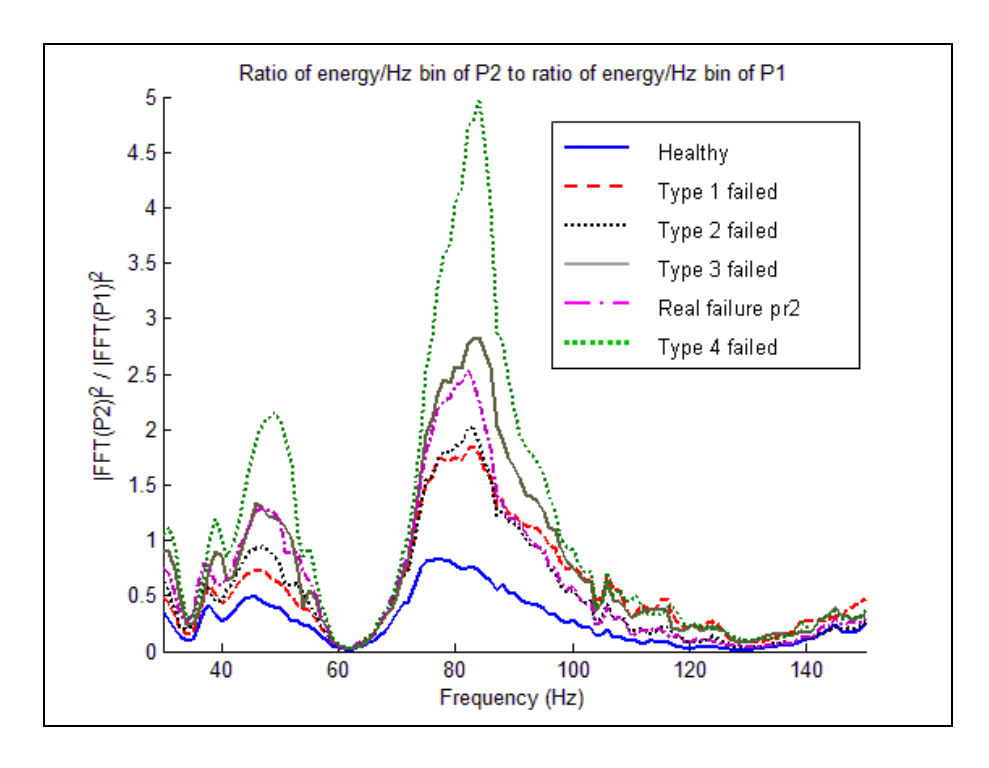


Figure A.5 Energy ratio plots for all LA92-cycle 1 for all filter cases



